UM-HSRI-PF-74-10

Hydroplaning and Tread Pattern Hydrodynamics

by

James F. Sinnamon
John T. Tielking

October 1974

Highway Safety Research Institute / University of Michigan

BIBLIOGRAPHIC DATA SHEET	1. Report No. UM-HSRI-PF-74-10	2.	3. Recipient's Accession No.

4. Title and Subtitle

Hydroplaning and Tread Pattern Hydrodynamics

5. Report Date: October 1974

6.

7. Author(s)

J. F. Sinnamon and J. T. Tielking

8. Performing Organization Rept. No. UM-HSRI-PF-74-10

9. Performing Organization Name and Address

Highway Safety Research Institute
University of Michigan
Huron Parkway and Baxter Road
Ann Arbor, Michigan 48105

10. Project/Task/Work Unit No. 329180

11. Contract/Grant No.

12. Sponsoring Organization Name and Address

Motor Vehicle Manufacturers Association
320 New Center Building
Detroit, Michigan 48202

13. Type of Report & Period Covered

14.

15. Supplementary Notes

Tire Traction Characteristics Affecting Vehicle Performance: Interim Document 7

16. Abstracts

This document presents the final report on analytical and laboratory studies directed toward the development of a set of tread pattern performance parameters containing those aspects of tread pattern geometry which are relevant to water expulsion effectiveness. Current knowledge of the hydroplaning phenomenon is reviewed and utilized in interpreting the results of experiments conducted with a laboratory apparatus designed to measure the water expulsion effectiveness of a tread pattern.

17. Key Words and Document Analysis. 17a. Descriptors

Hydroplaning
Tread Patterns
Squeeze Films

17b. Identifiers/Open-Ended Terms

17c. COSATI Field/Group

18. Availability Statement	19. Security Class (This Report)	21. No. of Pages
UNLIMITED	UNCLASSIFIED	126
	20. Security Class (This Page) UNCLASSIFIED	22. Price

UM-HSRI-PF-74-10

HYDROPLANING AND TREAD PATTERN HYDRODYNAMICS

James F. Sinnamon

John T. Tielking

Project 329180

Tire Traction Characteristics
Affecting Vehicle Performance

Interim Document 7

October 1974

Sponsored by

The Motor Vehicle Manufacturers Association

PREFACE

The study of pneumatic tire hydroplaning reported in this document was conducted as part of an ongoing tire research project entitled "Tire Traction Characteristics Affecting Vehicle Performance," sponsored by the Motor Vehicle Manufacturers Association. A major objective of this study was to collect current knowledge of the hydroplaning phenomenon and squeeze films in the tire-road contact region. This knowledge is utilized in interpreting the results of experiments conducted with a laboratory apparatus designed to measure the water expulsion effectiveness of a tread pattern.

In addition to increased understanding of tread pattern hydrodynamics, a major goal of this work is the development of a set of tread pattern performance parameters which would contain those aspects of tread pattern geometry relevant to water expulsion effectiveness. Two such descriptors, derived from the experimental and theoretical work reported herein, are proposed. Recommendations for future work to develop additional tread pattern descriptors are discussed.

CONTENTS

1.0 INTRODUCTION

Pneumatic tire hydroplaning, which results in sudden and catastrophic loss of vehicle control, has been intensively studied since the phenomenon was first identified in the late 1950's. During the past decade, a large number of investigations, both experimental and analytical, have been conducted to identify and analyze various aspects of the hydroplaning phenomenon.

The hydroplaning phenomenon is known to be exceedingly complex, involving the interaction of fluid dynamics with the contact mechanics of a load-carrying, pressurized, toroidal shell. Although a number of very useful empirical relationships have been derived from the extensive body of experimental data, analytic investigations have been far less successful. With the rational view that a theoretical analysis of wet tire traction and hydroplaning must be based on the theoretical analysis (as yet unachieved) of tire traction on a dry surface, it is logical to anticipate that increased understanding of the hydroplaning phenomenon will be derived from the continuation of empirical investigations. The foundations on which to build a theoretical analysis of wet tire traction are insufficient at present.

The empirical approach has been followed in the work reported herein, which is specifically directed toward the development of numeric descriptors for tread pattern geometry relevant to traction on a wet pavement. Such descriptors are required for the continued development of semi-empirical mathematical models designed to reproduce measured tire traction characteristics.

The project plan for the development of tread pattern descriptors, as originally conceived, involved primarily the design, construction, and operation of a laboratory apparatus which would simulate the process whereby a tread pattern expels water from the tire-road contact region. It became readily apparent, however, that to simulate certain aspects of the water expulsion process was a difficult task and that the interpretation

of data from the simulation would require a thorough understanding of the physics of high-speed tire-road contact in wet conditions. Consequently, a very extensive literature survey was undertaken prior to and during the design of the laboratory experiment to test the water expulsion efficiency of a tread pattern. A major portion of this document is devoted to describing the present state of knowledge anent tire hydroplaning and the influence of squeeze films on wet traction performance.

Section 2.0 reviews and discusses various aspects of hydroplaning phenomena which occur when a tire is traveling in deep or shallow water. A control volume analysis is used to derive the Horne hydroplaning equation from fluid momentum theory. A complementary equation for the traveling speed at which squeeze-film penetration (contact detachment) begins is derived from the Bernoulli equation of fluid mechanics. Empirical investigations of hydroplaning phenomena in various water depths are reviewed and a theoretical explanation for the "critical water depth," above which tire-road shear force generation is insensitive to water depth, is proposed. Current concepts of the viscous hydroplaning phenomenon are introduced and Moore's theory of viscous hydroplaning is discussed. A four-zone concept of wet traction phenomena is outlined.

Section 3.0 contains a discussion of squeeze-film theory relevant to wet traction phenomena. Fluid inertia effects in squeeze films are analyzed by numerical solution of a recently derived squeeze flow equation which contains local and convective inertia force terms as well as the classical viscous force term. The analysis shows that the water expulsion process is mainly an inertial flow process* and that experimental data from the tread pattern effectiveness experiment, reported in Section 5.0, may be interpreted in the light of inertial flow considerations.

Section 4.0 describes the rational selection of two tread pattern performance parameters. The groove capacity parameter, γ_1, which is the ratio of the water-interception rate to the

*Inertial forces are found to predominate in squeeze films of thickness greater than .005 in. while viscous forces dominate in films less than .005 in. thick.

groove-absorption rate, may be used to define the boundary between shallow and deep water as seen by a particular tread pattern on a smooth surface. The flow distance parameter, γ_2, which is the ratio of squeeze flow distance (averaged) to contact length, is a measure of the effectiveness of pattern geometry in locating reservoirs for the expelled squeeze film. The requirement for a third parameter, relating to flow resistance, is defined and additional parameters, relating to the effectiveness of sipes, are discussed.

Section 5.0 describes the design and construction of a laboratory apparatus to simulate tread pattern hydrodynamics in the thick-film penetration zone of the tire-road contact region. Data from this apparatus is presented and interpreted in relationship to findings of on-the-road wet traction test programs. The laboratory experiments showed the existence of a critical rib width which is influenced by groove volume and water depth. The critical water depth, analogous to that observed in tire hydroplaning experiments, was found to be influenced by groove volume and independent of groove depth. The limitations of the laboratory apparatus are discussed and suggestions are made for further work with the present apparatus and some modifications of it.

2.0 THE HYDROPLANING PHENOMENON

The reduction of the maximum shear force capability of a pneumatic tire by water and other road surface contaminants has long been a matter of concern to pavement and tire design engineers. Experimental measurements of tire-road friction using the locked-wheel stopping distance method began in the 1920's. Since that time, investigators in this field have gradually come to recognize the great complexity of this problem. In the past fifteen or so years, these investigators have attempted to carefully control and quantify such variables as water depth and pavement surface texture. Several theoretical analyses of certain aspects of the wet traction problem have been published recently. Most of the references found useful in the preparation of this document have appeared since 1960.

2.1 DEFINITIONS

It is generally agreed that the reduction of shear force capability of a tire operating on a wet road surface is due to a film of water separating part or all of the tire from the road surface. When such a lubricating film of water exists, the tire is said to be hydroplaning. When the water film pervades the entire contact region, the tire shear force capability is reduced to such a low level that directional control of the vehicle depending on this tire becomes impossible and the tire is said to be totally hydroplaning. If only a portion of the contact region is separated by water, shear force capability is substantially reduced but not totally lost and the tire is said to be partially hydroplaning.

The hydroplaning phenomenon is classified according to the basic physical mechanisms that produce it. Dynamic hydroplaning refers to the situation where fluid inertia or momentum change produces the hydrodynamic pressure distribution necessary to maintain a water film in the tire-road contact region. Viscous hydroplaning occurs when a thin water film in the contact region is maintained by flow resistance due to fluid viscosity.

In much of the literature, the term "hydroplaning" refers to what would, in this document, be called total dynamic hydroplaning. In this document, however, the term "hydroplaning" is applied to any situation in which maximum shear force capability is reduced by the presence of a lubricating water film. The adjectives "partial," "total," "dynamic," and "viscous" will be used to distinguish between the different hydrodynamic mechanisms which result in reduction or loss of tire shear force capability.

2.2 DYNAMIC HYDROPLANING

The depth of water on the pavement surface is of major importance in the study of dynamic hydroplaning. The following three sections devoted to dynamic hydroplaning discuss the phenomena occurring in conditions of (a) deep water (2.2.1) —depth such that most of the water intercepted by the tire must be displaced to the periphery of the tire contact patch rather than simply displaced into the tread grooves; (b) shallow water (2.2.2)—depth such that water need only be displaced into the grooves (flow through the grooves does not occur); and (c) intermediate water depths (2.2.3). Section 2.2.3 reviews experimental data which may be used to define the critical water depth for dynamic hydroplaning.

2.2.1 DEEP WATER. Extensive research in deep-water hydroplaning has been performed at the Langley Aeronautical Laboratory by Horne and his associates [1, 2, 3]*, and at the Road Research Laboratory in England [4].

When a tire rolls through deep water, it is observed that most of the water is displaced from the tire contact region by means of a forward and a lateral spray resulting from the impact between the leading edge of tire contact and the water covering the road surface. A so-called water wedge is formed (Fig. 1) and substantial hydrodynamic pressures develop in this region. As rolling speed increases, the hydrodynamic pressure increases and a portion of the contact region, where the hydrodynamic pressure exceeds the tire-road contact pressure, becomes supported by a water film.

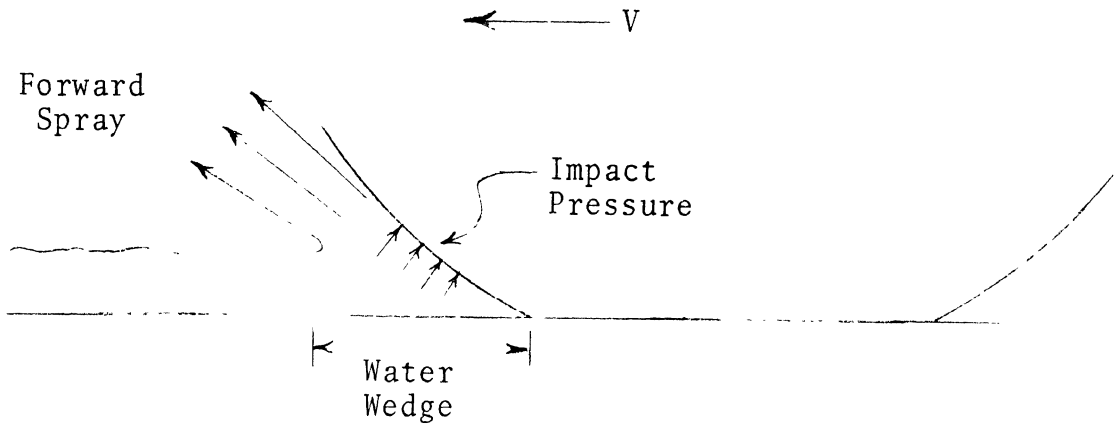

Figure 1. Water wedge formed by tire rolling in deep water.

*Numbers in brackets indicate literature references on page 118.

With further increases in speed, the entire contact region eventually becomes supported by a water film and total hydroplaning occurs. It is observed that, when total hydroplaning occurs, there is considerable water flow to the rear of the contact region and the foreward spray is greatly reduced.

It has been established that when the water is sufficiently deep, tire pressure is one of the most influential variables determining the speed at which hydroplaning occurs. Figure 2 shows the rolling speed at which wheel spin-down* occurs, plotted against inflation pressure. The data shown in Figure 2 was obtained with a standard production radial-ply automobile tire tested over a wide range of tire loads (indicated).

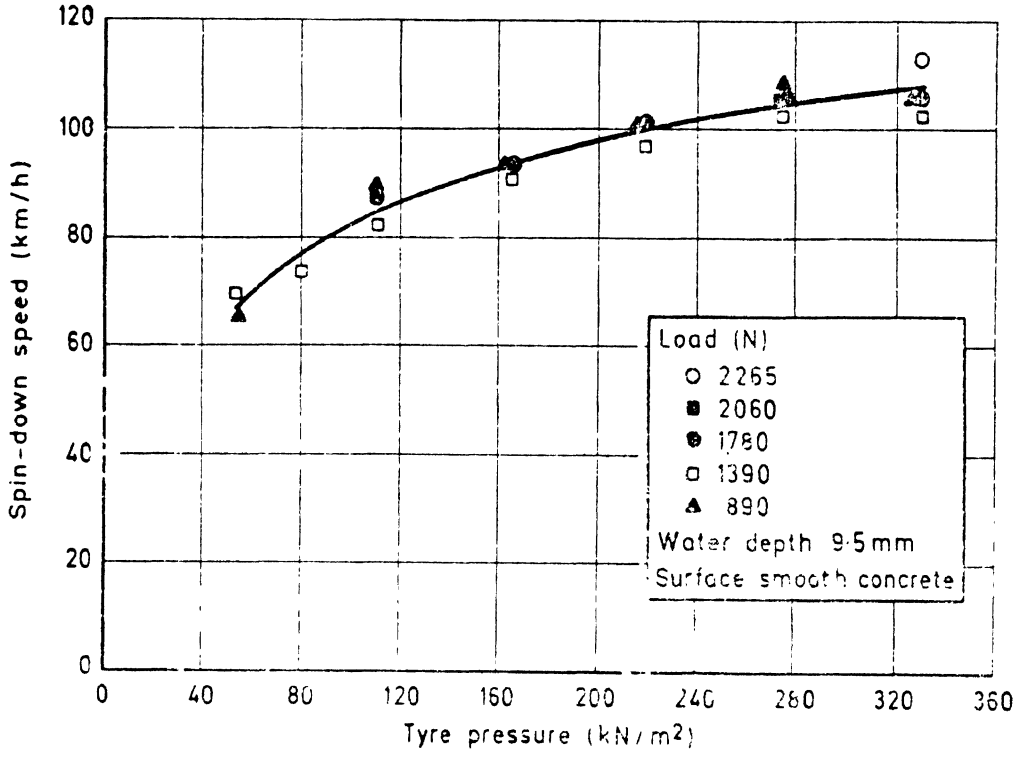

Figure 2. Effect of inflation pressure and tire load on the hydroplaning, or spin-down, speed of a radial-ply tire. From [4].

*Wheel spin-down, without a reduction in traveling speed, is one of the manifestations of total hydroplaning, and has been shown to occur at the speed where minimum friction is obtained [4].

Figure 2 shows clearly that tire load does not have a very significant influence on hydroplaning or spin-down speed, which definitely increases with increasing inflation pressure for the same tire operating in the same water depth. This finding is explained by the knowledge that total hydroplaning occurs when the average hydrodynamic pressure beneath the tire roughly equals the ratio of tire load to gross contact area,* and this ratio depends primarily upon inflation pressure.

Control Volume Analysis. If the assumption is made that, in deep water, hydrodynamic pressure is due to momentum change resulting from impact of the tire upon the initially stationary water layer, an equation relating hydroplaning speed to inflation pressure can be derived. This equation was first derived by Horne [1]. Because of its relevance to the theory of water expulsion presented later, a derivation of Horne's hydroplaning equation is given in this document. The derivation is based on the following analysis of the water wedge as a control volume.

Imagine a coordinate system attached to the tire and moving with the tire at speed V. An observer from this reference frame would see the water layer moving toward the tire with speed V. A control volume of the water layer impinging upon the tire is shown in Figure 3 by a dashed enclosure. Water enters the control volume with velocity V in the x-direction. The mass flow rate, $\dot{m}_i$, into the control volume is given by

$$\dot{m}_i = \rho w h V \qquad (1)$$

*Gross contact area refers to the total area within the contact boundary. For a patterned tread, the actual contact area is always smaller than the gross area.

where ρ = water density

w = tire tread width

h = water depth

The control volume includes the foreward spray so that water can leave the control volume only by a lateral spray. For simplicity, the lateral spray is assumed to have no x-component of velocity. Assuming a constant input velocity, V, application of fluid momentum theory shows that the longitudinal component of hydrodynamic force on the tire is

$$F_x = \dot{m}_i \cdot V = \rho w h V^2 \qquad (2)$$

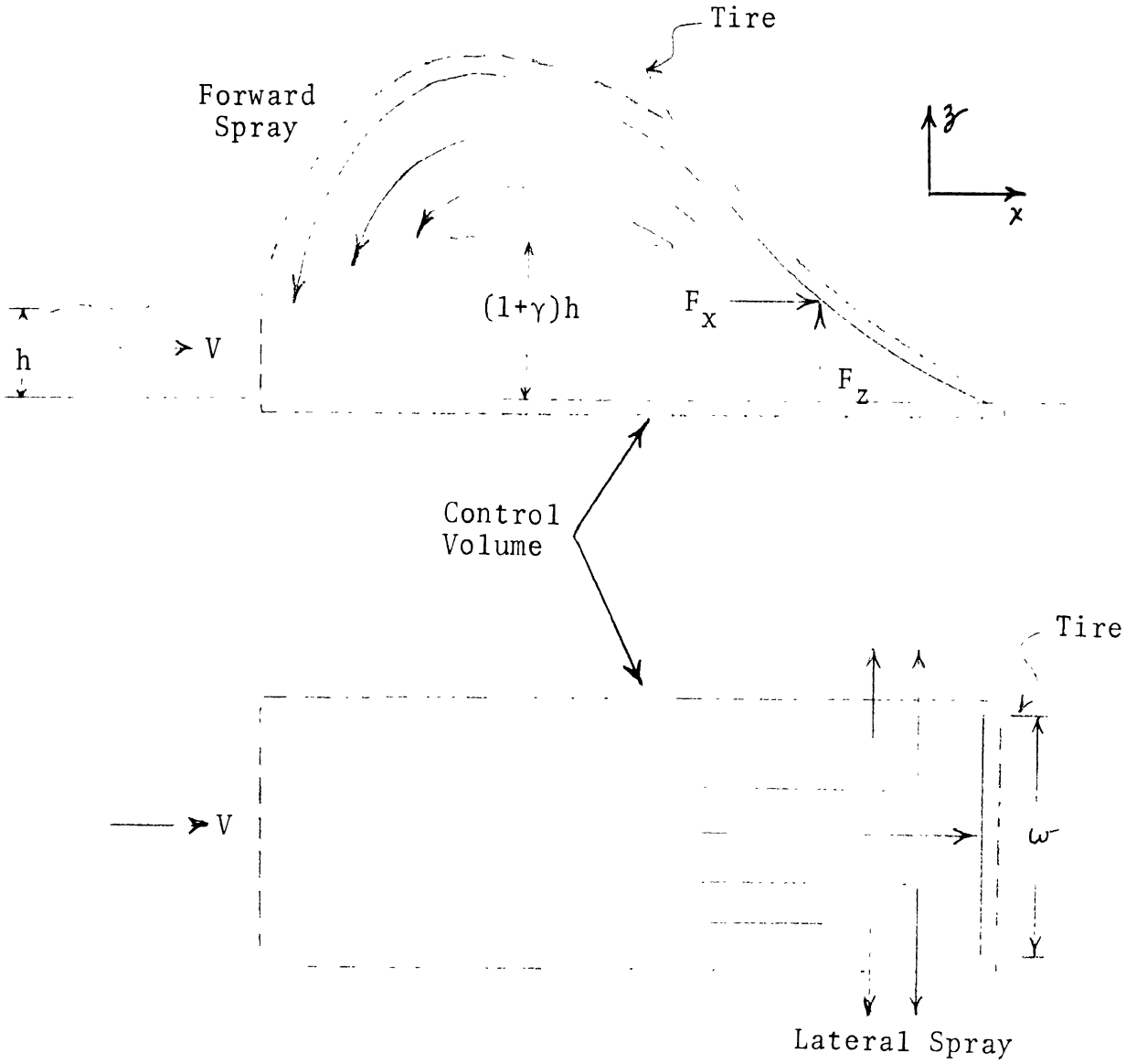

Figure 3. The control volume for application of the continuity and momentum theorems to determine hydrodynamic force on a tire rolling in deep water.

The foreward spray inside the control volume raises the water level to height h_{eff}. Let γ be the fraction of water volume recycled by the forward spray. Application of fluid continuity theory allows the effective water level to be determined.

$$\rho w h_{eff} V = \rho w h V + \gamma \rho w h V$$

$$h_{eff} = (1+\gamma)h \tag{3}$$

The dimension h_{eff} is the depth of the water wedge which impinges upon the tire. Figure 4 shows a water wedge of depth $(1+\gamma)h$ and length ℓ acting against a rolling tire.

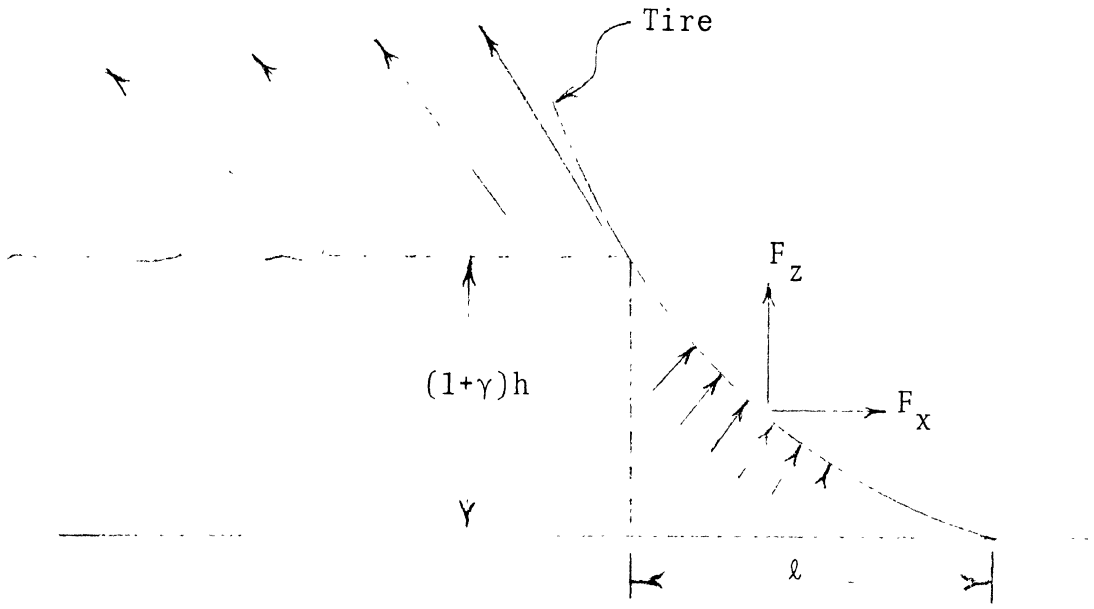

Figure 4. Hydrodynamic pressure and force components acting on a tire rolling in deep water.

The longitudinal force, F_x given by eq (2), is the horizontal component of the hydrodynamic pressure, P, developed in the water wedge acting on the tire. Referring to Figure 4, the horizontal and vertical force components of the hydrodynamic pressure are seen to be

$$F_x = P(1+\gamma)wh \tag{4}$$

$$F_z = Pw\ell \tag{5}$$

By equating the right-hand sides of eqs (2) and (4), the hydrodynamic pressure is found to be proportional to the velocity squared.

$$P = \frac{\rho V^2}{1+\gamma} \tag{6}$$

The substitution of eq (6) into eq (5) yields the vertical force component developed in the water wedge.

$$F_z = w\ell \cdot \frac{\rho V^2}{1+\gamma} \tag{7}$$

Although water depth, h, does not appear explicitly in eq (7), the vertical force, F_z, depends implicitly on h through the dependence of ℓ and γ on water depth.

If the vertical force generated in the water wedge were the only source of lift, extremely high speed would be necessary to induce total hydroplaning, and vertical load and tread width would be the primary variables to determine hydroplaning speed. In reality, as hydrodynamic pressure increases, the water wedge penetrates farther into the contact region and part of the tire becomes supported by a relatively thick water film. This thick-film penetration has been verified by contact region observations through a glass plate [1,2,3,25].*

*The observed penetration film is thick in comparison to the very thin lubricating films which may exist in apparently dry contact regions.

The portion of contact supported by thick-film penetration is viewed as a separate contact zone whose foreward boundary is the water wedge. The assumption of inviscid flow, which was used in the water wedge analysis, is no longer strictly valid in the film penetration region; hydrodynamic lift force is developed here by different mechanisms. The flow conditions in the water wedge are boundary conditions governing the flow in the film penetration region.

The Horne Hydroplaning Equation. A precise analysis of the water flow in the tire-road contact region is an extremely difficult task, yet to be accomplished. The semi-empirical approach taken by Horne [1], however, has produced a valuable approximate expression relating hydroplaning (total) speed to tire pressure. Horne reasoned that, for total hydroplaning, the average hydrodynamic pressure, P_{avg}, in the contact region must be proportional to the pressure at the water wedge which, in turn, is proportional to the square of the speed, according to eq (6). Thus

$$P_{avg} = K_1 \rho V^2 \tag{8}$$

where the constant γ, appearing in eq (6), has been set to zero because, in total hydroplaning, it is observed that the forward spray is suppressed. As mentioned earlier, total hydroplaning will occur when P_{avg} equals the ratio of tire load to gross contact area. If one now assumes that tire inflation pressure accounts for 80 percent of a tire's load-carrying capacity, the other 20 percent being supplied by carcass stiffness, then

$$P_{avg} = 1.2 P_i \tag{9}$$

where P_i is the tire inflation pressure. Equation (8), with P_{avg} given by eq (9), may be solved for the hydroplaning speed $V = V_h$.

$$V_h = \sqrt{\frac{1.2P_i}{\rho K_1}}$$

or

$$V_h = K\sqrt{P_i} \qquad (10)$$

The value of the constant K is related to fluid properties and flow dynamics. It must be determined from experimental data for a specific tire-road combination.

Equation (10) was developed by Horne for the prediction of the hydroplaning speed of aircraft tires. With V_h in mph and P_i in psi, Horne finds that K = 10.35 provides a good fit to experimental data on hydroplaning speeds of aircraft tires in the inflation pressure range of 25 to 150 psi [1]. However, for automobile tires, which are significantly different in tread pattern and construction, eq (10) tends to predict hydroplaning speeds which are too low.

Comparison With Experimental Data. The following data is presented to illustrate the range of validity of Horne's hydroplaning equation when used to predict the hydroplaning speed of passenger car tires. The influence of tread pattern is found to be nearly as important as the influence of inflation pressure on hydroplaning speed.

Figure 5 presents deep-water data showing that minimum cornering friction and spin-down for grooved automobile tires is encountered at speeds somewhat higher than that predicted by Horne's equation, while hydroplaning speed for the smooth tread tire is predicted very accurately. Although Figure 5

shows cornering force data, the small slip angle (4.5 deg.) should have little effect on flow beneath the tire, and Horne's equation, which was derived for straight-ahead motion, should be valid for predicting the spin-down speed for the data shown in this figure.

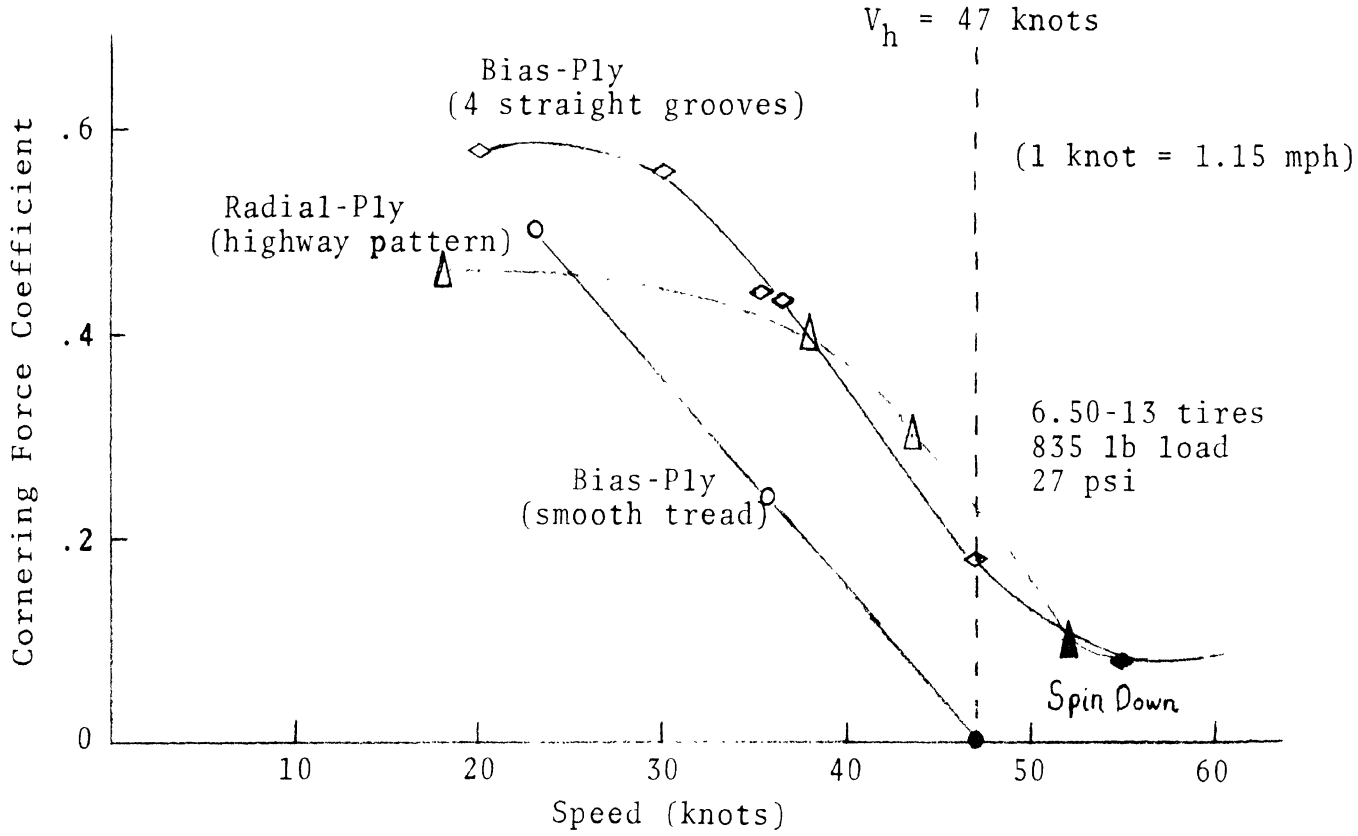

Figure 5. Cornering force coefficients vs. speed at 4.5° slip angle. Concrete surface with smooth macro-texture, sandblasted to produce harsh microtexture. Water depth = .4 inches. From [3].

A plot of spin-down speed versus inflation pressure data, taken from Reference [4], is given in Figure 6. The effect of tread pattern on hydroplaning speed is clearly seen in this figure. The spin-down speed predicted by Horne's hydroplaning equation has been plotted as a dashed curve and data points from Figure 5 have been added.

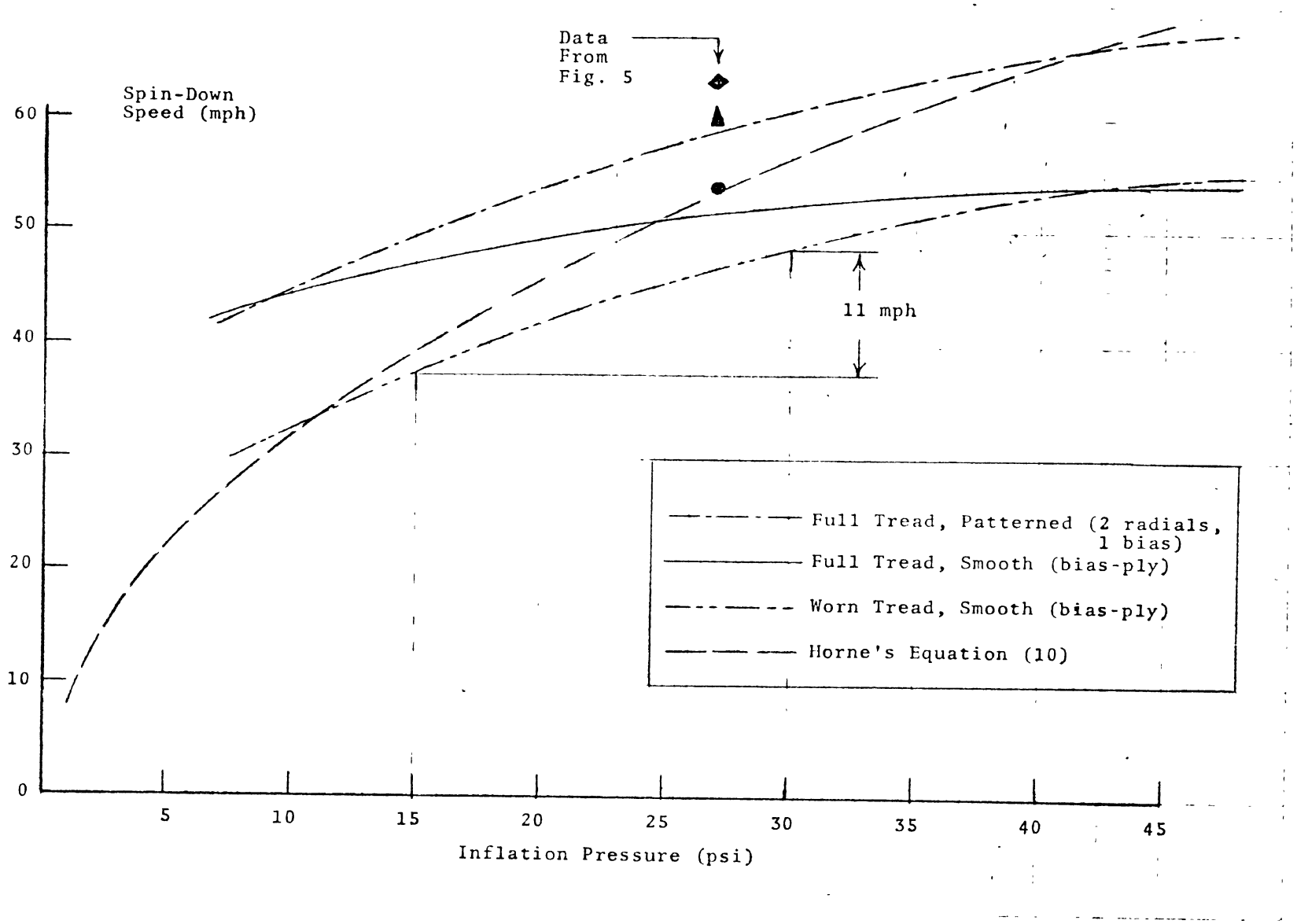

Figure 6. Effect of tread pattern on hydroplaning speed of passenger car tires.

The data in Figure 6 show that the hydroplaning speed for a new, fully patterned, automobile tire is about 10-12 mph higher than the hydroplaning speed of a similar tire which is worn smooth. It is also seen that approximately the same change in hydroplaning speed can be obtained by increasing the inflation pressure from 15 to 30 psi, the pressure range over which automobile tires are usually operated. Thus, it is concluded that, for automobile tires, tread pattern and inflation pressure are of about equal importance in determining the speed at which total hydroplaning occurs in deep water. The observation that tread pattern has such a significant effect on hydroplaning speed is not too surprising since additional pattern features (in addition to the straight rib pattern found on all aircraft tires) delay the build-up of hydrodynamic pressure by providing more channels for the escape of water from the contact region. Horne's hydroplaning equation does provide a useful approximation to the deep water hydroplaning speed of patterned tires since it appears to predict values that are intermediate between the values measured for a new patterned tire and for a tire with the tread worn smooth. Finally, the deviation from predicted values which is exhibited by the new tire with a featureless full tread is, in all likelihood, a result of the increase in bending stiffness of the tire structure due to the solid tread layer. The Horne hydroplaning equation presumes a uniform contact pressure at nearly the value of the tire inflation pressure; a uniform contact pressure will be obtained only with tires having minimal bending stiffness. It is quite likely that the nonuniform contact pressure produced by the tire with a featureless tread is responsible for the deviation of hydroplaning speeds from the values predicted by eq (10).

The general validity of Horne's hydroplaning equation, seen by comparison with experimental data, indicates that deep-water hydroplaning is a "dynamic" phenomenon, i.e., fluid inertia effects predominate. The term "total dynamic hydroplaning" is thus applied to phenomena predicted by the Horne equation.

Referring again to Figure 5, it is seen that tread pattern has a very important influence on tire-road friction capability at speeds below the total hydroplaning speed. However, as the total hydroplaning speed is approached, the patterned tires rapidly lose their advantage. An explanation for this behavior will be proposed after some observations on the role of squeeze films in partial hydroplaning are made (Chapter 3).

Surface texture has an effect on hydroplaning speed similar to that of tread pattern [6]. However, since the tread pattern is the primary concern of this document, surface texture effects will not be dealt with extensively herein.

2.2.2 SHALLOW WATER. Consideration is now given to a tire rolling on a paved surface covered by a water layer which is sufficiently thin so that the tread grooves do not become flooded. In this situation, water need only be displaced into the grooves of a patterned tire. Pressurized flow through the grooves to the contact periphery does not occur.

A dimensionless geometric ratio which quantifies the capability of a tread pattern to absorb a specific layer of water into its grooves can be derived in the following way. Consider a tire of tread width w which is rolling at speed V on a surface covered by shallow water of depth h. The volume rate, $\dot{Q}$, at which water is intercepted by the tire is given by

$$\dot{Q} = whV \quad . \tag{11}$$

Let g be the tread groove capacity defined as the groove volume per unit of gross contact area. The rate, $\dot{v}$, at which groove volume becomes available to absorb water is given by

$$\dot{v} = wgV \tag{12}$$

The water-absorption capability of a specific tread pattern operating in a specific layer of water is quantified by the dimensionless ratio $\dot{v}/\dot{Q}$ which will be designated γ_1

$$\gamma_1 = \frac{\dot{v}}{\dot{Q}} = \frac{wgV}{whV} = \frac{g}{h} \tag{13}$$

If the situation of a tire rolling in a certain depth of water is such that $\gamma_1 > 1$, then water need only be displaced into the tread grooves and flow through the grooves need not occur in order for the tread surface to make contact with the pavement surface. Thus, $\gamma_1 > 1$ is the criterion which determines the situation of a tire rolling in shallow water.

The preceding analysis is independent of pavement surface texture and is valid only for a free-rolling tire in water layers of depth h measured to the top of the surface asperities. Surface texture correction factors would be introduced if the action of the tread rubber draping over the asperities was considered influential on the water absorbing capability of a tread pattern. If braking is applied, the possibility of groove flooding arises in the sliding portion of the contact region.

A typical automobile tire, with highway-type tread pattern, has a groove capacity of about .08 when new. In water depths of .02-.04 inches, where many wet traction

tests are done, the grooves will not be expected to flood, except possibly at high values of longitudinal slip and/or at high speeds. It is highly unlikely that a fully patterned tire will hydroplane (totally) at ordinary highway speeds in shallow water, even on surfaces having smooth macrotexture.

A large number of measurements have been made of tire traction in shallow water, presumably because shallow water conditions usually prevail in normal wet weather driving.

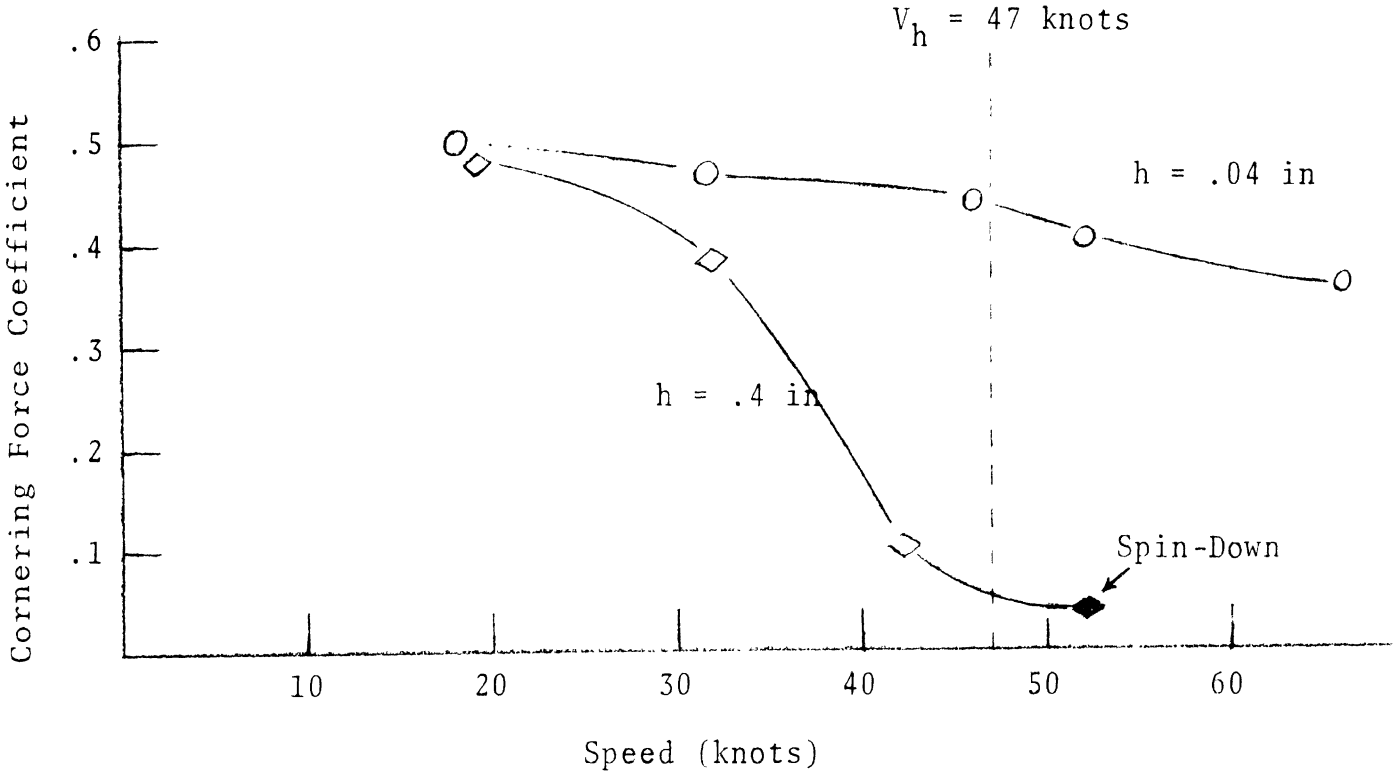

Figure 7. Covering force coefficients vs. speed at 4.5° slip angle. Concrete surface with smooth macrotexture, sandblasted to produce harsh microtexture. Automobile tire with highway-type tread pattern rolling in shallow (h = .04 in.) and deep (h = .4 in.) water. From [3].

Figure 7 shows typical cornering force versus speed data for a patterned automobile tire in both shallow and deep water. In this figure, it is seen that the rapid drop in friction capability, as the hydroplaning speed is approached, does not occur for the patterned tire rolling in shallow water. Apparently, the hydrodynamic pressure developed in the water wedge at the leading edge of tire contact does not provide a significant lift force on a patterned tire in shallow water. Quite different behavior is observed with a smooth tread tire in shallow water, for which analysis depends on the squeeze-film penetration concept to be discussed next.

Squeeze-Film Penetration. The reduction of traction with increasing speed in shallow water is usually explained by the progressive penetration of a relatively thick film of water, called a "squeeze film," into the contact region. This particular squeeze film is maintained and motivated by the hydrodynamic pressure generated in the water wedge. When a portion of the tread surface in the contact area is supported by such a squeeze film, the tire is said to be in "partial dynamic hydroplaning." This phenomenon has been observed on the glass plate facility at the Langley Landing Loads Track [3].

Clearly, a certain amount of time is required to squeeze a water film from the tread-road interface to permit tire contact with the paved surface. The time available for the squeezing process is inversely proportional to speed, and, as speed increases, a greater portion of the contact region becomes supported by the squeeze film and friction capability decreases accordingly. The time required to expel the squeeze film is hypothesized to be a function of (1) initial thickness of the squeeze film, (2) tire-road contact pressure distribution, (3) flexibility of the tire carcass and tread rubber, (4) tread pattern, and (5) surface texture.

Momentum and continuity considerations indicate that the hydrodynamic pressure at the leading edge of the contact region is independent of water depth (see eq (6)). This pressure will exist whenever there is a sufficient water cover to allow formation of a water wedge*. When this pressure exceeds the tire-road contact pressure at the leading edge of contact, a squeeze film presumably penetrates into the contact region, initiating the separation of the tire from the road surface.

An analysis of squeeze-film initiation can be made by application of Bernoulli's equation. Consider a mass particle, δ_m, of water moving with speed V in a longitudinal streamline to the center of the leading edge of the contact region. The mass particle will decelerate in the water wedge, come to rest at a stagnation point (A) near the leading edge of contact, and be abruptly expelled in a forward spray as shown in Figure 8.

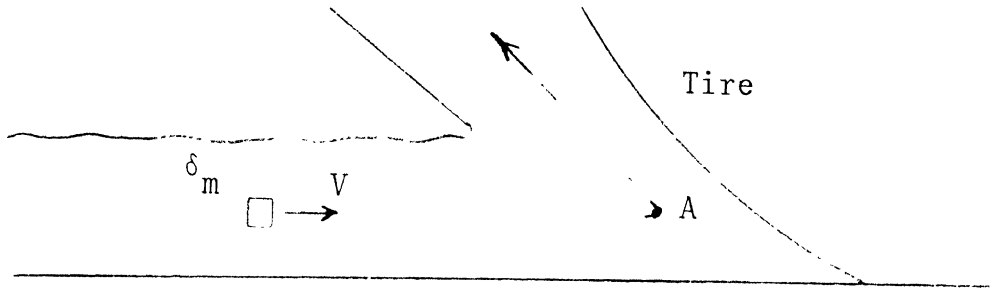

Figure 8. Streamline for application of the Bernoulli equation in the water wedge region.

*A water wedge will certainly exist if there is standing water above the surface asperities, and may form at lower depths as the tire tread will deform to partially fill surface voids and displace water from these voids.

The application of the Bernoulli equation to the flow along the streamline shown in Figure 8 requires that the stagnation pressure at point A be given by

$$P_A = 1/2\rho V^2 \tag{14}$$

where ρ is the mass density of water. The hydrodynamic pressure measurements of Horne and Joyner [2] tend to confirm the validity of eq (14) which is very similar to eq (6), a result obtained by a control volume analysis of the water wedge.

As mentioned earlier, the bending stiffness of the carcass and tread causes the contact pressure to deviate from a uniform distribution, usually producing higher pressure near the shoulders and lower pressure in the crown portion of the contact region. (Figure 9 illustrates a typical contact pressure distribution measured on an automobile tire.)

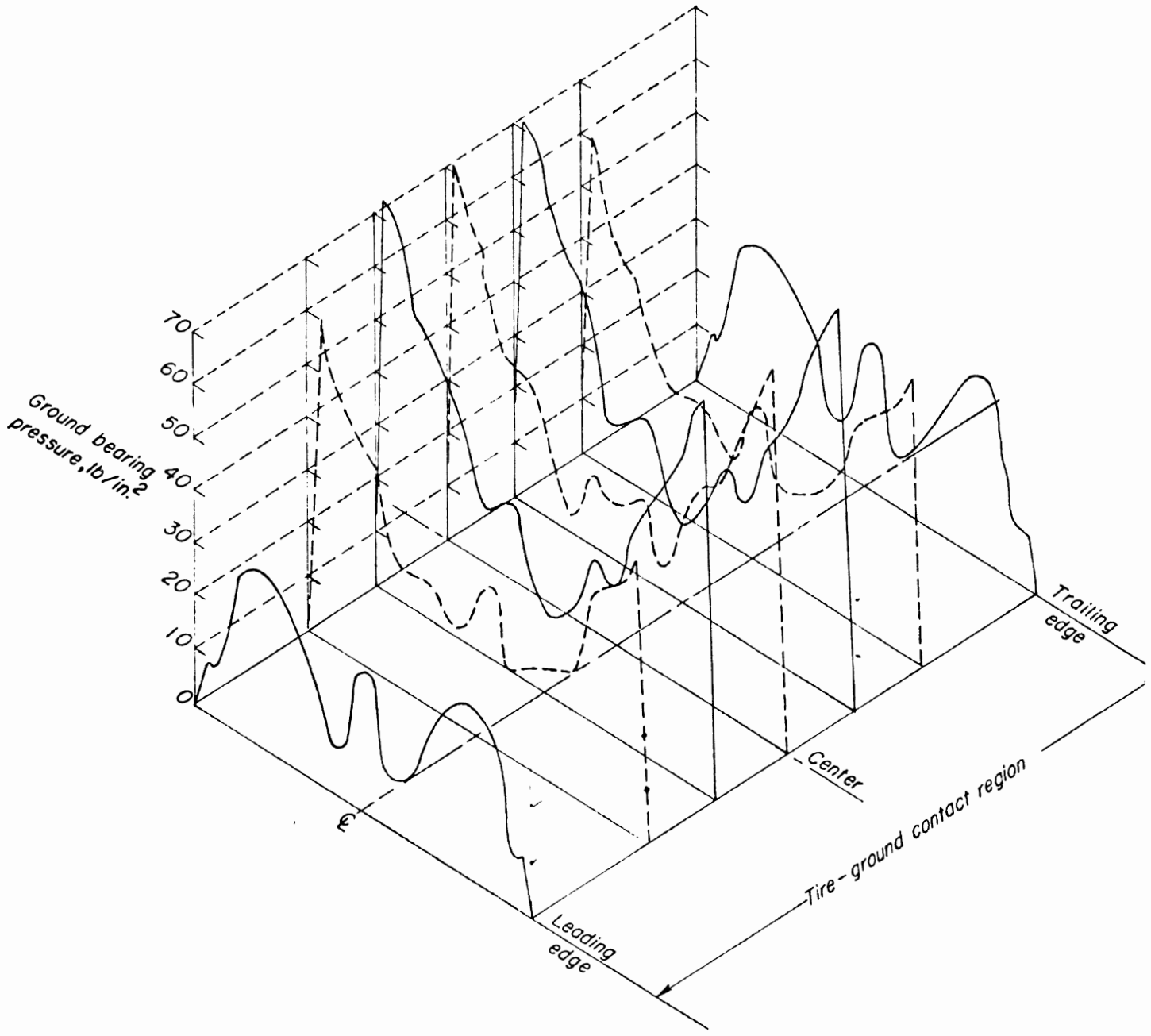

Figure 9. Standing contact pressure distribution for a 6.50-13 smooth tread passenger car tire. Tire load 835 lb; tire pressure 27 psi. From [2].

If the contact pressure on the tire equator at the leading edge of contact is estimated to be 75 percent of the inflation pressure, then, according to eq (14), squeeze-film penetration will be initiated when the speed, V, is such that

$$1/2\rho V^2 = .75\ P_i \ . \tag{15}$$

Letting V_p denote, in mph, the speed at which partial dynamic hydroplaning begins, eq (15) predicts (with $\rho = 1.938$ lb-sec^2/ft^4)

$$V_p = 7.2\sqrt{P_i} \tag{16}$$

where P_i is the inflation pressure expressed in psi.

Glass plate observations [3] tend to confirm the validity of eq (16) although the precise speed at which partial hydroplaning begins is difficult to determine visually. *

As speed increases, the stagnation pressure increases and tire deformation at the leading edge of contact accommodates the penetration of the squeeze film. The initial thickness of the squeeze film increases with increasing speed.

It has been observed [3, 25] that the squeeze film tends to first penetrate the central area of the contact region, while the sidewall regions remain in contact with the road surface. This observation is consistent with the measured contact pressure distribution shown in Figure 9, since it is expected that water would first penetrate those parts of the contact region where contact pressure is lowest. Thus, it appears that, with the penetration of the squeeze film, the tread surface in the contact region no longer conforms to the road surface but deforms upward in the central area of the contact

---

*Recent application of the Moiré fringe technique to the measurement of tire deformation during dynamic hydroplaning [25] shows that observation of Moiré fringes in the contact interface will facilitate visual determination of the speed at which partial dynamic hydroplaning is initiated.

region. Later in this document, it will be shown that this tread deformation has an important effect on the distribution of the hydrodynamic pressure supporting a hydroplaning tire.

Experiments with an automobile tire having a highway-type tread pattern have shown that, at the onset of total hydroplaning, the maximum of the minimum water film thickness in which hydroplaning occurs is about .05 inches and occurs in the central portion of the contact region [2]. It seems reasonable to expect that squeeze films which prevail under partial hydroplaning conditions are thinner than the maximum film thickness observed when total hydroplaning begins. Thus, in partial hydroplaning, tire deformation due to hydrodynamic pressure should be sufficiently small that the pressure available to squeeze a water film from beneath a tread element is essentially the dry-surface contact pressure. Hydrodynamic pressure measurements presented in Reference [2] support this assumption. It follows that an improvement in wet traction performance should accompany an increase in tire-road surface contact pressure. This can be accomplished in two ways.

1. The groove, or void, area can be increased, thereby decreasing the actual area of tire-road contact. The contact pressure for a given tire load will thus be increased.

2. The inflation pressure can be increased, thereby reducing the contact area and increasing the tire-road contact pressure.

Staughton and Williams [4] investigated the effect of inflation pressure on locked-wheel braking force coefficients produced by several tires operating in shallow and deep water on two smooth surfaces. Figure 10 shows some typical shallow-water data from this investigation. A definite reduction in speed sensitivity of the braking force coefficient is found when braking data from an overinflated (48 psi) tire is compared with braking data from the same tire (and the same load) in an underinflated condition.

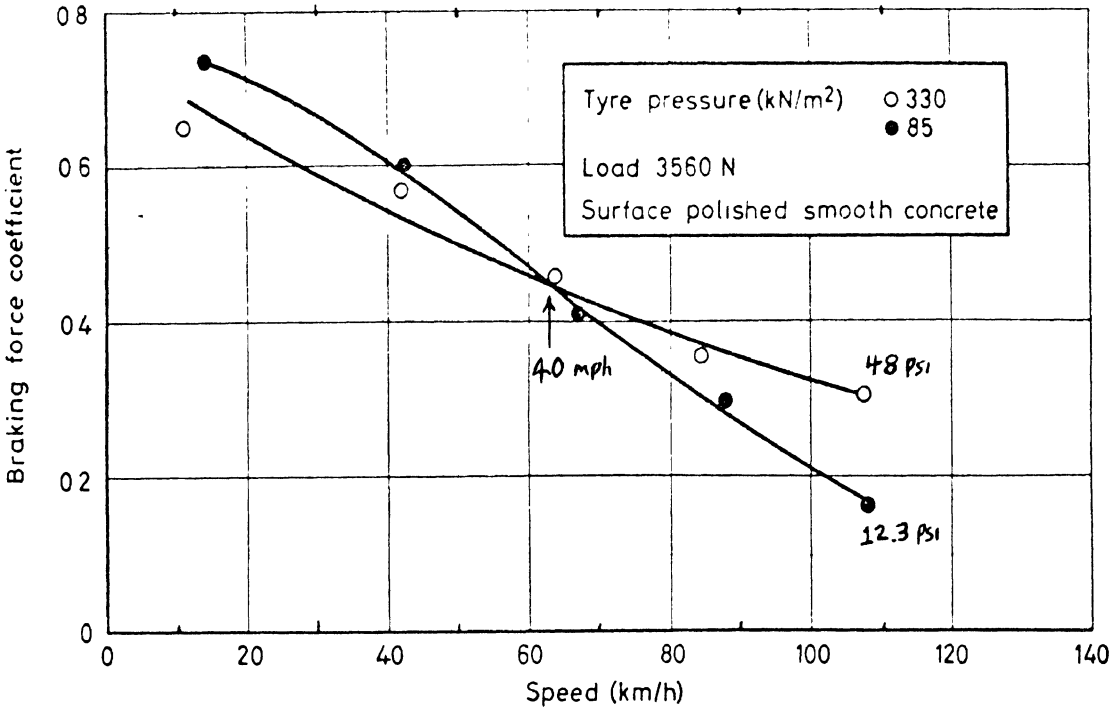

Figure 10. Effect of inflation pressure on locked-wheel braking force coefficients produced by a radial-ply automobile tire in shallow water (.03 in.). From [4].

The effect of inflation pressure seen in Figure 10 is small, however, in comparison to the effect of inflation pressure on braking force coefficients measured in deep water. Figure 11, also taken from [4], shows the effect of inflation pressure on locked-wheel braking force coefficients produced by a bias-ply automobile tire in deep water (.35 in.) on a smooth concrete surface.

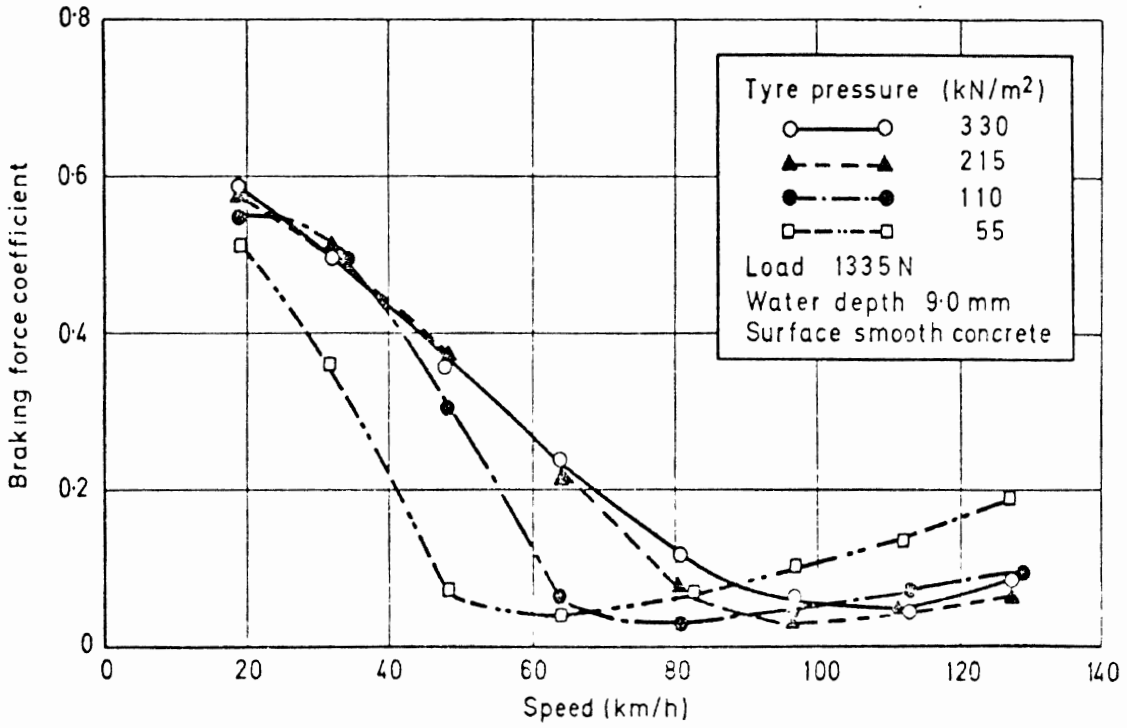

Figure 11. Effect of inflation pressure on locked wheel braking force coefficients produced by a bias-ply automobile tire in deep water (.36 in.). From [4].

The influence of surface on the speed sensitivity of braking force coefficients is seen in Figure 12 in which the difference between braking force coefficients at high (48 psi) and low (12.3 psi) pressures is plotted against speed. Each data point in Figure 12 is an average of data from four tires (two radial-ply and two bias-ply). These data show the asphalt surface to have a greater effect on the pressure sensitivity of braking force at speeds above and below a "cross-over" speed found at approximately 47 mph. At the cross-over speed, the asphalt and the concrete surfaces produced braking force coefficients which are insensitive to inflation pressure.

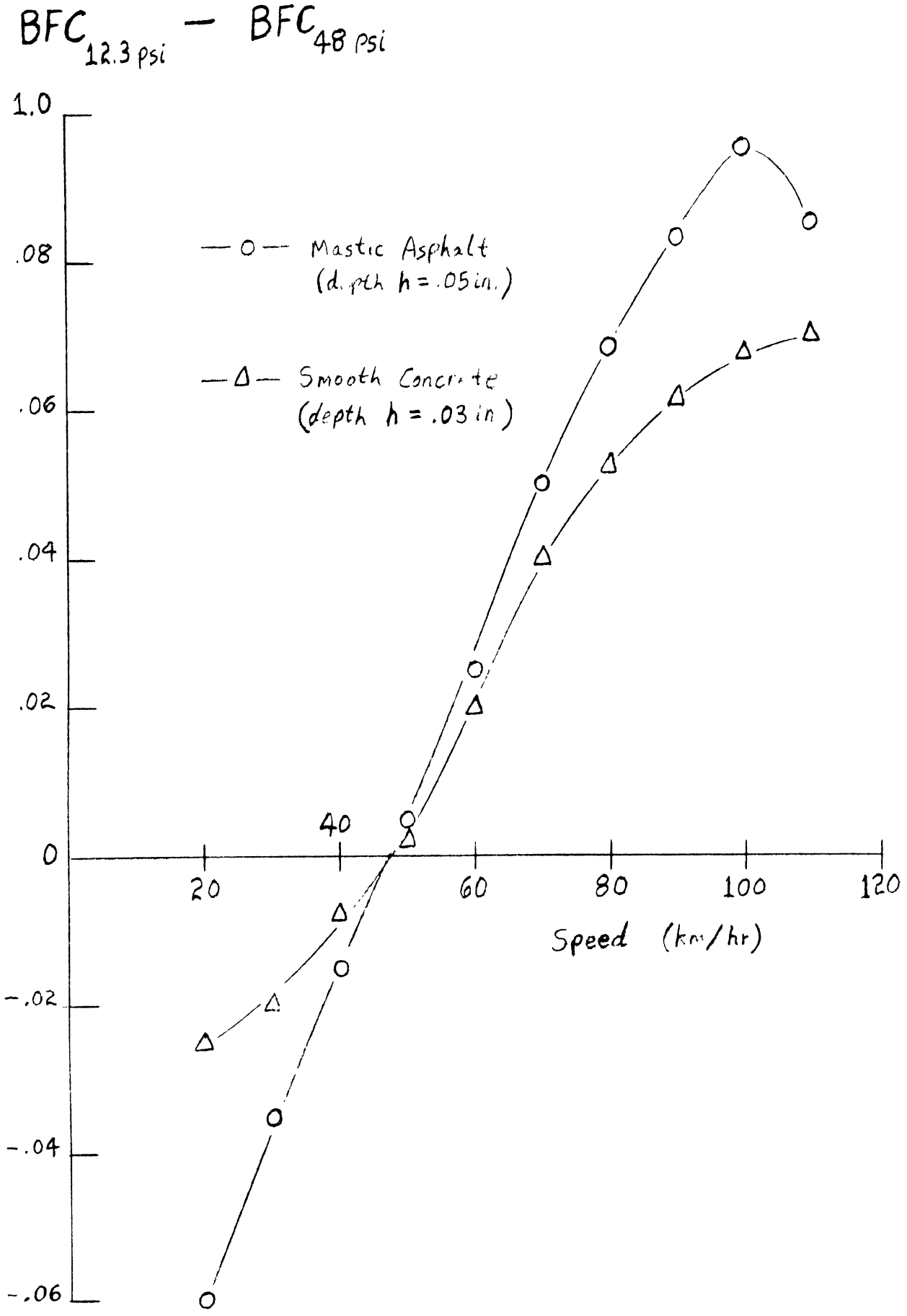

Figure 12. Effect of inflation pressure on locked-wheel braking force coefficient data obtained in shallow water on two paved surfaces. Plot constructed from data in [4]. Averaged data from 4 tires.

The effects of inflation pressure on the braking coefficient data shown in Figures 10, 11, and 12 are consistent with the squeeze film concept in the following two ways.

1. A comparison of Figures 10 and 11 shows that the effect of inflation pressure is much smaller in shallow water than in deep water. In shallow water on a given surface, the fraction of the contact patch supported by a water film will be inversely proportional to contact length* and contact pressure**. An increase of inflation pressure, while increasing contact pressure, decreases the contact length. The net effect of inflation pressure increases should, therefore, be small, as seen in Figure 10. A different, pressure-sensitive, mechanism exists in deep water, where the additional hydrodynamic pressure resulting from groove flow tends to retard squeeze film expulsion and causes an additional loss of friction.

2. The data in Figure 10 shows that at low speeds, in shallow water, an increase in inflation pressure results in a decrease in braking force, while at high speeds (above approximately 40 mph) braking force is increased. Rubber friction studies have shown that an increase in normal contact stress results in a decrease of the friction coefficient. A decrease in braking force is therefore expected when inflation pressure is increased at speeds below the speed at which partial hydroplaning begins. Equation (16) shows that the speed at which squeeze film penetration begins, i.e., partial hydroplaning, depends upon the inflation pressure; an underinflated tire shows reduced brake force capability at speeds

---

*A shorter contact length results in less time available for squeeze film expulsion. Thus, for a given velocity, the squeeze film fraction increases if contact length is decreased by means of a decrease in tire load or an increase in inflation pressure.

**A lower contact pressure results in a lower rate of water expulsion.

below the speed at which an overinflated tire will begin to lose brake force capability. The average cross-over speed seen at approximately 47 km/hr in the shallow-water data (Fig. 12) is, then, determined by a combination of two factors: (a) the dependence of rubber friction on inflation pressure, and (b) the dependence of the partial hydroplaning initiation speed on inflation pressure. The cross-over speed is bounded from below by the partial hydroplaning initiation speed of the low-pressure tire calculated from eq (16).

Inflation Pressure		V_p from eq (16)
(underinflated)	12.3 psi	40.6 km/hr
(overinflated)	48.0 psi	79.9 km/hr

For the underinflated tire (12.3 psi) tested by Staughton and Williams, the lower bound (40.6 km/hr) compares well with the average cross-over speed of 47 km/hr found in the shallow-water tests.

Tread Pattern Effects. The primary effect of the tread pattern is to reduce the size of the squeeze film in shallow water. In addition to reducing the actual contact area (and thus the lateral dimensions of the squeeze film), the grooves provide a low-pressure squeeze film boundary and a reservoir for the water being squeezed out from beneath a tread element. In shallow water, hydrodynamic pressures due to water flow through the grooves are not present because such flow occurs only when there is a sufficient water layer on the road to fill or "flood" the grooves. These considerations have led a number of researchers to perform experiments in which the effect of groove geometry on wet traction performance is studied.

Grime and Giles [7] tested several tires having smooth, straight rib, zig-zag rib, and various block-type tread

patterns. The test data were analyzed to yield locked-wheel braking force coefficient as a function of a dimensionless tread pattern parameter defined as

$$\frac{\text{perimeter of contact area}}{\sqrt{\text{contact area}}}$$

The resulting correlation, displayed in Figure 13, suggests that this parameter, or a related parameter, may be utilized as a meaningful descriptor of tread pattern geometry.

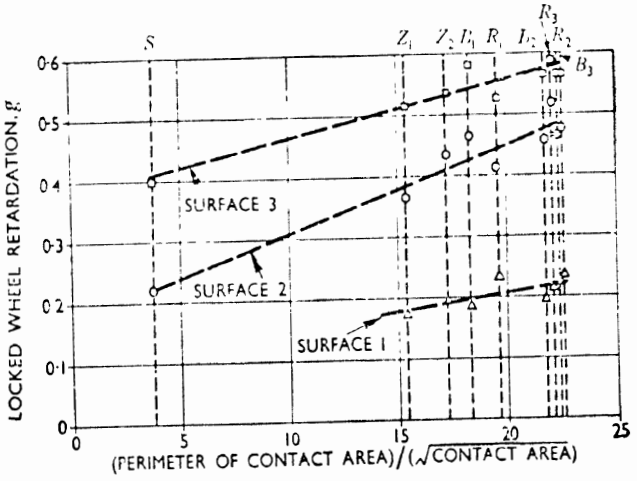

Figure 13. Correlation of locked wheel braking force coefficient with a dimensionless tread pattern descriptor. From [7].

Maycock [5] has measured both the peak and locked-wheel braking force coefficients (BFC) produced by tires with five different tread patterns, viz, a smooth tread and treads with 5, 7, 9, and 13 ribs. The rib treads had straight grooves with groove width varied such that the ratio of groove width to rib width was the same for all four tires. The tread pattern dimensions of the ribbed tires are listed in Table 1.

TABLE 1

TREAD PATTERN DIMENSIONS USED IN THE RIB WIDTH EXPERIMENTS OF MAYCOCK [5]

Number of Ribs	Groove Width (in)	Rib Width (in)	$\frac{\text{Groove Width}}{\text{Rib Width}}$	Groove Depth (in)	Groove Capacity* (in)
5	.28	.90	.31	.32	.095
7	.20	.65	.31	.32	.095
9	.16	.52	.31	.32	.095
13	.12	.36	.33	.32	.095

*Groove capacity, g, is defined as groove volume per unit gross contact area.

The water depth prevailing in these tests was roughly .035 in., so that the tread pattern parameter, γ_1, defined by eq (13), is nearly 3 and groove flow need not occur for the free-rolling tire to make contact with the road surface.

Maycock performed braking tests on six road surfaces having a wide variety of textures. Differences in peak braking performance of the four rib-type tires were detected only on the smoothest test surface. On this surface, the 5-rib tire showed a somewhat greater rate of decrease of BFC with increasing speed (Fig. 14).

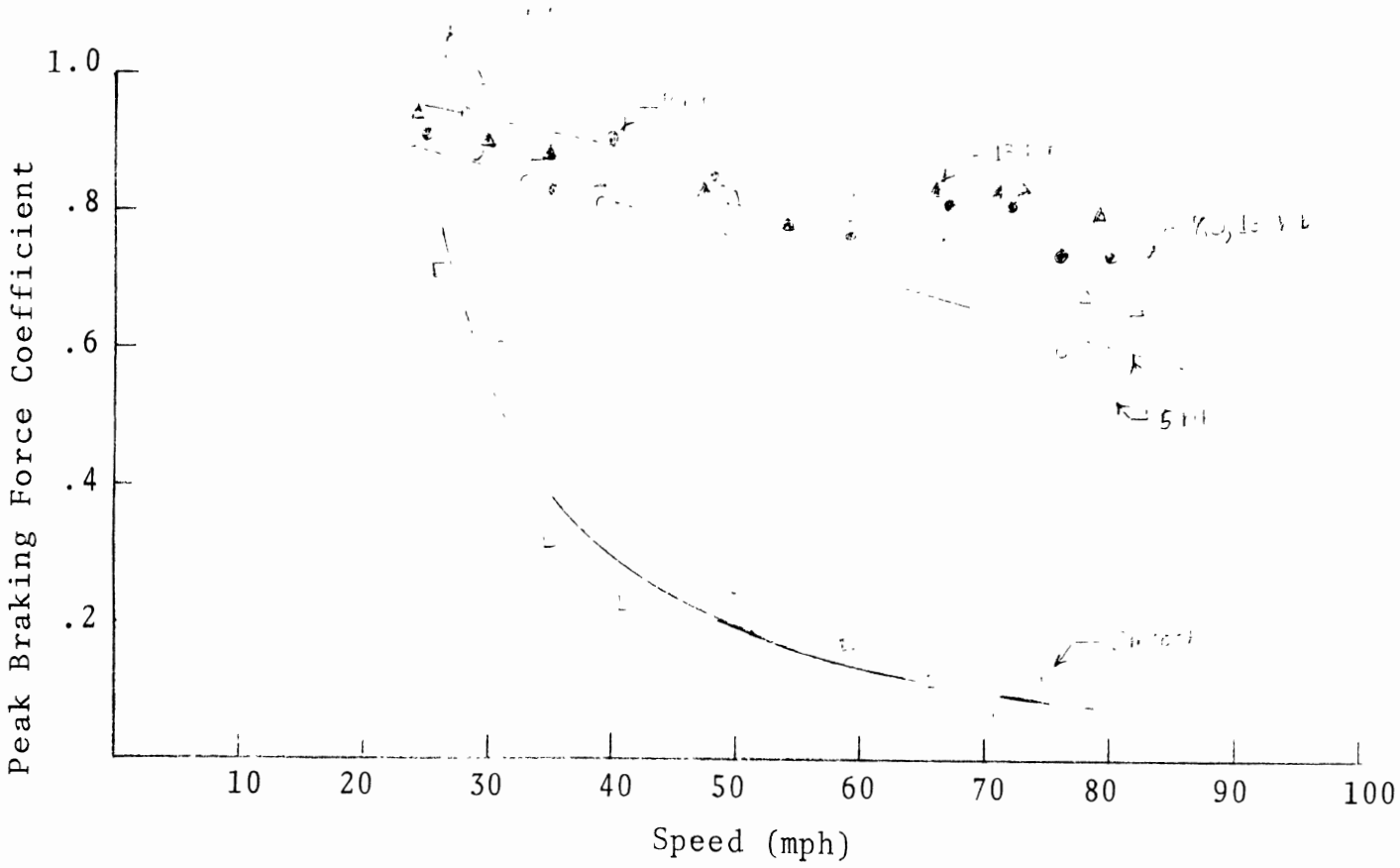

Figure 14. Peak braking force coefficients for smooth, 5,7,9, and 13-rib tires on smooth, polished concrete. Water depth about .035 in. From [5].

Since these tests were performed at speeds up to 80 mph, it is quite likely that partial hydroplaning occurred on the smooth, polished concrete surface.

Maycock attributes the decrease in BFC with increasing speed of the 7,9, and 13-rib tires to thin-film viscous-lubrication effects. The greater decrease seen with the 5-rib tire is attributed to partial hydroplaning produced by penetration of a thick squeeze film into the contact region. The thick squeeze film penetration theory, described earlier, is supported by the fact that on the other three test surfaces, which are sufficiently coarse in texture to provide good drainage and perhaps prevent the formation of a water wedge, the rate of decrease of BFC with speed is

the same for all the patterned tires. It might be concluded that on even the smoothest highway surfaces likely to be encountered, there is little advantage in having a rib width less than that of the 7-rib tire (about .65 in.). It appears that the expulsion of a squeeze film from beneath a rib of width less than .65 in. is sufficiently rapid that partial hydroplaning does not occur to a significant extent at typical highway speeds and in water depths most commonly encountered.

The results of Maycock's investigations lead to another interesting observation concerning the speed sensitivity of peak brake force coefficients in comparison with locked-wheel brake force coefficients. On all surfaces, the locked-wheel braking force produced by tires with good drainage decreases faster with increasing speed than peak braking force decreases with increasing speed. The opposite result was found with poorly drained and smooth tread tires. Other investigators have also noted that a tread pattern is more effective in maintaining high values of peak force as speed increases than is the case for locked-wheel braking forces.

The finding that a tread pattern is less effective in maintaining high locked-wheel braking force can be explained, in part, by hydrodynamic considerations. In shallow water, a rolling tire displaces water into the grooves which serve only as a temporary water reservoir. The grooves also provide a low-pressure boundary (approximately atmospheric level) for squeeze films existing beneath adjacent ribs. Peak braking force is generated at longitudinal slip parameter* values in the neighborhood of .1 to .25. When the wheel is locked, however, all water entering the contact region must be displaced to the contact periphery—a process which necessitates

---

*Considering a longitudinal slip parameter defined such that 0 corresponds to free-rolling and 1 corresponds to a locked wheel.

groove flow. The groove flow, which accompanies locked-wheel braking, requires a pressure gradient raising groove pressure to above atmospheric level. The resulting elevated pressure at the squeeze-film boundary retards the rate of displacement toward the groove, thereby reducing tire-road friction. Since groove flooding is inevitable (unless the water depth is extremely small) in locked-wheel braking, the configuration of the tread pattern may be expected to have little influence on the generation of locked-wheel braking force.

Maycock also performed similar experiments (on the same surfaces, with the same wetting conditions and speeds) using tires on which groove widths are varied while rib width is kept constant. The tread pattern dimensions for this series of experiments are listed in Table 2 and test results obtained on the smooth, polished concrete are shown in Figure 15.

TABLE 2

TREAD PATTERN DIMENSIONS USED IN THE GROOVE WIDTH EXPERIMENTS OF MAYCOCK [5]

Number of Ribs	Groove Width (in)	Rib Width (in)	$\frac{\text{Groove Width}}{\text{Rib Width}}$	Groove Capacity* (in)
5	.02	.50	.04	.013
5	.10	.51	.20	.063
5	.215	.49	.44	.142
5	.29	.52	.55	.173
5	.36	.54	.67	.211

*Groove capacity, g, is defined as groove volume per unit gross contact area.

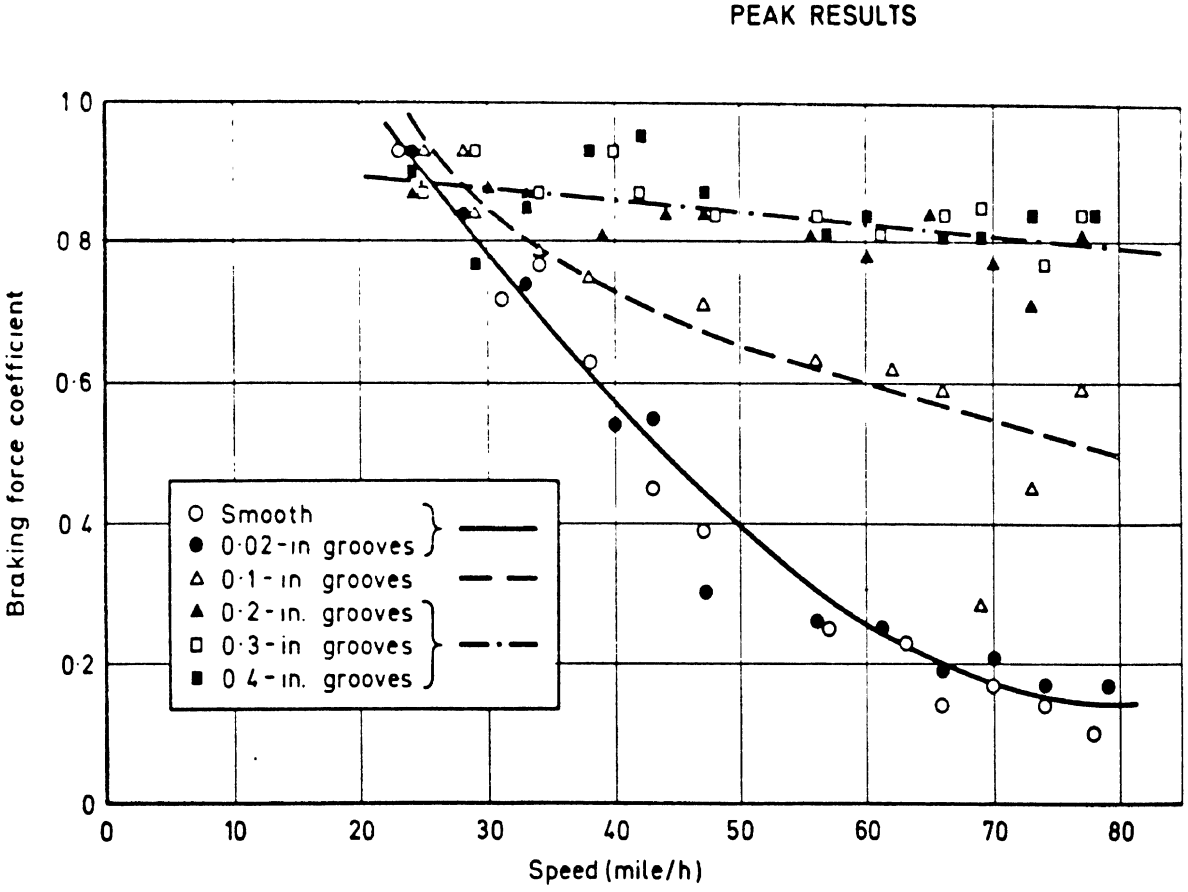

Figure 15. Peak braking force coefficients for smooth and rib-type tires, each having 5 ribs and grooves of various widths. Smooth, polished concrete. Water depth approximately .035 inches. From [5].

The data shown in Figure 15 indicate that there is a critical groove width, above which there is no further improvement in shallow-water traction performance. For the conditions prevailing in these experiments, the critical groove width appears to be somewhere between .1 and .2 inches.

Figure 16 shows similar results found on a coarse textured asphalt surface—a surface very different from the one on which the data shown in Figure 15 were obtained. Although the critical groove width appears to be independent of surface texture (at least for these test conditions), the coarse-textured surface shows a smaller loss of friction capability with groove widths below the critical value.

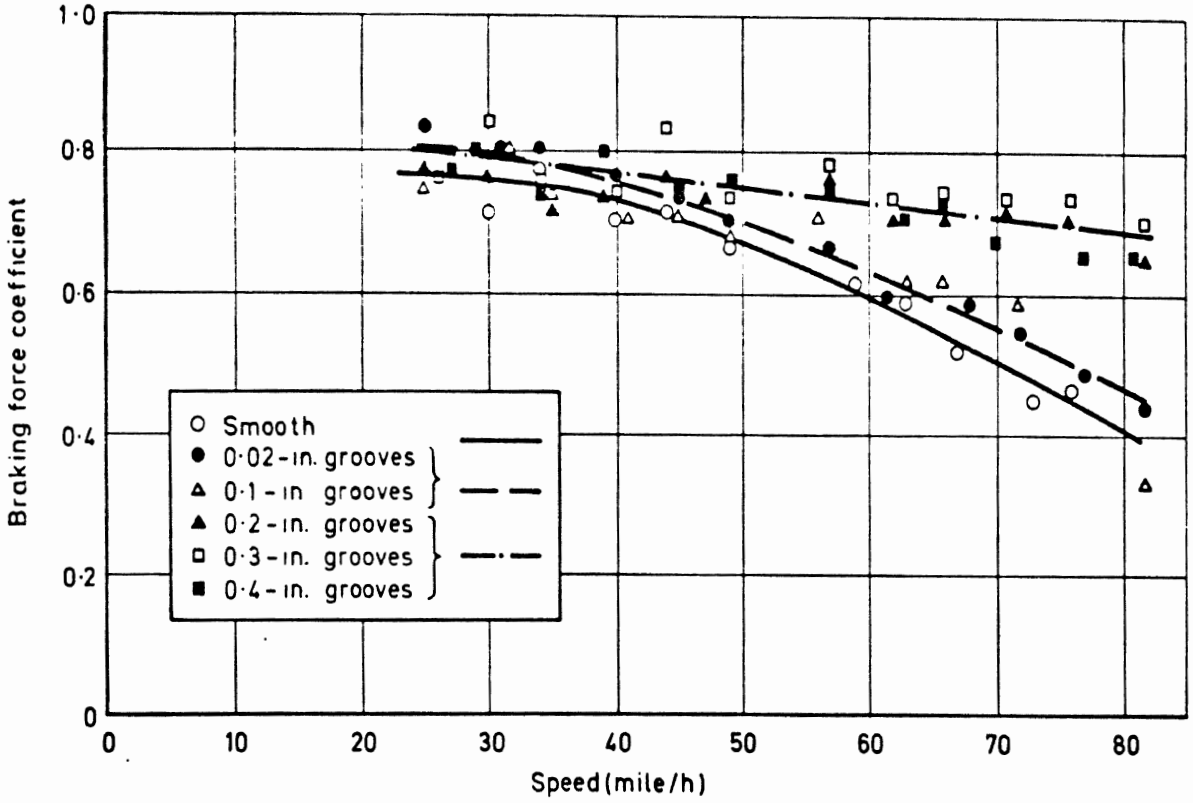

Figure 16. Peak braking force coefficients for smooth and rib-type tires, each having 5 ribs and grooves of various widths. Coarse, textured, asphalt. Water depth about .035 inches. From [5].

For the groove width experiment described above, the same amount of water was applied to all test surfaces and all test tires had the same groove depth. No data was obtained on the effect of water depth, or groove depth, on critical groove width.

Gengenbach [9] performed experiments to study the effect of water depth on the maximum cornering friction coefficient obtained in a wetted internal drum laboratory test device. Straight-rib tires, for which the ratio of groove area to gross contact area was varied by changing the groove width, were tested in three water depths. The Gengenbach experiments were thus similar to those of Maycock except that, by use of the internal drum device, water depth can be carefully

controlled and accurately measured. The results, shown in Figure 17, indicate that the critical groove width increases with increasing water depth.

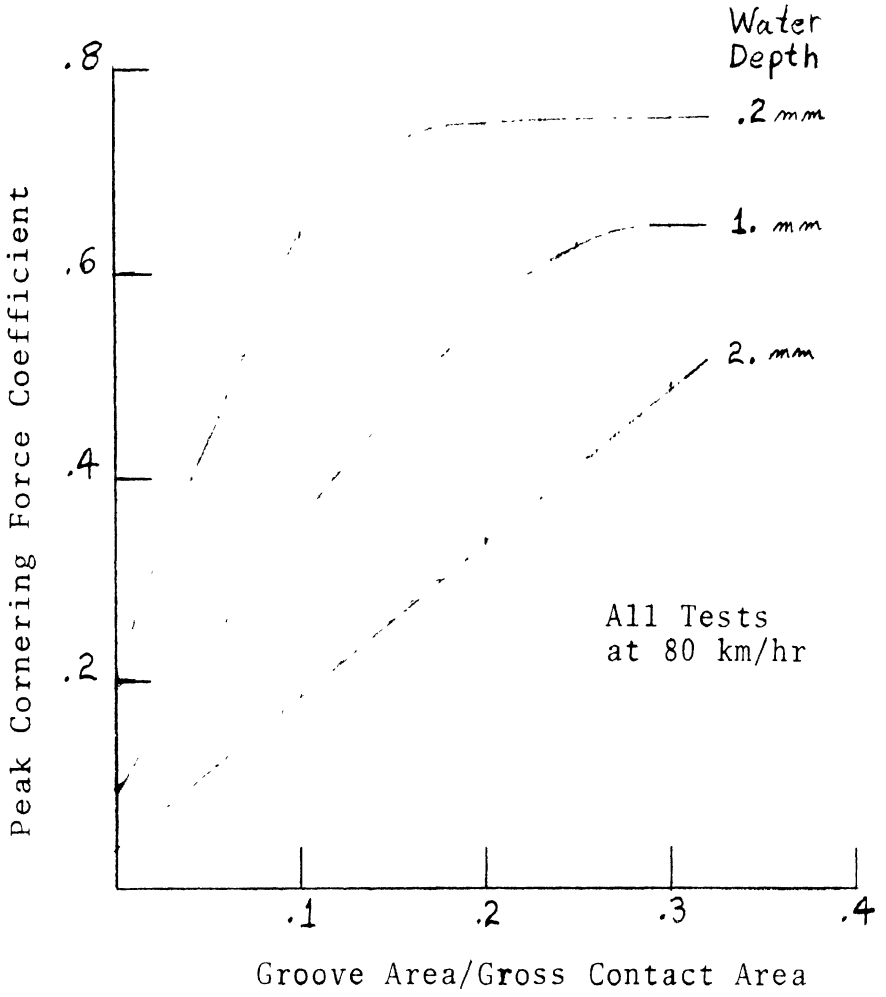

Figure 17. Effect of the ratio (groove area)/(gross contact area) on maximum cornering friction coefficient obtained at the indicated water depths. From [9].

The effect of tread wear has been investigated at the Road Research Laboratory by Staughton [10]. A pair of high-way-type automobile tires with four zig-zag circumferential grooves and sipes, opening into the grooves, was tested for

peak and locked-wheel braking force coefficients at three speeds (50, 80, and 130 km/hr) on six different surfaces. The grooves were initially 8.4 mm deep. Tread wear was obtained by normal driving and tires were tested at 5000 km intervals until the tread had worn to a groove depth of 2 mm. The braking tests were then continued at 500 km intervals until the tires were smooth.

The peak braking friction coefficients obtained on two smooth-textured surfaces are shown in Figure 18. The 50 km/hr data exhibit a definite break point on both surfaces shown in Figure 18. Braking force decreases very rapidly with decreasing groove depth beyond the break point, or critical groove depth, which appears to depend on water depth. (Since both surfaces are smooth-textured, they may be expected to show similar drainage capabilities.)

The 80 and 130 km/hr data shown in Figure 18 do not exhibit well-defined break points, possibly because, at higher speeds, the drainage provided by the sipes becomes important. At low speeds, drainage by the main grooves is adequate—provided the grooves exceed the critical groove depth.

The data of Maycock, Gengenbach and Staughton, reviewed above, clearly show that groove width, groove depth, and water depth are somehow interrelated with respect to wet traction performance. The dimensionless parameter, γ_1, defined earlier as the ratio of groove capacity, g, to water depth, h, (eq (13)),

$$\gamma_1 = \frac{g}{h} \tag{13}$$

contains all three of these factors. It thus is reasonable to expect that experimental data on the effects of groove width, groove depth, and water depth from separate investigations

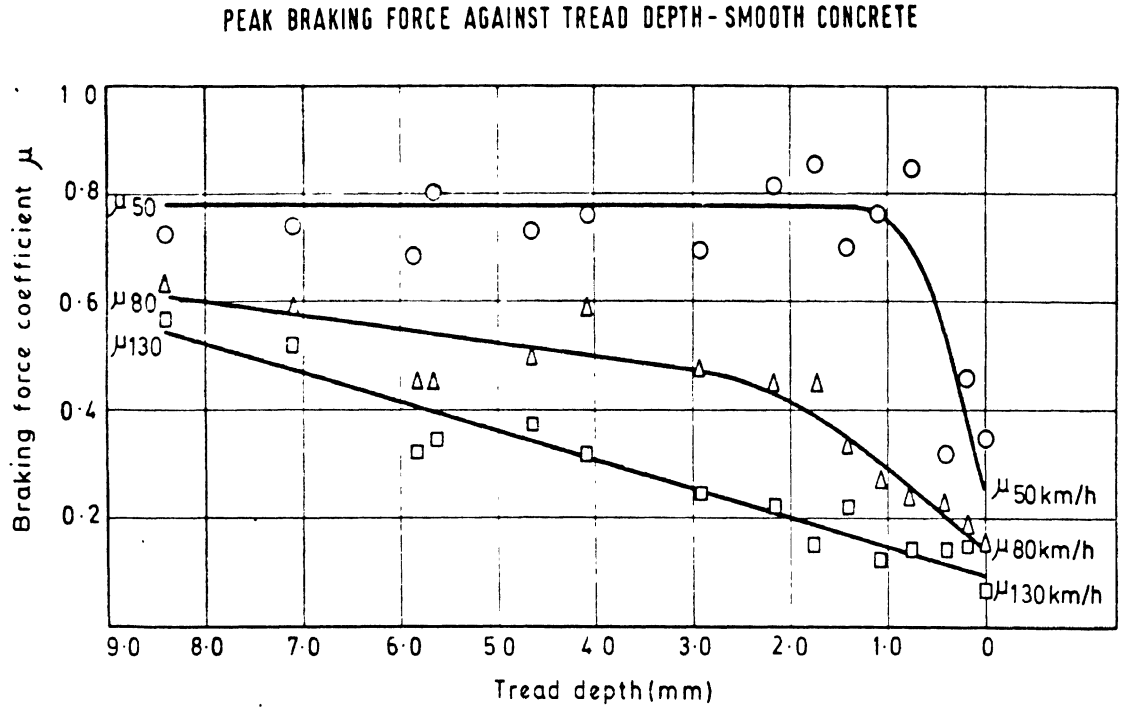

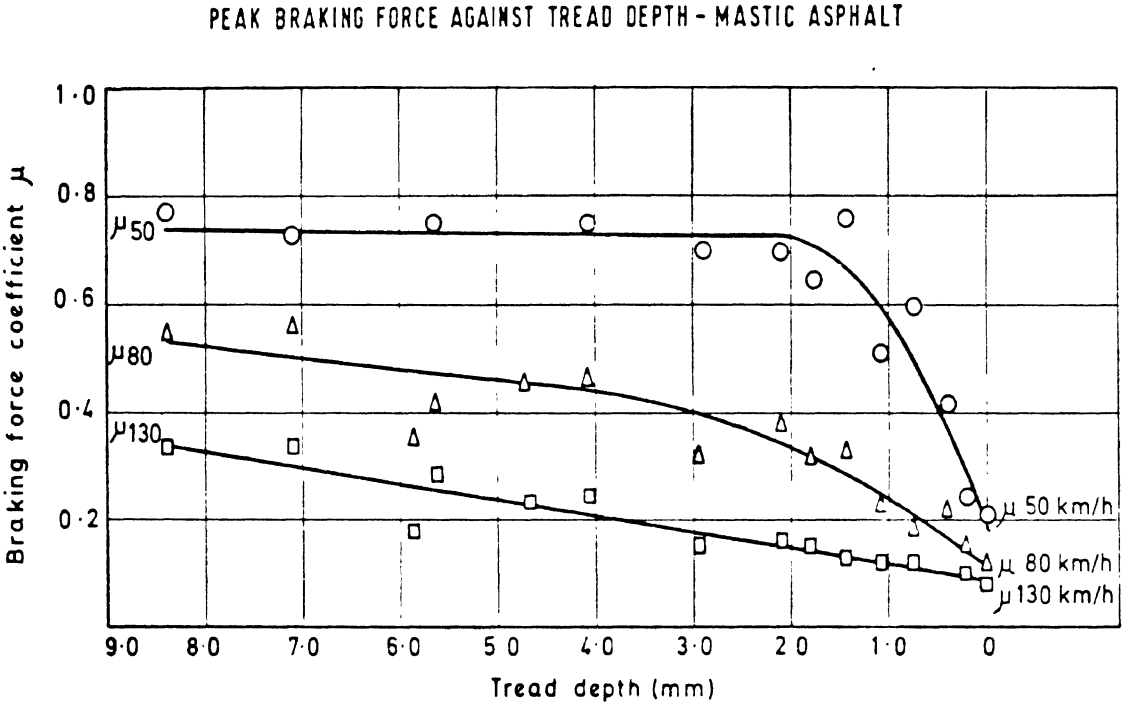

Figure 18. Effect of tread wear on peak braking friction coefficient measured on two smooth-textured surfaces with average texture depth of .1 mm (sand patch measurement). From [10].

could be correlated by using the parameter γ_1. In practice, however, this is rarely possible because researchers seldom describe their test tire treads in sufficient detail to enable one to evaluate g and because there has been no standard procedure used for measuring water depth.

In the case of Maycock's groove width experiments, the values of g can be easily computed and are listed in Table 2. The value of water depth, held constant in these experiments, is subject to some uncertainty but is stated to be .02-.04 inches. Figure 19 shows peak braking force coefficients, measured by Maycock, plotted against γ_1, computed with an assumed water depth of .03 inches.

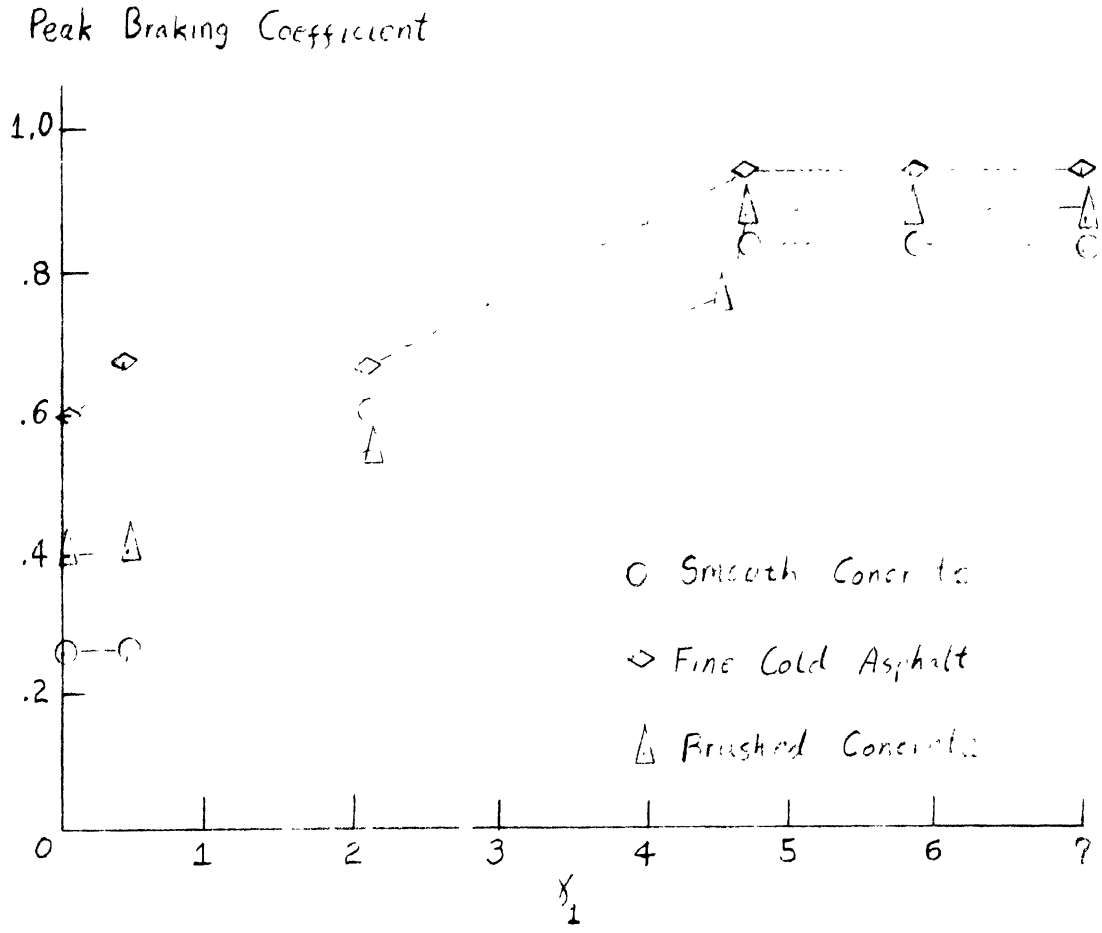

Figure 19. Peak braking force coefficient vs. γ_1 for straight-rib tires on three surfaces. Rib width, groove depth, and water depth held constant. Groove width varies from .02 to .36 inches. Data from [5].

The small quantity of data used in constructing Figure 19 is insufficient to permit definite conclusions to be drawn concerning the usefulness of the parameter, γ_1. Moreover, in Maycock's experiments, only groove width was varied. However, the data in Figure 19 appears to indicate that when tire and surface conditions are such that γ_1 drops below about 4.0, a definite decrease in wet braking friction may be expected in shallow water.

Surface Texture. Pavement surface texture facilitates the removal of the squeeze film by providing drainage passages that remain open even when the tire makes contact with the surface asperities. It is well known that, if surface texture is sufficiently rough (macrotexture), a smooth tire will perform at least as well as, and sometimes better than, a patterned tire. Testing for tread pattern effects should therefore be done on surfaces having a negligible macrotexture so that tread pattern drainage effects will dominate. However, the test surface should have a harsh microtexture to provide a high initial (low speed) friction while providing very little drainage.

2.2.3 INTERMEDIATE WATER DEPTHS. The preceding sections have examined tire behavior at the two extremes of wet traction performance: in shallow water where groove flow does not occur, and in deep water where groove flow must occur. Some profound differences in tire hydroplaning behavior were noted: in particular, the rapid loss of friction capability which occurs in deep water as the hydroplaning speed is approached does not occur in shallow water (see Fig. 7). To explain these differences in tire behavior, the influence of groove flow on the squeeze film process in intermediate water depths is considered below.

Groove Flow Effects. Glass plate observations [3] show that partial hydroplaning due to penetration of a squeeze film into the contact region occurs in deep water in much the same manner as in shallow water. In deep water, however, as the total hydroplaning speed is approached, the water film is observed to spread rapidly throughout the contact region, producing an equally rapid loss of friction capability. It is also well known that total hydroplaning occurs at a much lower speed in deep water than in shallow water. This phenomenon, viz, the abrupt onset of total hydroplaning in deep water, can be explained by consideration of the hydrodynamic pressure developed in the tread grooves, which are flooded at all speeds in deep water.

It was stated previously that a primary function of the tread grooves is to provide a low pressure boundary to the squeeze film trapped beneath the tread ribs. If the grooves are not flooded, as is the case in shallow water, atmospheric pressure prevails as the low-pressure boundary to the squeeze film. In deep water, groove pressure increases in order to motivate the flow of water.

Horne and Joyner [2] have measured hydrodynamic pressures in the grooves and beneath the tread ribs of an aircraft tire having straight, circumferential grooves. The pressures found in the center groove and beneath an adjacent rib are shown as a function of speed in Figure 20. Distributions of pressure over the contact length are shown in Figure 21, taken from [2]. The data in Figure 20 show that as speed increases, groove pressure builds up and the difference in pressure between groove and rib decreases.

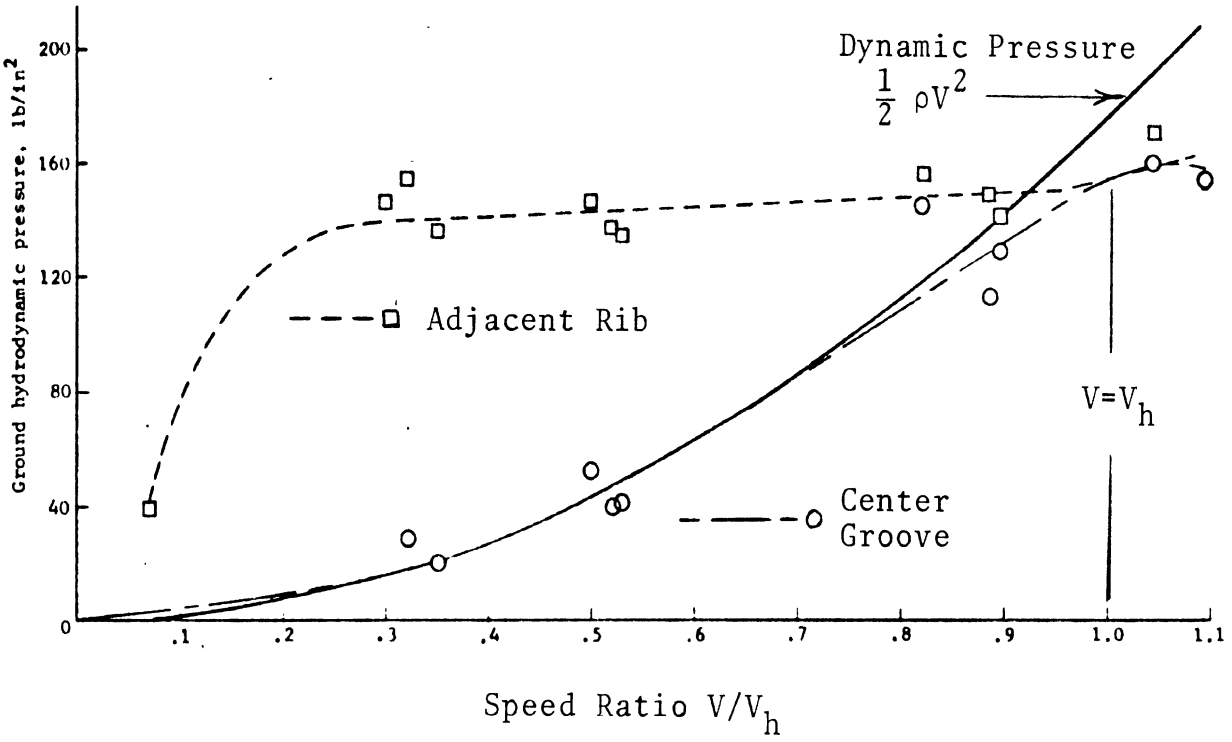

Figure 20. Speed sensitivity of hydrodynamic pressure in center groove and beneath an adjacent rib. Water depth about 1 inch. From [2].

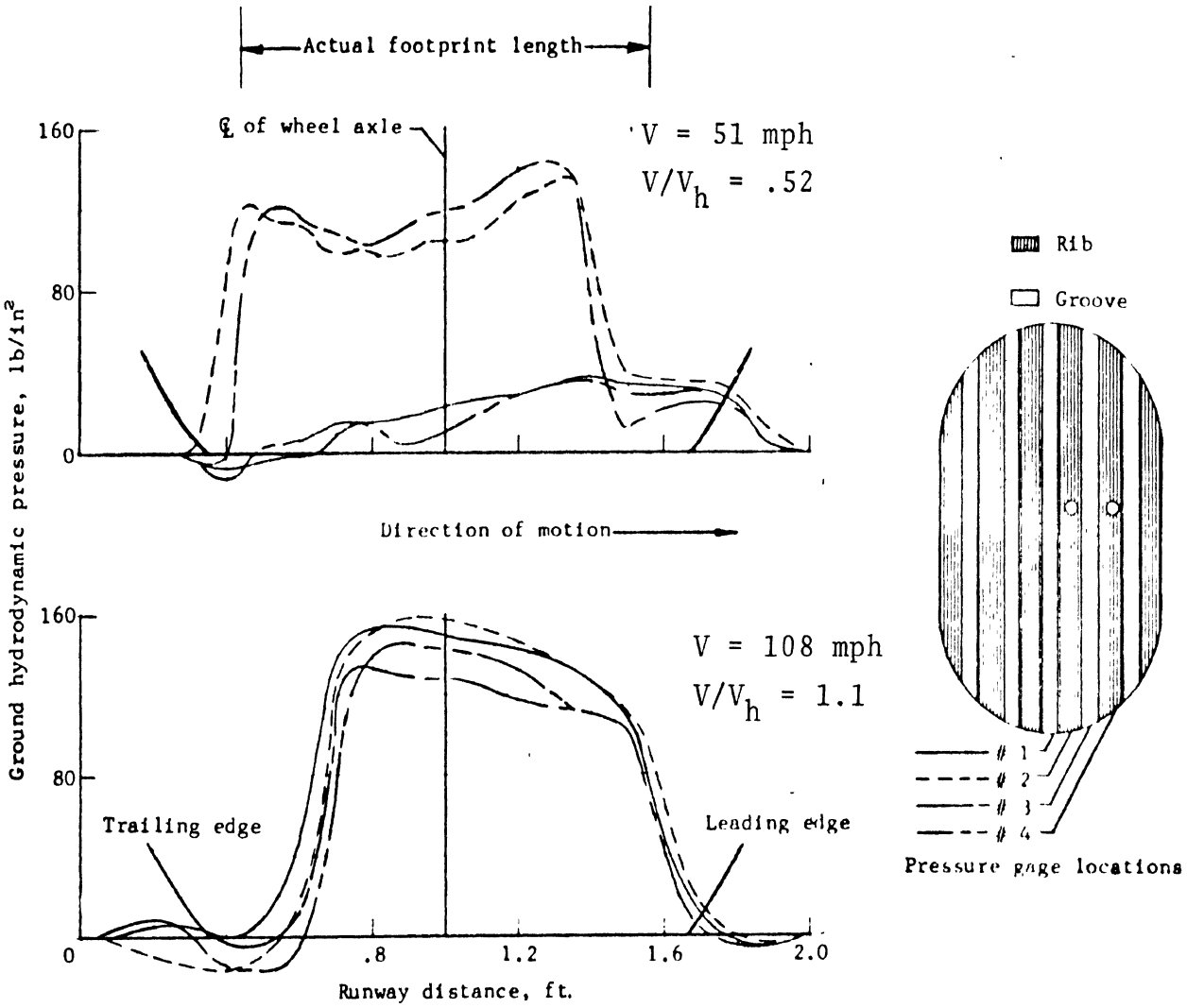

Figure 21. Typical hydrodynamic pressure distributions for a 32 x 8.8 type VII aircraft tire. Water depth about 1.0 inches. From [2].

Since the rate of squeeze film expulsion from beneath the rib depends on the groove-rib pressure difference, it follows that the build-up of groove hydrodynamic pressure will inhibit squeeze film expulsion and result in more of the contact region being supported by a water film than would be the case at the same speed in shallow water.

At a certain speed, groove pressure becomes equal to the pressure on the squeeze film beneath the ribs. At this speed, the grooves are said to be "choked" and no longer provide a low-pressure boundary for the squeeze film beneath a rib. A further increase in speed cannot increase the groove flow rate so the water entering the contact region is accommodated by separation of the tire from the road surface. The groove choke speed is also the speed of total dynamic hydroplaning.

Critical Water Depth. At this point, two questions naturally arise: (1) how does hydroplaning occur in intermediate water depths, and (2) how thick must the water film be in order that the statements regarding deep-water hydroplaning are valid?

Staughton and Williams [4] have measured spin-down speed and locked-wheel braking force coefficients for several production tires in various water depths on a smooth concrete surface. The results of the spin-down tests are shown in Figure 22. For all but one of these tires, an increase of water depth above about 5 mm (.20 in.) has no effect on the hydroplaning speed. Tire 1, which maintained friction capability in deeper water than the other tires, is a radial-ply tire with an open tread pattern which contains transverse grooves. Tires 2 and 3 have standard, highway-type patterns; tires 4 and 5 have no effective pattern.

Figure 23 shows the influence of water depth on the speed sensitivity of locked-wheel braking force coefficients. Moderate water depths (.06-.16 in.) are found to have a significant influence on braking performance, while increasing the depth from .16 inches to .40 inches has very little effect. Horne [1] conducted a similar water depth study using a 6.70-15 bias-ply, rib-tread, automobile tire and found that increasing water depth caused a decrease in friction coefficient up to a depth of about .2 inches and no further loss of friction occurred at a water depth of .3 inches. It appears that, for a typical patterned automobile tire, most of the loss of friction capability, as water depth increases, occurs in depths below a film thickness of .16-.20 inches. The experimental data appear to exhibit a definite water depth, above which no further loss of tire-road friction will occur. This level is called the "critical water depth" and may be viewed as a lower bound to the water depths in which deep-water hydroplaning phenomena will occur.

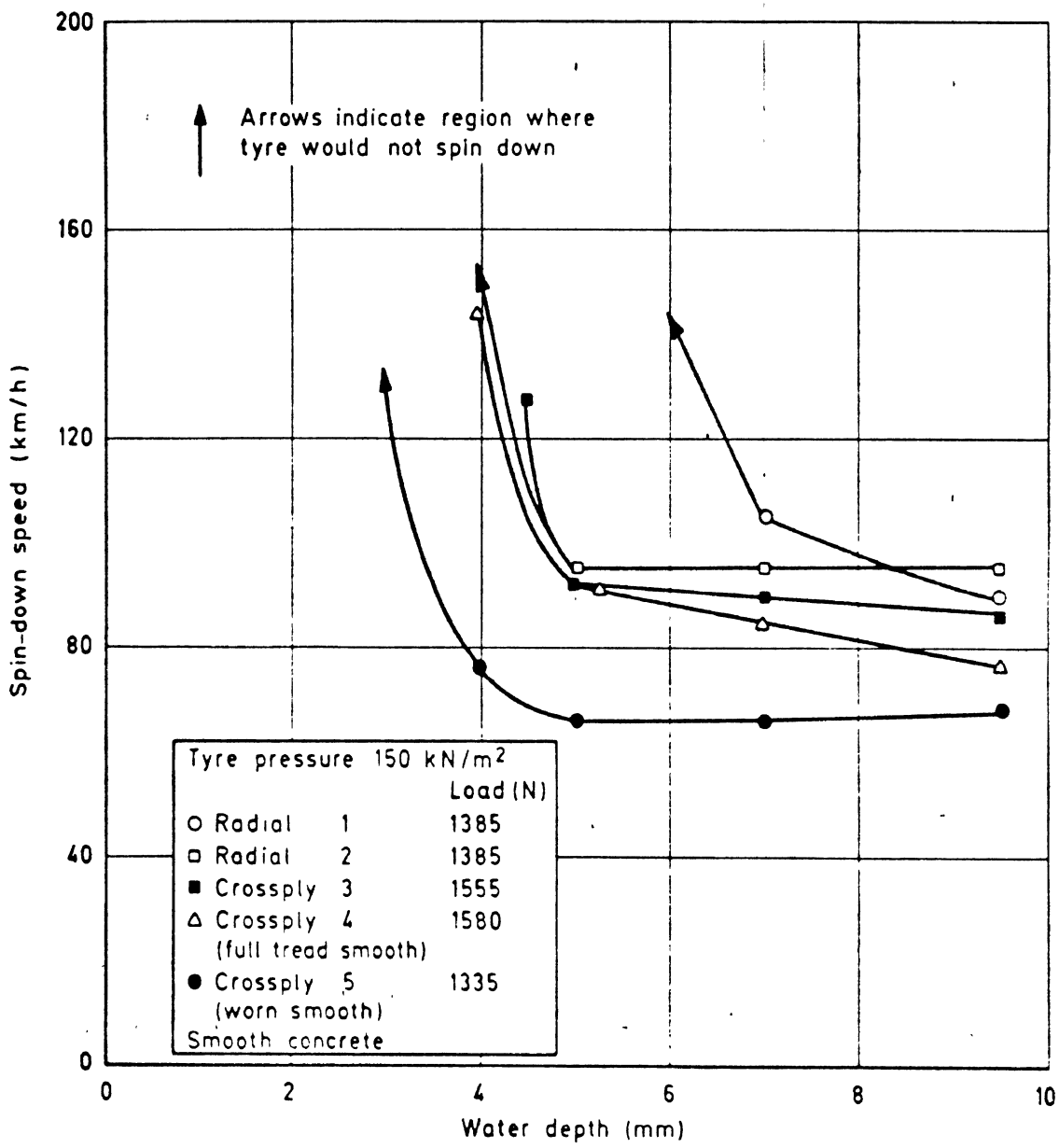

Figure 22. The effect of water depth on hydroplaning speed.

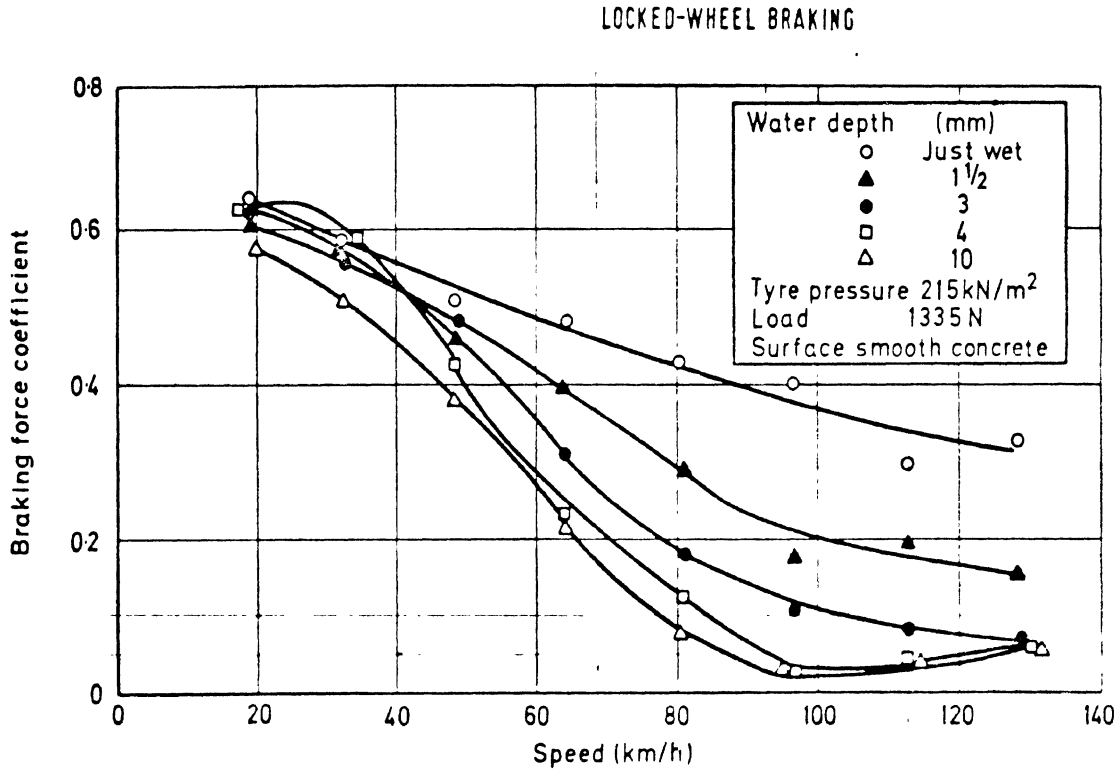

Figure 23. Effect of water depth on locked-wheel braking coefficients. Fully patterned bias-ply tire. From [4].

If it is assumed that the test tires had an average groove capacity, g, of roughly .08 inches (a value which is typical for highway-type passenger car tires), then it may be speculated that deep-water hydroplaning conditions prevail if the parameter $\gamma_1 = g/h$ is less than .5. There is, at this time, no experimental substantiation of this value, since water depth studies have not been performed on tires having tread patterns which exhibit a broad range of groove capacities.

It has also been suggested that the critical water depth is equal to the average groove depth, but there is insufficient experimental data to substantiate this. Such substantiation would result from an experimental study of the effect of water depth on the braking forces produced by several tires having different groove depths but equal groove capacities.

It has been experimentally established that, at a certain speed, the grooves of a tire traveling through deep water become "choked" when groove flow rate is such that groove pressure equals the tire-road contact pressure. It is reasonable to expect that choking will occur at smaller water depths (depths below those classed as deep water) provided there is a sufficient quantity of water on the road surface to induce groove flow. It is evident, referring to the data in Figure 23, that hydrodynamic pressure in the grooves is strongly dependent on water depth at depths below the critical value. Nevertheless, it is difficult to explain precisely why wet traction performance is extremely sensitive to water depth below some critical value and relatively insensitive to water depth above the critical value. The following theory is offered as a partial explanation.

Consider the hydrodynamic pressure measurements shown in Figure 21. At speeds below that of total hydroplaning, the pressure in a particular groove is maximum at the leading edge of contact and decreases to a minimum near the trailing edge. The groove flow rate, $\dot{Q}_g$, depends on the water-wedge pressure, P, and the groove flow resistance, R.

$$\dot{Q}_g = \frac{P}{R} \tag{17}$$

The rate at which water is intercepted by the tire, $\dot{Q}$, is given by eq (11), repeated below.

$$\dot{Q} = whV \tag{11}$$

Since the pressure at the leading end of the groove is proportional to the square of the speed (cf. eq (2)), the groove flow rate must also be proportional to the square of the speed.

$$\dot{Q}_g = \frac{K}{R} V^2 \tag{18}$$

Comparing equations (11) and (18) it is seen that while groove flow rate increases as the square of the speed, water-interception rate increases linearly with speed and water depth.

Figure 24 illustrates the above situation. The parabolic line in Figure 24 is the groove flow rate versus speed curve that would result if the flow rate were determined only by the dynamic pressure in the water wedge. The straight lines represent the rates at which different depths of water are intercepted by the tire—the steepest straight line represents a depth greater than the critical depth, h_c, and the lowest slope line represents the interception rate when the depth is less than the critical depth.

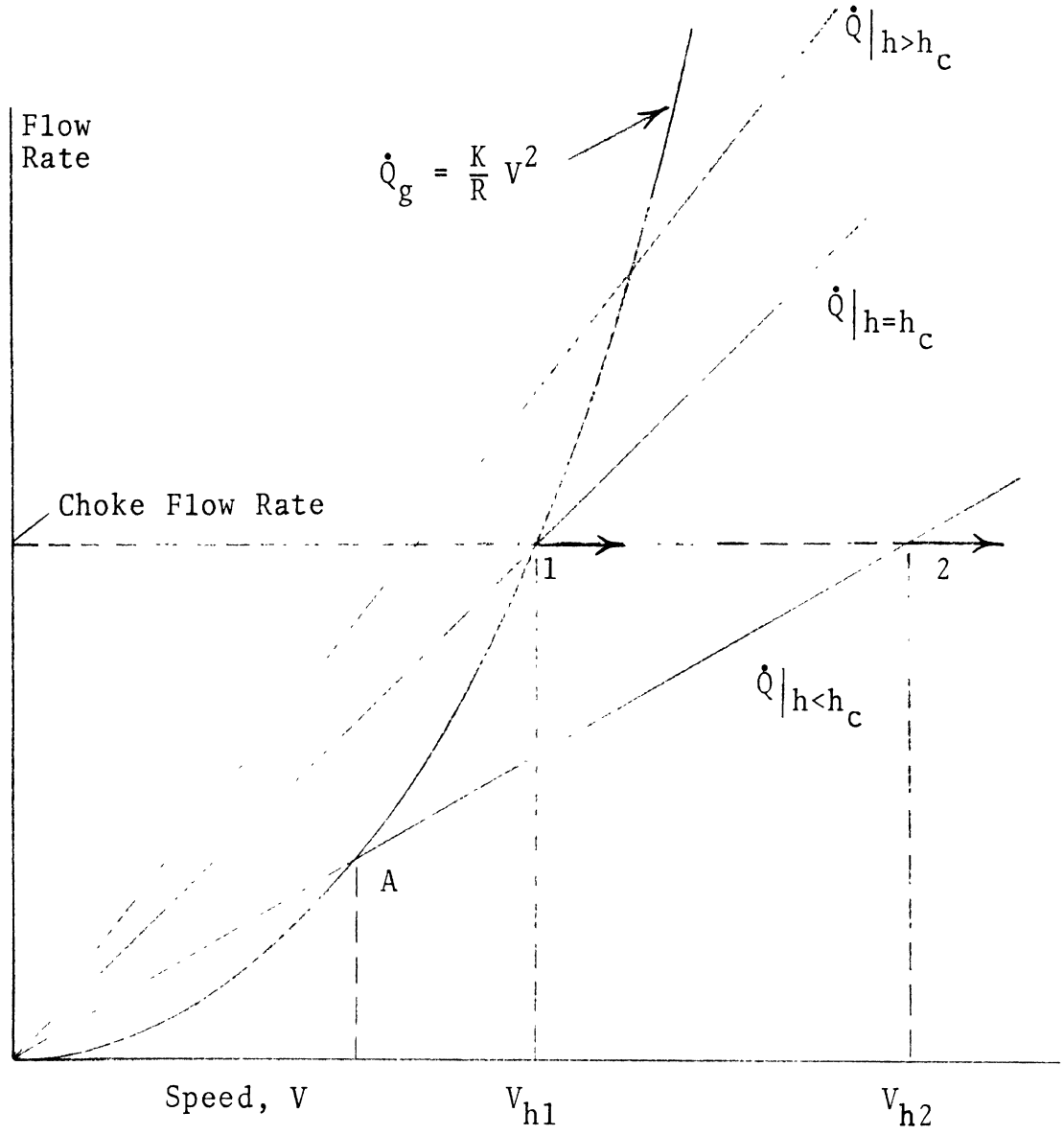

Figure 24. Effect of water depth and speed on groove flow rates.

When the depth is above critical, the amount of water intercepted by the tire exceeds the amount flowing through the grooves at all speeds up to the total hydroplaning speed* V_{h1}, at which time the grooves become choked. When the depth is below critical, there is a speed (at point A in Figure 24) for which the groove flow rate is limited by the water-interception rate, $\dot{Q}$. Beyond this speed the groove flow rate simply follows the interception rate line and choking will occur at a much higher speed. At speeds below the cross-over point (A), there is a sufficient amount of water available to maintain a water wedge and the corresponding groove flow rate, $\dot{Q}_g$. At speeds above point A, the water wedge is suppressed because the quantity of water required to maintain a groove flow rate compatible with the existance of a water wedge (viz, a $\dot{Q}_g$ which varies parabolically with speed) is not available. Some investigators have, in fact, noted a suppression of the water wedge and the accompanying forward spray as speed is increased in moderate water depths [11].

At water depths below critical, a speed $V_{h2} > V_{h1}$ is required for groove choking, and total hydroplaning**, to occur. When groove flow rate is limited by water interception rate, the groove flow rate, and hence the groove pressure is proportional to water depth. This analysis explains why tire traction capability is dependent on water depth at depths below the critical value.

Also shown in Figure 24 is the water-interception rate line corresponding to critical water depth. The intersection of the line with the groove flow rate, $\dot{Q}_g$, curve occurs at the speed of total dynamic hydroplaning (predicted by the Horne equation).

---

* This is the deep-water hydroplaning speed predicted by the Horne equation (10).

** Failure to expel the squeeze film can cause total hydroplaning at a speed lower than V_{h2}.

At this particular point, groove flow rate no longer increases and the additional water intercepted at higher speeds simply slides beneath the hydroplaning tire, groove pressure becomes independent of water depth, and tread pattern influence is lost.

If the above theory is correct, critical water depth can be defined as that depth necessary to supply a sufficient quantity of water to choke the tread grooves while maintaining a water wedge. The critical value would depend on the ease with which water can be made to flow through the grooves, which would, in turn, depend upon groove capacity (number of grooves, groove width, and groove depth) as well as the pattern of the grooves, e.g., a zig-zag groove would offer greater flow resistance than a straight groove.

In the above theory, it is necessary to distinguish between phenomena occurring in the contact region of locked and rolling wheels. With a locked wheel, all water intercepted by the tire is available for groove flow. When the wheel is rolling, some of the water is effectively absorbed by the tread grooves as they pass through the contact region. The amount of water available for groove flow under a rolling tire is given by

$$\dot{Q} = whV - wgV = w(h-g)V \qquad (19)$$

The above equation indicates that the critical water depth for a free-rolling tire should exceed that of a locked-wheel tire by an amount equal to the groove capacity, g. When the wheel is braked but not locked, as in the generation of peak traction force, the critical water depth would be reduced proportionately. Unfortunately, no data has been found in the literature which either supports or refutes this conclusion.

Although there is insufficient data to prove the validity of the critical water depth theory presented above, this theory

is consistent with several aspects of tire behavior that have been observed in tests conducted in deep water and in intermediate water depths.

Additional experimental evidence in support of the proposed theory consists of the observation that water depth has very little effect on the wet traction performance of a smooth-tread tire on a smooth surface. No critical water depth is apparent and total hydroplaning has been observed at the speed predicted by the Horne equation in water depths as low as .04 in. [3]. This finding is consistent with the above theory, in that, as groove capacity approaches zero, the critical water depth should also approach zero.

2.3 VISCOUS HYDROPLANING

The preceding section on dynamic hydroplaning has been concerned with phenomena which involve the movement of relatively large quantities of water, namely, water-wedge flow, groove flow, and the formation of relatively thick squeeze films, as are observed in the contact region of tires traveling over glass plates. In these cases the hydrodynamic pressures which develop to the point of separating the tire from the road surface result primarily from the inability of tire contact pressure to overcome fluid inertia forces. This does not imply that viscosity has no effect on tread pattern hydrodynamics leading to dynamic hydroplaning. In considering water flow through tread grooves, for example, there is little doubt that the pressure gradient which sustains the flow in a groove channel is influenced by viscosity. However, the pressure that initiates and motivates groove flow originates in the water wedge region where viscosity effects are negligible.

In the case of squeeze films which can exist beneath tread ribs, it can be shown* that fluid inertia effects dominate until the film thickness is reduced to about .005 in., where viscous shear forces will dominate. Under certain conditions, thin, viscous films will form in the tire-road contact region and produce a different type of hydroplaning phenomena, called "viscous hydroplaning."

Surface Texture. As discussed previously, large scale asperities — usually called macrotexture — perform a function similar to that of the tread grooves in providing drainage channels which remain open as the tire makes contact with the road surface. Experimental studies of the effect of surface texture on wet braking friction [6] have shown that, for a given speed, there is a value of average texture depth above which there is no further improvement in wet traction. For typical highway speeds, this value appears to be about .025 in.

*This will be shown in Section 3.2 by an analysis of the squeeze-film equation derived by Kuzma [22].

Sabey [12] has measured the effect of texture depth on the wet braking friction of a smooth tread automobile tire. In this investigation, she found that, with a texture depth of .01 in., a very low value of braking friction can be expected at 80 mph even if the value at 30 mph is high. However, a texture depth of .025 in. will generally insure that the braking friction at 80 mph is at least 75 percent of the value of 30 mph. It thus appears that macrotexture determines the rate at which speed degrades the wet friction of a smooth treaded tire. The influence of macrotexture on the friction generated by a patternless tread is evident in the .01 to .025 in. range of average texture depth.

It has often been observed, however, that even rough surfaces can produce a low level of friction at low speeds. This result occurs on surfaces whose gross roughness features have been worn to a polished smoothness. Such a surface is said to lack microtexture, although the macrotexture is retained. When such a surface is wet, a thin lubricating water film, only a few thousands of an inch thick, or less, can separate the tire from the road surface at points where contact would normally occur were the surface dry. The resulting thin, viscous film is extremely tenacious and, once formed, can continue to exist throughout the contact transit. The problem of preventing this occurrence, namely, viscous hydroplaning, is not so much one of penetrating the viscous squeeze film as it is of inhibiting the formation of this viscous film.

It is the "microtexture" of the pavement that serves to inhibit viscous film lubrication. As the name implies, this texture is of microscopic dimension, involving asperity heights of a few thousandths of an inch or less. These micro-asperities provide points of tire-road contact which are extremely small in area and involve extremely high contact

stresses. Substantial tire-road friction is generated at these contact points where viscous squeeze film formation is inhibited.

All surfaces appear to be subject to thin-film lubrication to some extent, since a drop in friction at low speeds is almost always observed after the application of very small quantities of water. As previously noted, the extent of this friction loss appears to depend upon the degree of surface polish, or the lack of microtexture. It is also observed that there is relatively small speed effect, provided the surface has adequate macrotexture. These observations are illustrated in Figure 25.

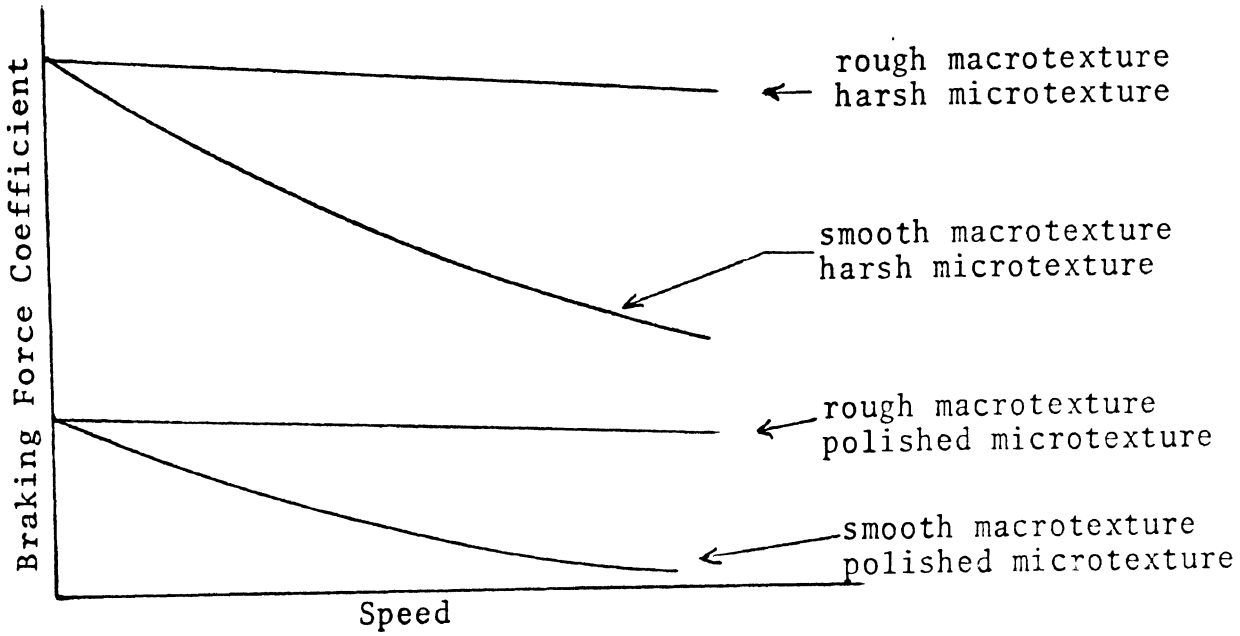

Figure 25. The effects of microtexture and macrotexture on the speed sensitivity of wet tire-road friction.

The term microtexture is generally taken to mean asperities of microscopic size that are superimposed upon the larger macro-asperities. However, high contact stresses over small areas can also be obtained if the macro-asperities have sharp points and edges. Just how sharp the points and edges must be, and how long they can be maintained under traffic conditions, are questions that have yet to be answered in evaluating the influence of macrotexture on viscous hydroplaning.

Grooves and Sipes. The fact that low friction is observed on coarse textured, but polished, surfaces indicates that lubricating water films can form over areas as small as the tips of individual surface macro-asperities. Since tread grooves are spaced at large distances relative to the size of such water films, it might be expected that grooves are not effective in preventing viscous hydroplaning. On polished surfaces, grooved tires do, in fact, exhibit very low wet friction and show little or no improvement over smooth tires [5].

Sipes, or knife cuts, do appear to give a significant improvement on smooth, polished, surfaces. The mechanism by which sipes improve wet friction is still a matter of speculation. The following four mechanisms have been suggested.

1. The sharp edges of a sipe act like squeegees in wiping away the water film so that the following tread can make contact with the road surface.
2. The sharp edges of a sipe provide points of high contact pressure which permits penetration of the water film.
3. The sipes provide temporary low-pressure storage cavities for squeeze film water trapped beneath the tread ribs, thereby reducing the size of the squeeze film.
4. The sipes that have at least one end opening into a groove will provide additional drainage in much the same manner as surface macrotexture. (This mechanism has been confirmed by glass plate observations [3].)

It is possible that all of the above mechanisms have a role in the prevention of viscous hydroplaning under certain conditions. The first mechanism (squeegee action) could operate only if there is a component of sliding velocity which is perpendicular to the sipe. The orientation of the sipe is therefore important. The second mechanism could make a contribution when there are shear forces perpendicular to the sipe to deform the tread in such a way that the sipe edge is pressed against the pavement. Sipe orientation would be important here also. The third mechanism would apply to sipes that are "land-locked" (do not open into a groove) and would only be effective for a rolling tire. If the sipes are not "land-locked," as with the fourth mechanism, drainage will occur in both rolling and sliding tire motion.

It would seem that the orientation of the sipes may determine the relative contribution of the first two mechanisms in cornering and braking. A transverse sipe should be more effective in braking than in cornering, and the opposite would be true of a longitudinal sipe. Most production tires have sipes that are cut at an angle, or at several angles, to the tire plane.

There is quite likely a road surface influence on the effect of sipes. The drainage mechanisms (3 and 4) will contribute to traction only on surfaces that lack macrotexture. The first and second mechanisms would tend to compensate for lack of microtexture and would appear to be effective only on polished surfaces.

The preceding statements have identified six tire and tire operating variables that determine the effectiveness of sipes.

1. Number of sipes
2. Depth of sipes
3. Orientation of sipes

4. Position relative to the grooves ("land-locked" or open)

5. Slip condition: braking or cornering, locked or rolling

6. Surface macrotexture and microtexture

It should also be mentioned that many tires have sipes cut in such a way that they are open to the grooves when the tire is new but become "land-locked" as the tire wears. The sipes frequently disappear as the tread wears, even when a significant groove depth remains.

There is insufficient data in the published literature to permit the influence of the above variables on sipe effectiveness to be evaluated. A tire test program necessary for such an evaluation would be a major undertaking.

Moore's Theory. In Section 2.2.2, dealing with dynamic hydroplaning in shallow water, it was noted that locked-wheel braking force shows a greater rate of decrease with increasing speed than does peak braking force. It is well known that a non-rolling tire will hydroplane at a lower speed than will a rolling tire. A partial explanation, based on the ability of the rolling tread grooves to absorb some of the water, was proposed in Section 2.2.2. A more complete explanation can now be given by considering the influence of viscosity.

Apart from groove and other pattern effects noted previously, the primary kinematic difference in the wet contact region of rolling and sliding tires is that extensive shear deformation occurs in the water film in the sliding case. This observation leads to the hypothesis that fluid viscosity effects are more important in sliding than in rolling. Moore [13] has constructed a theory in which a tire sliding over a road surface asperity is modeled as a foil bearing (tension tape) sliding over a smooth sinusoidal asperity (macrotexture) which is lubricated by a thin, viscous, water film. The details of this theory will not be summarized here but the results show that when a tread rib slides over an asperity, a water film can be maintained, whereas, if there were no sliding, the film would be squeezed away. The

thickness of the film that can be maintained is shown to increase with increasing sliding speed. The theory also shows that tractive forces due to viscous shear of the fluid film and tread rubber hysteresis cannot account for the levels of locked wheel braking force that are usually obtained experimentally and, therefore, an adhesion component of tractive force must exist. The adhesion component can certainly exist if the film thickness maintained is smaller than the height of the micro-asperities which may be superimposed upon the macrotexture. Presumably, as sliding speed increases, film thickness increases and some of the micro-asperities become ineffective. This is the mechanism by which Moore's theory of viscous hydroplaning explains the loss of adhesion due to sliding at the tire-road interface.

Moore's theory also suggests another explanation (in addition to the four listed previously) for the effectiveness of sipes. The rubber tread that slides over the macro-asperity must be continuous to maintain a lubricating water film in the manner predicted by Moore's theory. The sipe, being a discontinuity in the tread surface, could cause a breakdown of the water film in the immediate vicinity and thereby inhibit viscous squeeze-film formation and viscous hydroplaning.

2.4 THE FOUR-ZONE CONCEPT

The preceding discussion of the hydroplaning literature has noted several mechanisms by which tire shear force capability can be lost as a result of a water cover on a paved surface. These mechanisms are influential in different tire and road conditions. It is useful to visualize events in the contact region in terms of a multi-zone theory. This concept was first suggested by Gough and was later extended by Moore. A four-zone concept, following Moore, is described below and illustrated in Figure 26.

Zone 1 - Impact Zone

In this zone, a water wedge is formed by impact of the moving tire against the stationary water cover. Hydrodynamic pressure, which results from momentum transfer by impact, increases as the square of the speed. At a certain speed, hydrodynamic pressure becomes sufficiently high to initiate squeeze-film penetration into the contact region. Although hydrodynamic pressure in the impact zone has a strong influence on the flow within the contact region, this pressure contributes a relatively small vertical lift because of the small size of this zone.

Zone 2 - Thick-Film Zone *

If speed and water depth are sufficiently high, a thick squeeze film will penetrate the contact region designated as Zone 2. The extent of squeeze-film penetration (and Zone 2) depends upon the ratio of the time required for water expulsion to the contact transit time. If this ratio exceeds unity, the entire contact region becomes supported by a water film and total dynamic hydroplaning occurs.

Surface macrotexture and tread pattern are important variables in this zone.

---

*Recent measurements of tire deformation during dynamic hydroplaning [25] show that the boundary of the thick-film zone is horseshoe shaped, due to inward bending of the tread in the central portion of the contact region.

Zone 3 - Draping Zone

After the main bulk of water has been removed from the impact and thick-film zones, the tire tread begins to make contact with the road surface by draping over the asperity tips. A thin, viscous, lubricating water film may form at the asperity tips which lack sharpness or microtexture (i.e., polished). If the macro-asperities are polished to such an extent that a lubricating film is formed over most of the areas where tire-road contact normally occurs, very low values of friction will be obtained.

Road surface microtexture and the viscous hydrodynamic effects of relative sliding between tire tread and road surface are important in the draping zone. It may also be important to consider the structural dynamics of the draping process (cf. Moore [14]).

Zone 4 - Dry-Contact Zone

If speed and water depth are not high enough to induce total dynamic hydroplaning, and if the road surface possesses sufficient microtexture so that viscous hydroplaning is not extensive, a dry-contact zone will exist, in which large frictional shear stresses are developed. Whether or not there is truly dry contact is a matter of current controversy, but it is generally believed that the extremely high contact stresses which develop at the tips of micro-asperities in this zone enable the tread rubber and road surface to come into sufficiently close proximity to produce high sliding shear stresses. It is known that as a liquid film is reduced in thickness to molecular dimensions, the apparent viscosity of the film becomes very large. It is therefore possible to generate high shear stresses without completely removing the water film.

Zone 1 - Impact of leading edge of contact patch against water film.

Zone 2 - Thick film; inertia forces dominate, tread pattern and surface macrotexture important.

Zone 3 - Thin film; viscous squeeze film at tips of the larger asperities.

Zone 4 - Dry contact; surface microtexture penetrates viscous squeeze film.

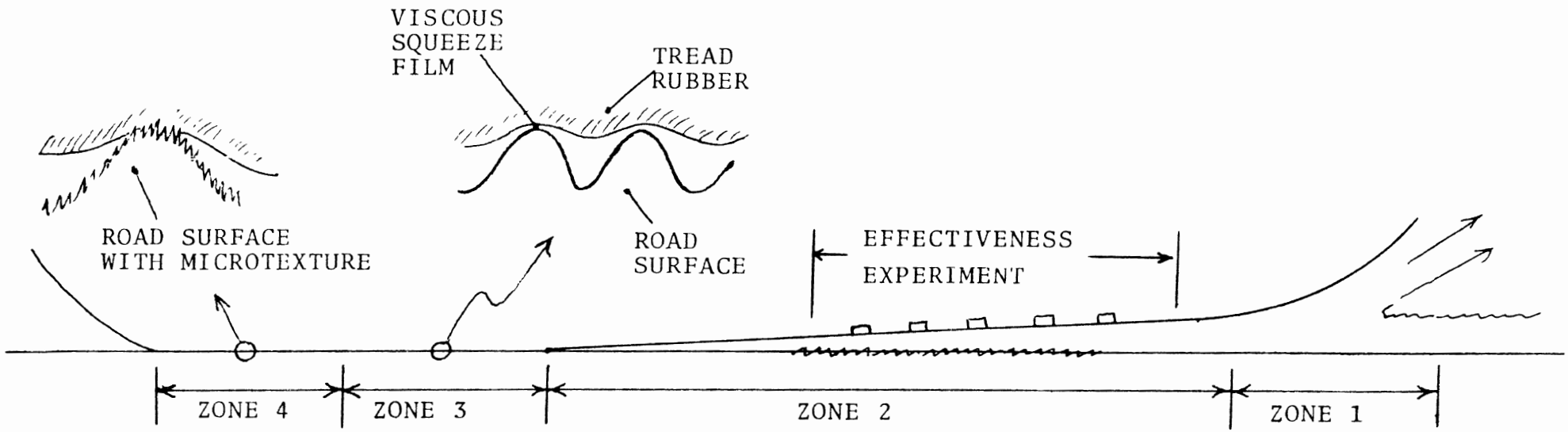

Figure 26. The four-zone concept.

3.0 SQUEEZE-FILM THEORY

The preceding chapter has emphasized the importance of the squeeze-film concept in wet traction phenomena, although the squeeze film itself was not carefully defined and analyzed.

This chapter will discuss those aspects of squeeze-film theory which have important implications relative to the understanding and analysis of hydroplaning and tread pattern hydrodynamics. A primary distinction is made between classically viscous squeeze films and squeeze films in which inertia forces may dominate over viscous forces.

3.1 VISCOUS SQUEEZE FILMS

The simplest case of squeeze film flow, and, historically, the first to be analyzed is the flow generated by a flat, rigid, circular or elliptical plate in parallel approach to a flat, rigid, infinite surface submerged in an incompressible Newtonian fluid. The equation of motion for this situation, derived by Reynolds [15], is

$$-\frac{dh}{dt} = \frac{W}{\pi ab} \cdot \frac{a^2 + b^2}{3a^2b^2} \cdot \frac{h^3}{\eta} \tag{20}$$

where

h (t) = gap between plate and surface

W = vertical force on the plate

a = major semi-axis of the elliptical plate

b = minor semi-axis of the elliptical plate

η = fluid viscosity

t = time

For a circular plate of radius r, this equation reduces to

$$-\frac{dh}{dt} = \frac{2}{3} \frac{Wh^3}{\pi r^4 \eta} \tag{21}$$

In the derivation of the equation of motion (20), all inertia force terms were neglected and the film thickness was assumed to be small in comparison to the plate surface dimension, thus permitting the vertical component of fluid velocity to be neglected.

Equation (21) may be directly integrated to obtain

$$\frac{1}{h^2} = \frac{1}{h_o^2} + \frac{4W}{3\pi r^4 \eta} t \tag{22}$$

where h_o is the initial separation. For plates that are neither circular nor elliptical, an equation of form similar to (22) can be used [16], viz:

$$\frac{1}{h^2} = \frac{1}{h_o^2} + \frac{W}{K\ell^2\eta} t \qquad (23)$$

where ℓ is a characteristic length dimension and K is a constant which is determined by the shape of the plate. For a circular plate, $K = 3\pi/4$; and for a square plate, $K=.21$. The rate of sinkage for a square plate is found to be about 12 percent greater than the sinkage rate of a circular plate of the same area.

Moore [17] has developed a theory for the sinkage of an inclined rectangular plate. The angle of inclination is permitted to vary linearly with time from an initial value α to a final value β. An important conclusion, derived from Moore's theory, is that small angles of inclination cause large increases in the sinkage rate. For an initial angle $\alpha = 1.6°$ and a final angle $\beta = 0$, the inclined plate has a sinkage rate approximately four times that of the same plate in parallel approach.

Moore [18] has developed several methods of predicting the influence of surface roughness on sinkage rate and has verified these methods by laboratory experiment. Figures 27 and 28 illustrate some typical calculations for parallel approaches to both a smooth and rough surface.

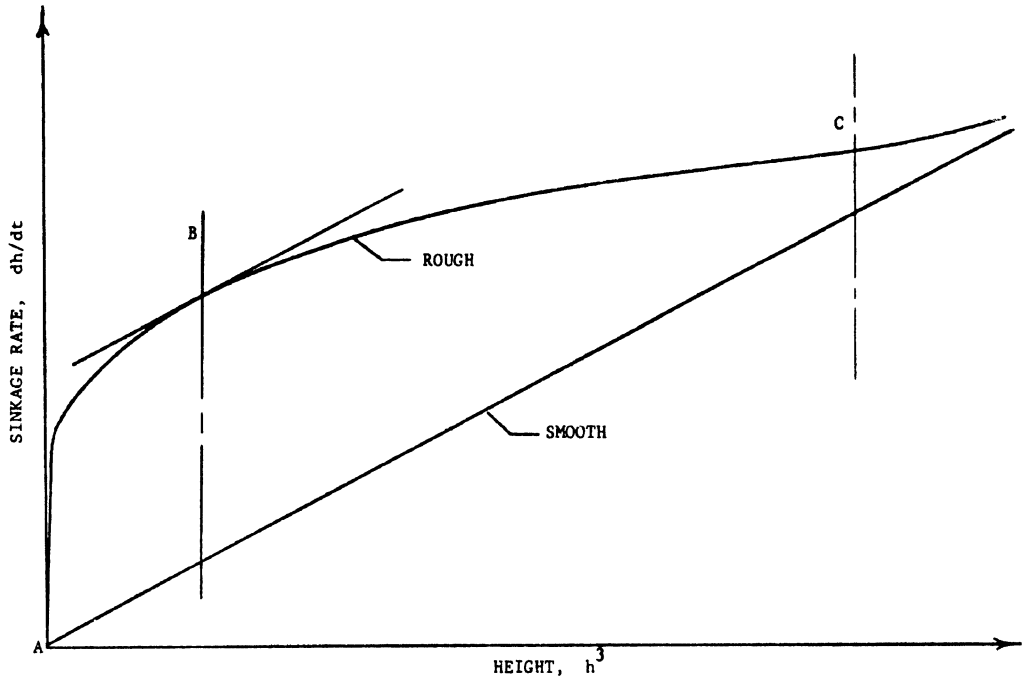

Figure 27. The effect of surface roughness on the parallel approach rate, $\dot{h}$, of a circular plate. From [18].

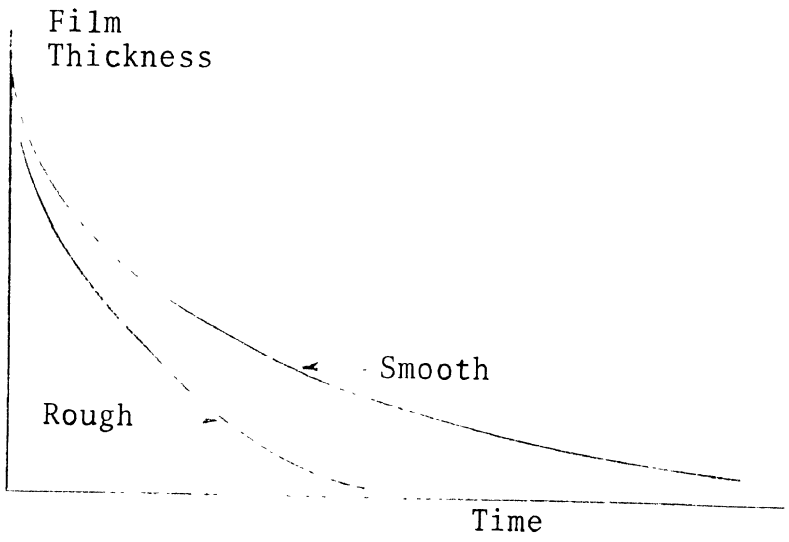

Figure 28. The effect of surface roughness on film thickness vs. time for parallel approach of a circular plate. From [18].

Finally, Moore has extended the well-known concept of the "hydraulic radius," which has long been applied to the analysis of one-dimensional channel flow, to include the case of two-dimensional viscous flow through the voids of a randomly rough surface. The success of Moore's analysis led to a device called the "outflow meter" designed for the purpose of evaluating the drainage capability of a paved road surface. Efforts to correlate outflow meter readings with tire skid test results have been moderately successful [14] but there is insufficient experience with this device to define the extent of its usefulness.

One of the first attempts to use squeeze-film theory to explain the loss of tire-road shear force capability on wet surfaces was made by Saal [19] in 1936. Saal proposed that the tire footprint, or an element of tread surrounded by grooves, could be modeled as a flat, rigid plate approaching the road surface in a parallel manner while submerged in a viscous liquid with the flow between the surfaces being governed by eq (22), as previously derived by Reynolds. A laboratory apparatus was used to measure the friction developed by a small model pneumatic tire which was skidded across various road surfaces covered by liquid films having several values of viscosity. The variation of friction force with speed and viscosity was shown to be qualitatively consistant with the predictions based on eq (22) and data from full-scale tire-road experiments.

Since the appearance of Saal's paper [19], viscous squeeze-film effects have frequently been invoked to explain the decrease in friction coefficient with increasing speed, the explanation being based on the progressive penetration of a squeeze film into the tire-road contact region [20].

To further investigate the applicability of viscous squeeze-film theory, eq (22) was used to calculate sinkage curves for the parallel approach of circular plates having areas and

vertical loads comparable to those prevailing in a tire contact patch or to the loads on a tread element. Calculations were performed for a plate having a radius of 3.0 inches and carrying a vertical load of 1000 pounds, producing a vertical pressure distribution of approximately 35 psi, a value typically found in the contact region of a tire. The tread element calculation was performed for a plate of .5 inch radius carrying a vertical load of 28 pounds which produces the same contact pressure, 35 psi, as the plate simulating the total contact patch. The sinkage curves resulting from these calculations are shown in Figure 29. In both calculations, the initial film thickness was set at h_o = .05 inch to correspond to the maximum value observed at the onset of total hydroplaning [2]. The water viscosity was taken as $\eta = 2 \times 10^{-5}$ lbf-sec/ft^2.

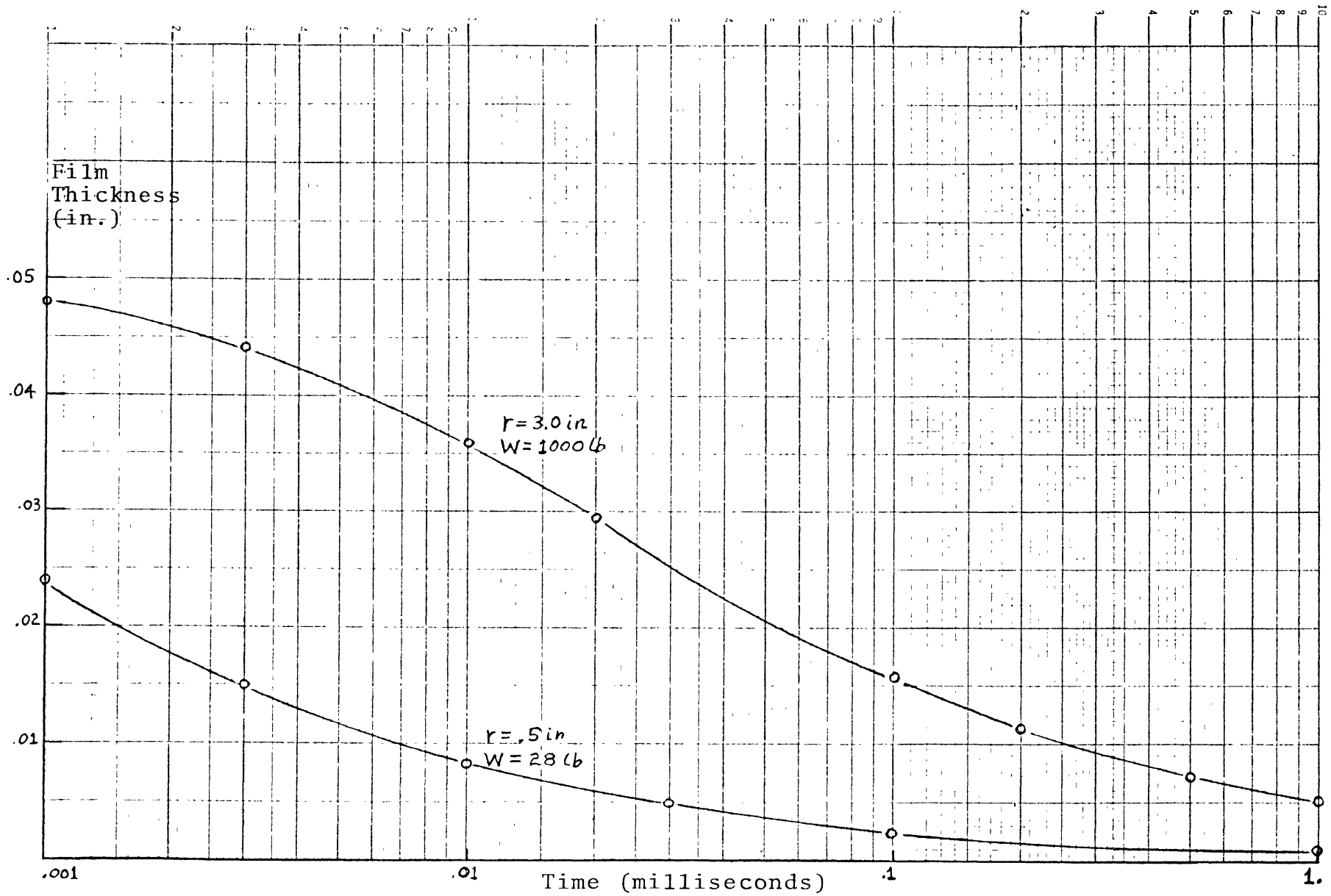

Figure 29. Viscous sinkage curves from eq (22) for circular plates in water. Initial film thickness: .05 in. Plate pressure: 35 psi.

It is interesting to observe that for the 3-inch plate, film thickness is reduced from .05 in. to .01 in. in about .13 milliseconds. The .5-inch plate achieved the same film thickness reduction in less than .01 milliseconds. These calculations should be placed in context with the case of a real tire which exhibits inclined sinkage toward a surface having significant roughness, which roughness would influence the sinkage rate. The work of Moore has demonstrated that both inclination and surface roughness produce large increases in sinkage rate. If these factors were accounted for in the theory which produces the results shown in Figure 29, viscous sinkage rates would be calculated that are substantially higher than the rates shown in Figure 29.

On a real tire, rolling at 60 mph, a tread element requires approximately 4-5 milliseconds to pass through the contact region, this time being several orders of magnitude greater than the time span of the very conservative viscous sinkage calculations shown in Figure 29. Clearly, hydrodynamic pressure due to viscous forces alone is insufficient to account for the time required to penetrate the squeeze films that are observed to accompany partial and total hydroplaning. Moreover, the influence of tread grooves and surface macrotexture would be imperceptible if viscous forces alone prevailed.

However, it should be noted that when film thickness is reduced to, say, .005 in., the sinkage rate is substantially reduced (see Fig. 29). Such films are very tenacious (not easily expelled) and viscous forces can, in this situation, result in a loss of friction, with this phenomenon presumably occurring on surfaces of very low microtexture. The low sinkage rates found in very thin viscous films also explain the negligible influence of speed on viscous hydroplaning, as described previously in Section 2.2.

3.2 INERTIA EFFECTS IN SQUEEZE FILMS

Recently, there has been considerable interest in fluid inertia effects in hydrodynamic lubrication. Some techniques for the analysis of bearing films, including convective inertia effects, have been developed. Browne [21] has applied these techniques in an analysis of dynamic hydroplaning, and the analysis was validated experimentally. Browne found that convective inertia forces are the dominant source of hydrodynamic pressure supporting a tire in total hydroplaning.

Kuzma [22] has derived a theory for the parallel approach of a circular plate which includes the effect of viscous forces, convective inertia forces, and local inertia forces. Kuzma arrived at the following equation:

$$W = \frac{\pi r^2}{4}\left(\frac{6\eta\dot{h}}{h^3} + \frac{3\rho\ddot{h}}{5h} - \frac{15\rho\dot{h}^2}{14h^2}\right) \tag{24}$$

where ρ is the fluid density and the other variables are those defined with eq (20). If the density, ρ, is set equal to zero, eq (24) reduces to eq (22) for a viscous squeeze film. The terms involving $\dot{h}^2$ and $\ddot{h}$ account for convective and local inertia forces, respectively.

Equation (24) was used to calculate water sinkage curves for plates having dimensions comparable to a tire contact region or a tread element surrounded by grooves. As assumed in the viscous-film calculations (Fig. 29), forces, W, were applied to the plates which would correspond to a force per unit plate area of 35 psi. The plates are assumed to be massless*, the initial film thickness is .05 in., and the initial sinkage rate is assumed to be zero.**

---

* This is equivalent to assuming that the inertia forces associated with the tread mass are small compared to the forces due to inflation and hydrodynamic pressure.

** Calculations were performed with initial sinkage rates other than zero; the results do not alter the conclusions derived herein.

Figure 30 shows the circular plate sinkage curves calculated from Kuzma's equation (24) for a family of plates with radius varying from .125 in. to 3.0 in. Two viscous sinkage curves, from eq (22), for plates of radius .5 in. and 3.0 in. are shown for comparison purposes. It is interesting to note that when film thickness is greater than .005 in., the sinkage time is much longer when fluid inertia effects are included. However, for very thin films, less than say .002 in., the viscous forces dominate and essentially the same sinkage rate is predicted by the Kuzma equation as is obtained from eq (22).

It is also of interest to observe the manner in which the three components of hydrodynamic force, viz,

F_A - local inertia force

F_C - convective inertia force

F_V - viscous force

vary with film thickness, as plotted in Figure 31. Figure 31 shows that inertia forces dominate until film thickness is reduced to approximately .008 in., after which the viscous force becomes greater than the sum of the two inertia forces, F_A and F_C.

With smaller plates, of radius less than 3 in., the viscous force does not become dominant until still smaller film thicknesses are attained. In Figure 30, a curve has been drawn through those points on the sinkage curves at which $F_V = F_A + F_C$. Above this curve, inertia forces dominate, and below it, viscous forces dominate.

On the basis of the above calculations, it appears that the progressive penetration of a squeeze film into the contact region with increasing speed is primarily a "dynamic" phenomenon, i.e., it can be explained by consideration of the effects of fluid inertia. As a result of fluid inertia effects, it appears that sinkage times (in squeeze films of the thicknesses known to exist beneath a smooth-tread tire, or beneath a relatively wide rib)

can be long enough (on the order of a few milliseconds) to account for the decrease in friction with increasing speed and the observed dependence of speed-sensitive friction on tread pattern.

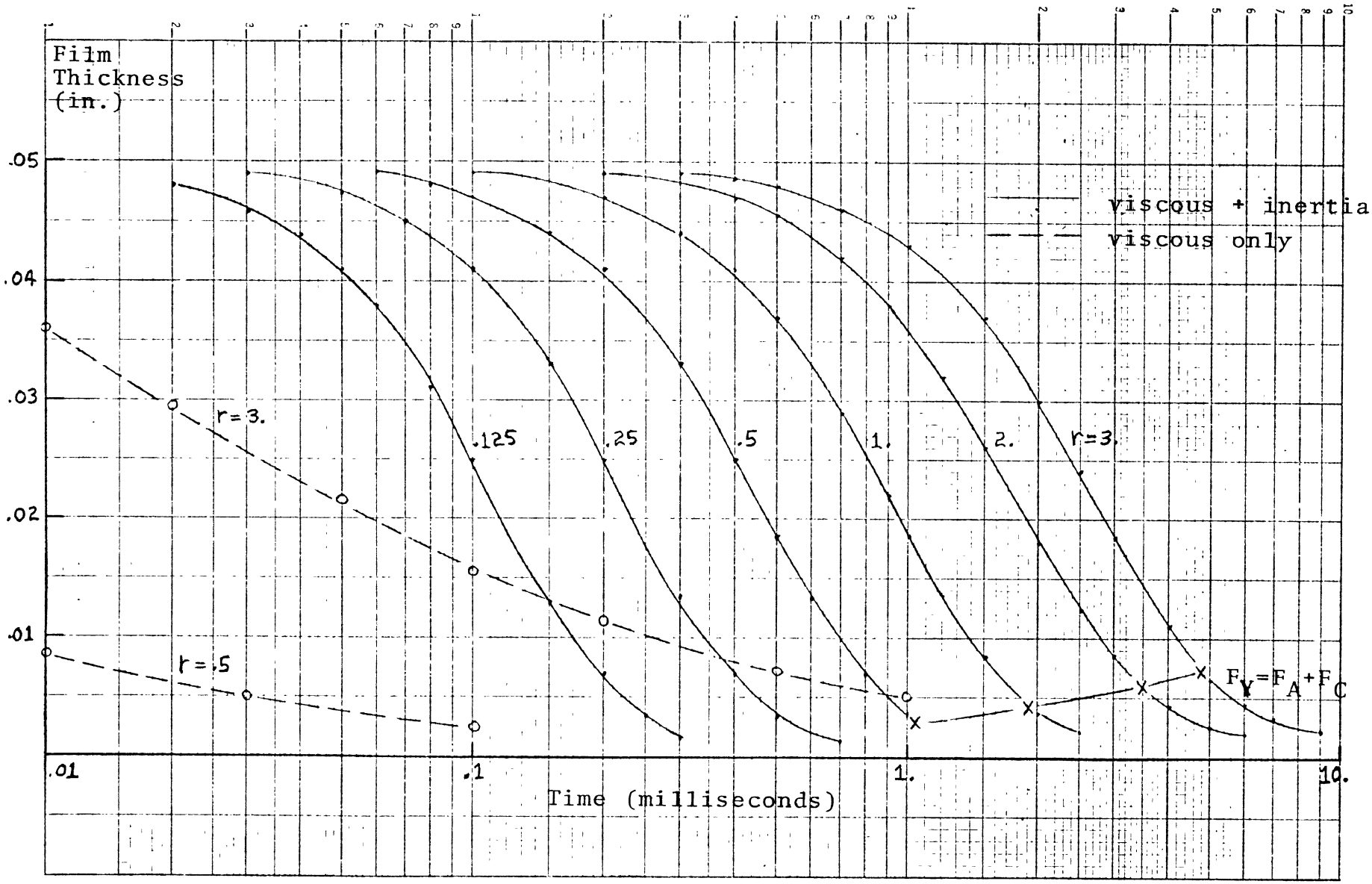

Figure 30. The influence of fluid inertia on sinkage curves for circular plates of various radii. Initial film thickness: .05 in. Plate pressure: 35 psi.

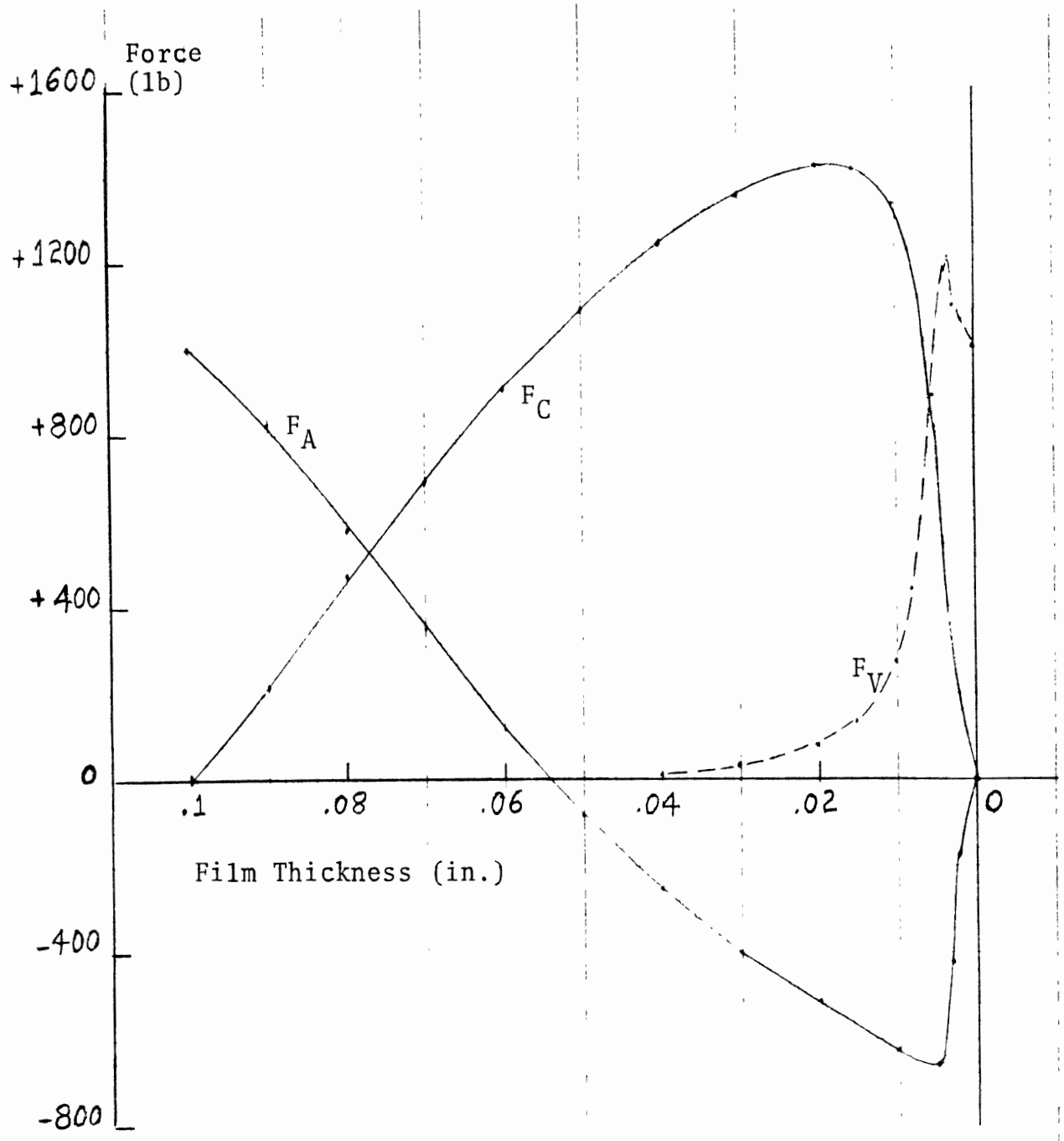

Figure 31. Inertia (F_A, F_C) and viscous (F_V) components of hydrodynamic force vs. film thickness. Circular plate (r=3) with 1000 lb. load. Initial film thickness: .1 in.

4.0 TREAD PATTERN PERFORMANCE PARAMETERS

The conclusions drawn from (1) the preceding discussion of the wet-tire traction literature and (2) calculations based on squeeze-film theory have been used to assist in the rational selection of tread pattern performance parameters which should have a bearing on the water expulsion effectiveness of the tread. Two such parameters (viz, groove capacity and flow distance) are proposed below, followed by a discussion of the requirements for additional parameters.

4.1 GROOVE CAPACITY PARAMETER

The groove capacity, g, is defined as the groove volume per unit of gross contact area. Groove capacity, being a measure of the water-holding capacity of a tread pattern, is meaningful to wet traction in relation to the amount of water encountered by the tire.* It is therefore logical to form a dimensionless performance parameter, γ_1, as the quotient of groove capacity divided by water depth.

$$\gamma_1 = \frac{g}{h}$$

A derivation of this parameter as the ratio of water-interception rate to groove-absorption rate has been given previously (see Section 2.2.2).

*The data of Maycock, Gengenbach, and Staughton (reviewed in Section 2.2.2) clearly show that groove width, groove depth, and water depth are closely interrelated with respect to wet traction performance.

4.2 FLOW DISTANCE PARAMETER

It was noted, in Section 2.2.2, that Grime and Giles [7] attempted, with some success, to correlate locked-wheel braking coefficients measured on three wet surfaces with the dimensionless parameter

$$\frac{\text{perimeter of contact area}}{\sqrt{\text{contact area}}}$$

A similar dimensionless parameter derives from the following consideration of the squeeze-film expulsion process.

Consider a flat plate of area A and perimeter C which carries a load, W, while expelling a squeeze film of thickness $h(t)$ as it approaches an infinite surface. The mass expulsion rate of the squeeze film is given by

$$\dot{m} = -\rho A \dot{h}$$

The rate at which fluid crosses the boundary defined by the plate perimeter is

$$\dot{m} = \int_C \rho h V(c) dc = \rho h C V_C$$

where $V(c)$ is the flow velocity at the perimeter which has the average value V_C. The average flow velocity at the perimeter is found by equating the above mass flow rates.

$$V_C = -\frac{A}{C}\frac{\dot{h}}{h} \qquad (25)$$

Arguments were presented in Sections 2.3 and 3.2 which imply that inertia forces are dominant in film thicknesses for which tread grooves are influential. The role of the tread

geometry, then, is to enable transfer of water from beneath a tread rib into a groove to occur with minimum momentum change. Equation (25) shows that, at a given film thickness, h, and sinkage rate, $\dot{h}$, the average flow velocity at the plate perimeter, and therefore the momentum change, depends on the value of the parameter A/C. A larger value of A/C means, according to this equation, that a fluid particle must be accelerated to a higher velocity (V_c) at the plate perimeter in order to achieve a given sinkage rate, $\dot{h}$. For a particular A/C, a higher velocity, V_c, will require a larger force, W. Conversely, for a given force, W, a plate with a larger value of A/C will exhibit a lower sinkage rate.

The following arguments are given to show that the parameter A/C can be the basis of a dimensionless "flow distance parameter." Consider a fluid particle of the squeeze film shown in Figure 32 and denote, by s, the minimum distance from the particle to the squeeze-film boundary (defined by the plate perimeter). The

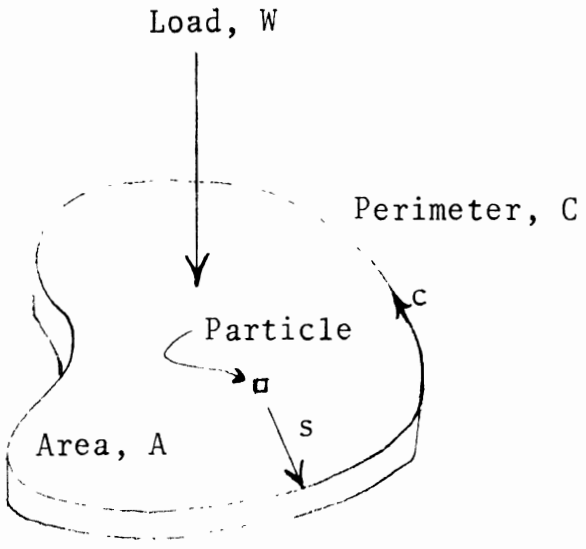

Figure 32. Squeeze film used in definition of the average flow distance, AFD.

average flow distance, AFD, is defined by

$$AFD = \frac{1}{A}\int s\, dA \tag{26}$$

For example, the average flow distance for a square of side ℓ

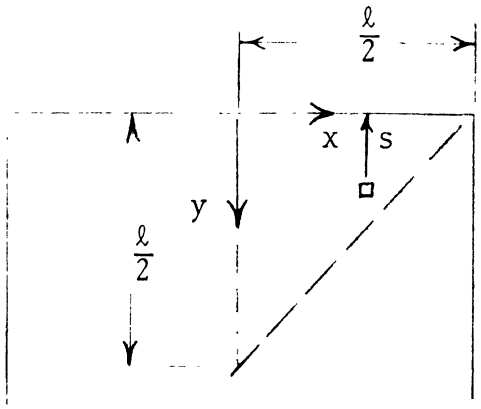

is computed by the following integration.

$$\int s\, dA = 8\int_0^{\ell/2}\int_0^{x} y\, dy\, dx = 8\int_0^{\ell/2} \frac{1}{2}x^2\, dx = \frac{\ell^3}{6}$$

$$AFD = \frac{\ell^3/6}{\ell^2} = \frac{\ell}{6}$$

Table 3 lists values of AFD and A/C computed for six simple geometric shapes. If A/C is plotted as a function of AFD for these six geometric shapes (see Figure 33), it appears that there is an excellent correlation between A/C and AFD

TABLE 3

Shape	AFD	A/C
Straight Rib (1 in. wide)	.250	.500
Square (1 in. sides)	.167	.250
Rectangle (2 in. x 1 in)	.208	.333
Circle (.5 in radius)	.167	.250
Equilateral Triangle (1 in height)	.111	.167
Diamond (1 in diagonal)	.118	.176

except for the straight rib, which has a value of A/C that is 20 percent too high. However, for

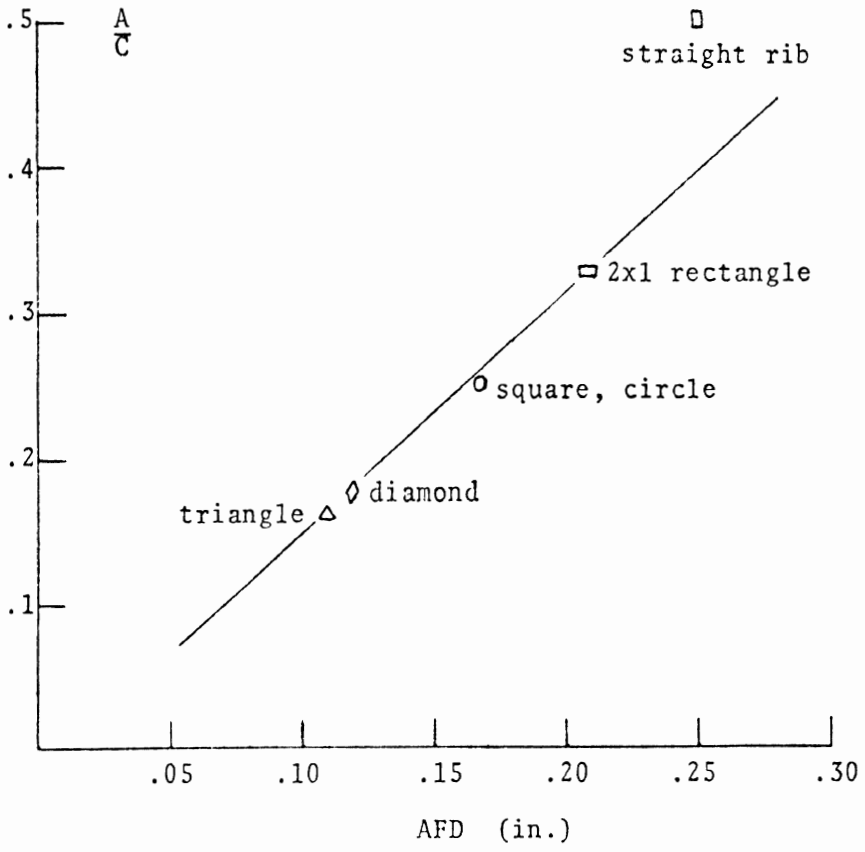

Figure 33. Correlation between area/perimeter ratio (A/C) and average flow distance (AFD).

rib-type tires having transverse grooves, or kerfs, the area/perimeter ratio, A/C, can be considered as a squeeze film flow distance parameter and a measure of the difficulty of a particular pattern in expelling a squeeze film from beneath a tread element.

At a given speed, the time available for squeeze film expulsion is proportional to the contact length. It is therefore logical to form the desired dimensionless performance parameter γ_2 as the quotient of the area/perimeter ratio divided by the contact length.

$$\gamma_2 = \frac{A/C}{L}$$

where

A = actual tire-road contact area

C = perimeter of the actual contact area

L = contact length

4.3 FLOW RESISTANCE PARAMETER

In the discussion of wet traction performance in intermediate water depths (Section 2.2.3), it was observed that tread grooves can delay the onset of total hydroplaning and thereby enable the tire to generate useful tire-road shear forces at speeds beyond the hydroplaning speed of a smooth tread tire. The effectiveness of a tread pattern in delaying the onset of hydroplaning depends on the ease with which the water intercepted by the tire can flow through the grooves to the contact region. An effective tread pattern geometry will be one which minimizes the total resistance to flow which is offered by the aggregate groove geometry.

The total flow resistance of a groove network depends on many factors, such as groove width and depth, average length of the flow path, and the linearity of the groove channels. (Clearly, a straight groove will have lower flow resistance than a zig-zag groove,)

The formulation of a tread performance parameter that relates to flow resistance appears to be an extremely complex task. The successful formulation of such a parameter will require analytical and experimental work yet to be accomplished. Appendix B describes a laboratory apparatus (as yet unbuilt) which is designed to measure the flow resistance property of simple groove patterns.

4.4 SIPE PARAMETERS

In the discussion of viscous hydroplaning (Section 2.3), it was mentioned that sipes improve wet road friction on smooth surfaces where it is generally difficult to penetrate a thin viscous film. Some possible mechanisms explaining the effectiveness of sipes were discussed. Among the possible mechanisms are those of a sipe acting like a squeegee to wipe away the water film and providing a sharp edge at which high contact pressures are generated, enabling the tread to break through the tenacious water film. If these mechanisms are operative, then the effectiveness of sipes should depend upon the total length of sipes projected in the direction of tire slip. The following sipe parameters may therefore be useful in predicting sipe effectiveness in braking (γ_{SB}) and cornering (γ_{SC}).

γ_{SB} = total longitudinally projected length of sipe per unit tread area

γ_{SC} = total laterally projected length of sipe per unit tread area

It has been observed that if the sipes open into a groove, they provide additional drainage passages for squeeze film water trapped beneath the tread elements. In this case it seems appropriate to add the length of sipes opening into a groove to the contact perimeter, C, used in the flow distance parameter, γ_2.

5.0 LABORATORY STUDY OF TREAD PATTERN EFFECTIVENESS

A thorough review of the published literature on wet traction has yielded insufficient data to establish the usefulness of the tread pattern performance parameters proposed in the preceding chapter. The primary difficulty with utilizing previously published test results is that the reports rarely document the tread pattern in sufficient detail to permit evaluation of the parameters. It is also very difficult to quantify, in a meaningful way, such test conditions as water depth and surface texture, and no standard procedures exist for measuring these test conditions.

One possible method of establishing the relevance of the tread pattern performance parameters would be to undertake a full-scale test program using actual tires on actual road surfaces. This program would be an extremely ambitious undertaking. A large sample of tires, specially produced to provide a wide range of values of the geometric description parameters (while keeping other factors, such as rubber compound, constant), would have to be tested at several water depths and speeds on a variety of surfaces. In addition to the great expense of such an extensive test program, the previously mentioned problems of controlling and quantifying water depth and surface texture would have to be overcome.

To avoid some of these difficulties, a laboratory apparatus was designed to simulate certain features of the water expulsion process which occurs when a tire rolls on a wet surface. The apparatus was designed specifically to reproduce the action of the tire tread in zone 2 of the contact region, namely, the squeeze film region where film thickness varies from approximately .05 inches at the leading edge of contact to a few thousandths of an inch at the beginning of zone 3 (see Fig. 26). It was intended that the laboratory experiments would yield useful information pertaining to the groove capacity parameter, γ_1, and the flow distance parameter, γ_2, defined in Section 4.0.

5.1 DESCRIPTION OF THE APPARATUS

The laboratory apparatus, diagrammed in Figure 34, utilizes a tread specimen plate which is mounted on bearings in a manner such that the axis of rotation (pivot axis) lies on a horizontal, fixed plate representing the road surface. The tread plate is motivated by a torsion spring which applies a torque about the pivot axis to force the tread plate toward the plate representing the road surface and to expel the intervening water film in the process. The tread specimens are flat aluminum plates into which various groove patterns are cut. The road surface is a stainless steel plate with the contacting surface ground flat and smooth. The road surface plate is mounted on three adjustable set screws for leveling and alignment with the pivot axis of the tread plate. The water is contained by sheet aluminum walls and a cover plate (as indicated in Fig. 34). The water depth above the road surface plate is measured by a micrometer probe mounted on the cover plate. A plexiglass window in the forward wall permits visual observation of the experiment.

The experiment is prepared by preloading the torsion spring, raising the tread plate with a lever, and attaching the knife-edge trigger mechanism to the preloaded tread plate. The water expulsion process is initiated by releasing a trigger which permits the tread plate to rotate through the measured water film until it contacts the road surface plate, the road surface plate having been pre-aligned for parallel surface contact. The lever for raising the tread and the trigger mechanism are mounted on a superstructure (not shown in Fig. 34) above the cover plate.

The torsion spring, which has a relatively low stiffness, is given a large preload (approximately 90 deg. twist) to insure that, during the operation of the experiment, the motivating torque is essentially constant. A uniform motivating torque is necessary in order for the instrumentation to sense variations in the hydrodynamic pressure which is developed during the water expulsion process. The experiment is designed such that the

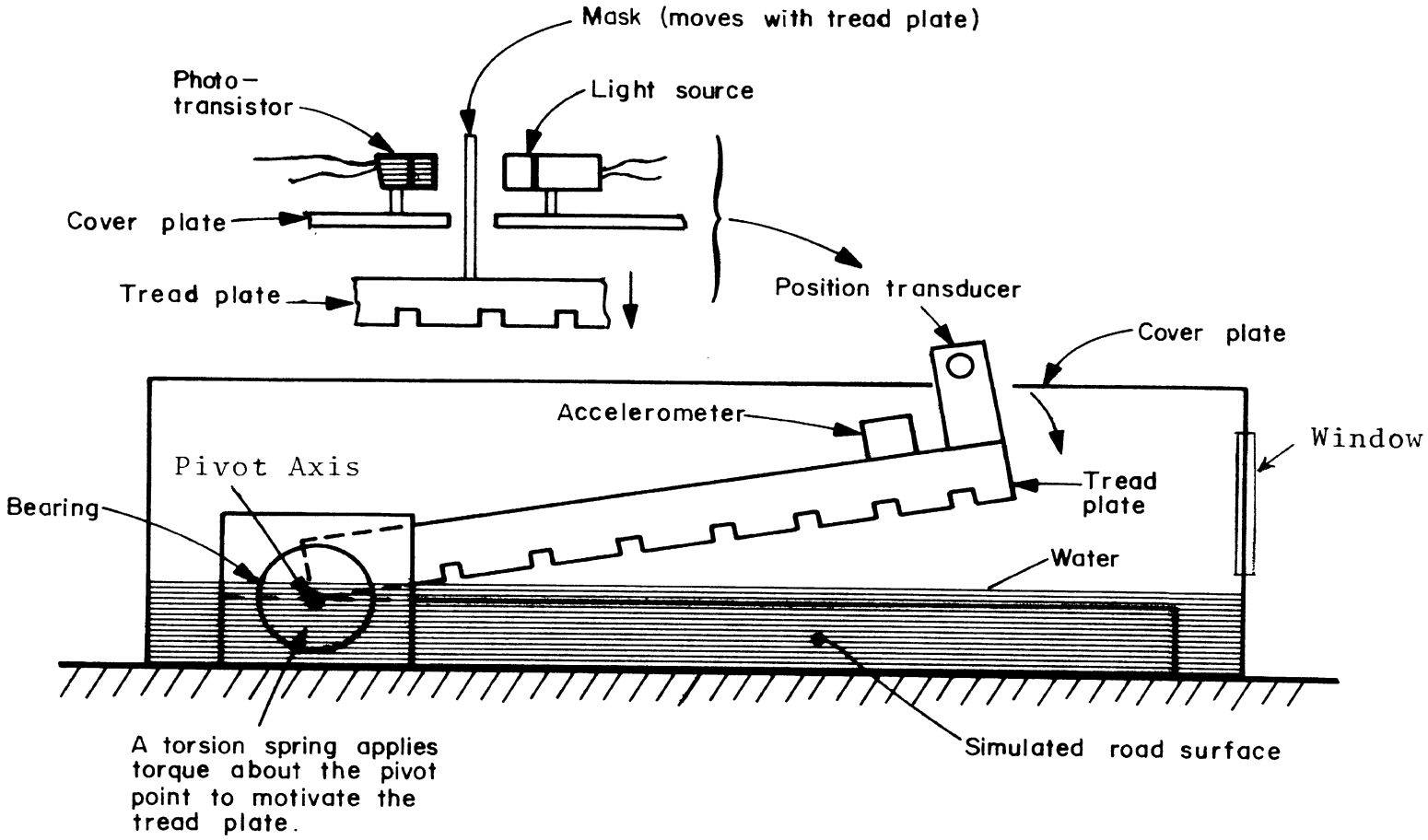

Figure 34. Laboratory apparatus for study of tread pattern effectiveness.

hydrodynamic pressure beneath the tread plate is approximately the interface pressure in the contact region of a fully hydroplaning tire, viz, the tire inflation pressure. Thus, the tread specimens which have geometries similar to that of an actual tire tread will have realistic sinkage rates and the nature of tread pattern hydrodynamics can be studied under realistic flow conditions.

The choice of a rotational motion for the tread plate, instead of a parallel approach to the road surface, is believed to be a closer approximation to actual tire operation. On a real tire, the tread translates toward the road surface at an angle of inclination which is zero at the forward contact boundary. Although, in the experiment, the tread specimen approaches the road surface plate with pure rotational motion, it is believed that the resulting simulation of the water expulsion process is more realistic than would be achieved by causing the "tread" to translate toward the "road" while keeping the "tread" parallel to the "road" at all times.

5.2 INSTRUMENTATION

The laboratory apparatus is equipped with the following measurement devices:

1. A position transducer, consisting of a photo-transistor facing a light source, is mounted on the cover plate as shown in Figure 34. A mask, attached to the leading edge of the tread plate, is positioned between the photo-transistor and light source such that the amount of light striking the photo-transistor is proportional to the position of the tread plate relative to the road surface plate. The position transducer is calibrated by inserting feeler gages of various sizes between the tread plate and road surface plate.

2. An accelerometer is mounted on the tread plate to measure its angular acceleration. The accelerometer output is integrated, by an operational amplifier circuit, to obtain the tread plate sinkage rate.

3. A torque transducer, consisting of a strain gage attached to the torsion spring, measures the motivating torque applied to the tread plate. The output from the tread plate accelerometer is summed with the torque transducer signal in order to correct for the constant signal due to the motivating torque. An output signal proportional to the hydrodynamic pressure moment about the tread plate pivot axis is obtained. Since the distribution of hydrodynamic pressure is unknown, due to the extreme difficulty in obtaining an analytical solution, the magnitude of the integrated hydrodynamic pressure cannot be derived from measurements made by this instrumentation.* Tread pattern effectiveness is assessed by measurement of the pressure moment.

Test data is acquired by photographing a storage oscilloscope display of signals corresponding to tread plate position, velocity and acceleration, and the motivating torque as a function of sinkage time.

5.3 EXPERIMENTAL RESULTS

Figure 35 presents data obtained for a smooth-surfaced tread plate subjected to a motivating torque of 10 ft-lbs. The tread plate was released at an initial displacement of .20 in. into a water depth of .30 in., the plate surface thus being totally immersed throughout its travel. With these test conditions, tread plate deceleration (solid line in Fig. 35) rises to a peak value of 5,000 rad/sec^2 at a displacement** of .05 in., and then decays toward zero. Using a value of .008 ft-lb-sec^2 for the moment of inertia of the tread plate about the axis of rotation, a deceleration of 5,000 rad/sec^2 corresponds to a net moment of

---

*The integrated pressure could be derived from measurement of the pressure moment if the moment arm were known; the moment arm depends on the pressure distribution.

**Displacement is measured at the tread plate edge farthest from the axis of rotation.

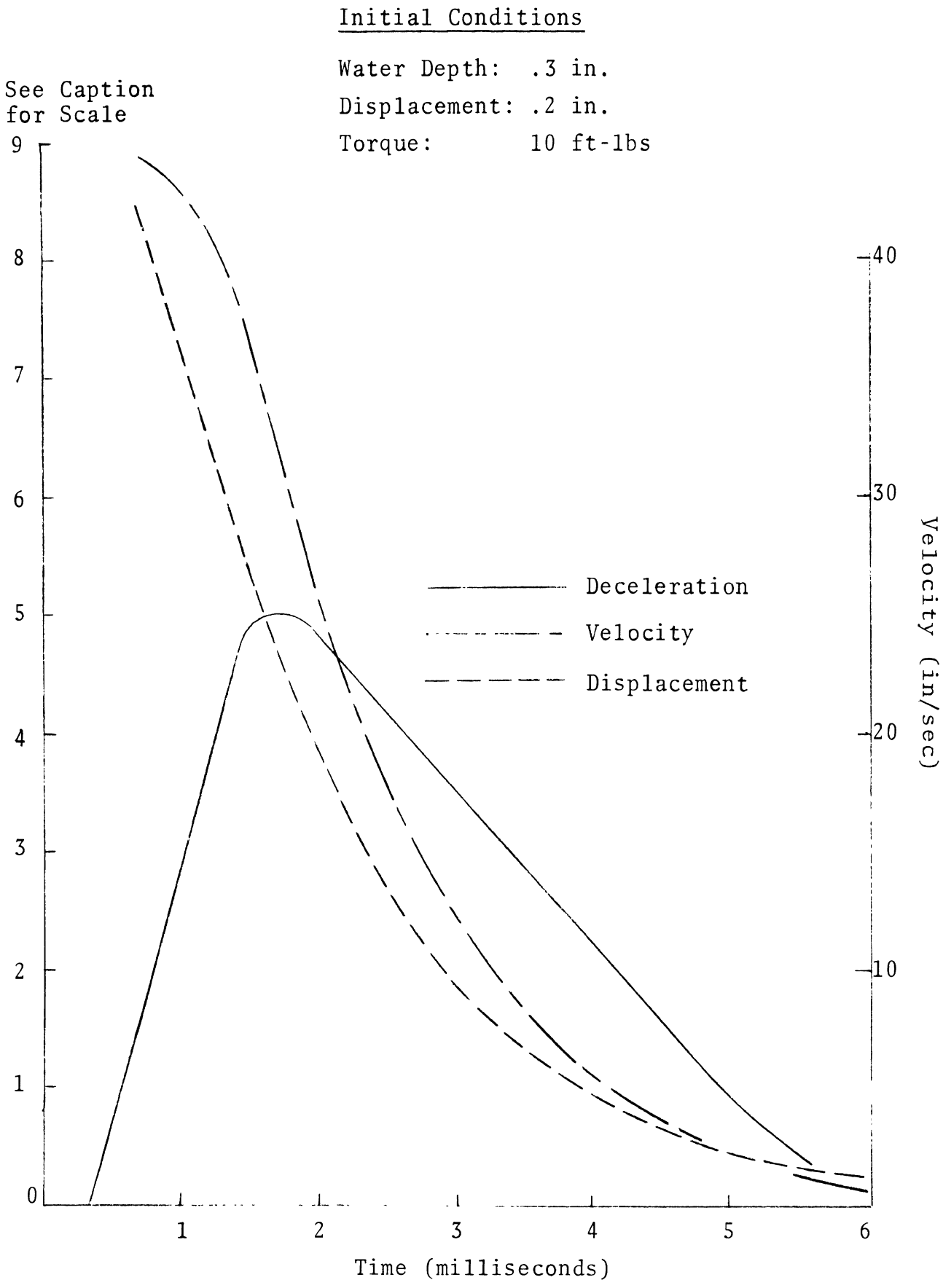

Figure 35. Smooth plate sinkage data. Left scale: angular deceleration (x 10^3 rad/sec^2) and displacement (x 10^{-2} in).

40 ft-lbs. The addition of the 10 ft-lb moment from the torsion spring gives a peak value of 50 ft-lbs for the hydrodynamic pressure moment.

Although the apparatus is not instrumented to measure hydrodynamic pressure directly, a value for the integrated pressure can be estimated if a general form for the pressure distribution is assumed. The pressure distribution sketched in Figure 36 is believed to be a reasonable assumption. This distribution is parabolic in planes perpendicular to the x-axis and elliptic in the plane of symmetry (p-x plane). The distribution is described by a surface function, $p(x,y)$, which has the following boundary conditions:

$$p(x,w/2) = p(x, -w/2) = 0 \qquad 0 \leq x \leq L$$

$$p(L,y) = 0 \qquad -w/2 \leq y \leq w/2$$

The following considerations led to the choice of the pressure distribution defined in Figure 36. If the plate were to approach the surface by parallel translation, a parabolic profile in the p-x plane would be appropriate (based on theoretical calculations [16]). In the present experiment, however, rotation of the plate about the y-axis forces the sinkage rate to increase with increasing distance from the axis of rotation. The increasing sinkage rate produces an increase in pressure toward the leading edge of the tread plate and is the reason for choosing an elliptical profile (rather than parabolic) in the plane of symmetry. No theoretical solution exists for the hydrodynamic pressure distribution between two smooth plates which approach by pure rotation.

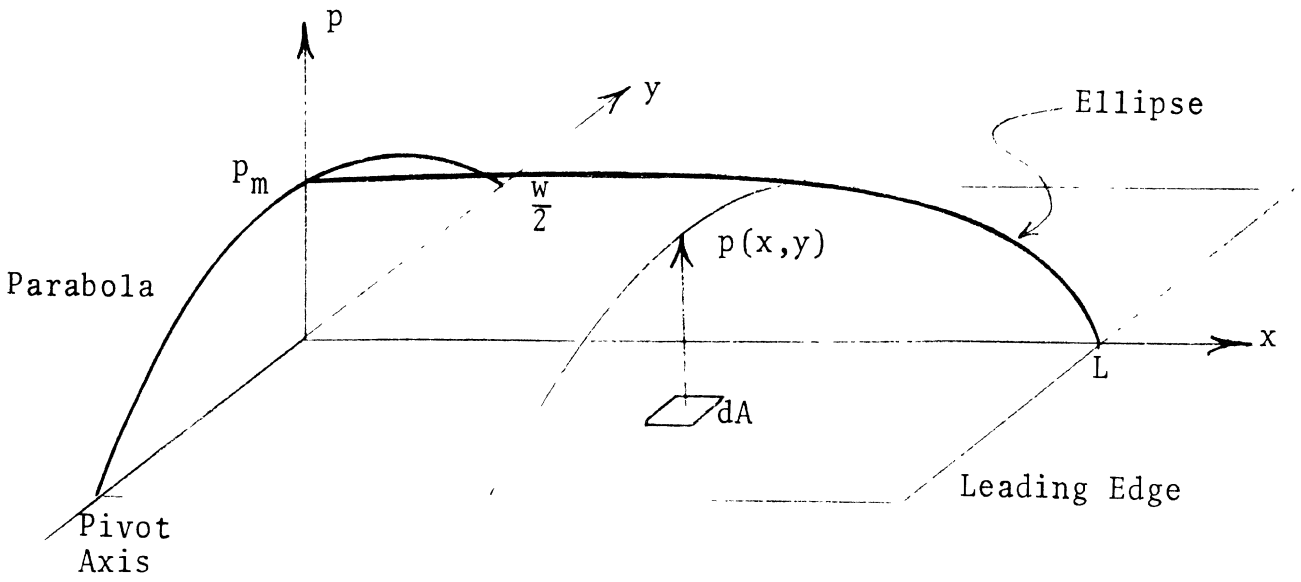

Figure 36. Hydrodynamic pressure distribution assumed for the purpose of computing the average hydrodynamic pressure for a tread plate in pure rotational approach.

With the hydrodynamic pressure distribution described above and sketched in Figure 36, the pressure moment about the y-axis (measured in the laboratory experiment) is given by

$$M_x = \int_A p(x,y)x \, dA = \frac{2}{g} p_m w L^2$$

and the average pressure is

$$P_{avg} = \frac{1}{wL} \iint_A p(x,y)\,dA = \frac{\pi}{6} p_m$$

By eliminating the maximum pressure, p_m, from the above two equations, the average pressure is found to be

$$P_{avg} = \frac{3\pi M_x}{4\ w\ L^2}$$

where

M_x = hydrodynamic pressure moment (measured)

L,w = length and width of the tread plate

For the smooth tread plate, of dimensions w = 3 in. and L = 4 in., a peak pressure moment M_x = 50 ft-lb was measured. For a pressure distribution as shown in Figure 36, the average pressure is P_{avg} = 29 psi. It is interesting to note that if a parabolic rather than an elliptic profile is assumed in the plane of symmetry, the value P_{avg} = 33 psi is found. The higher value is to be expected as the centroid for a parabolic profile is closer to the pivot axis than is the centroid for an elliptic profile. In either case, the resulting values for P_{avg} are merely rough estimates, because the actual pressure distribution has not been measured or calculated.

Figure 37 presents data obtained for a 3 in. x 4 in. tread plate having two straight, longitudinally cut grooves .25 in. deep and .25 in. wide. The initial displacement, water depth, and motivating torque used were the same as for the smooth tread plate (Fig. 35). As expected, the sinkage rate for the grooved tread is substantially greater than that of the smooth tread. At the .05 in. displacement level, the grooved tread velocity

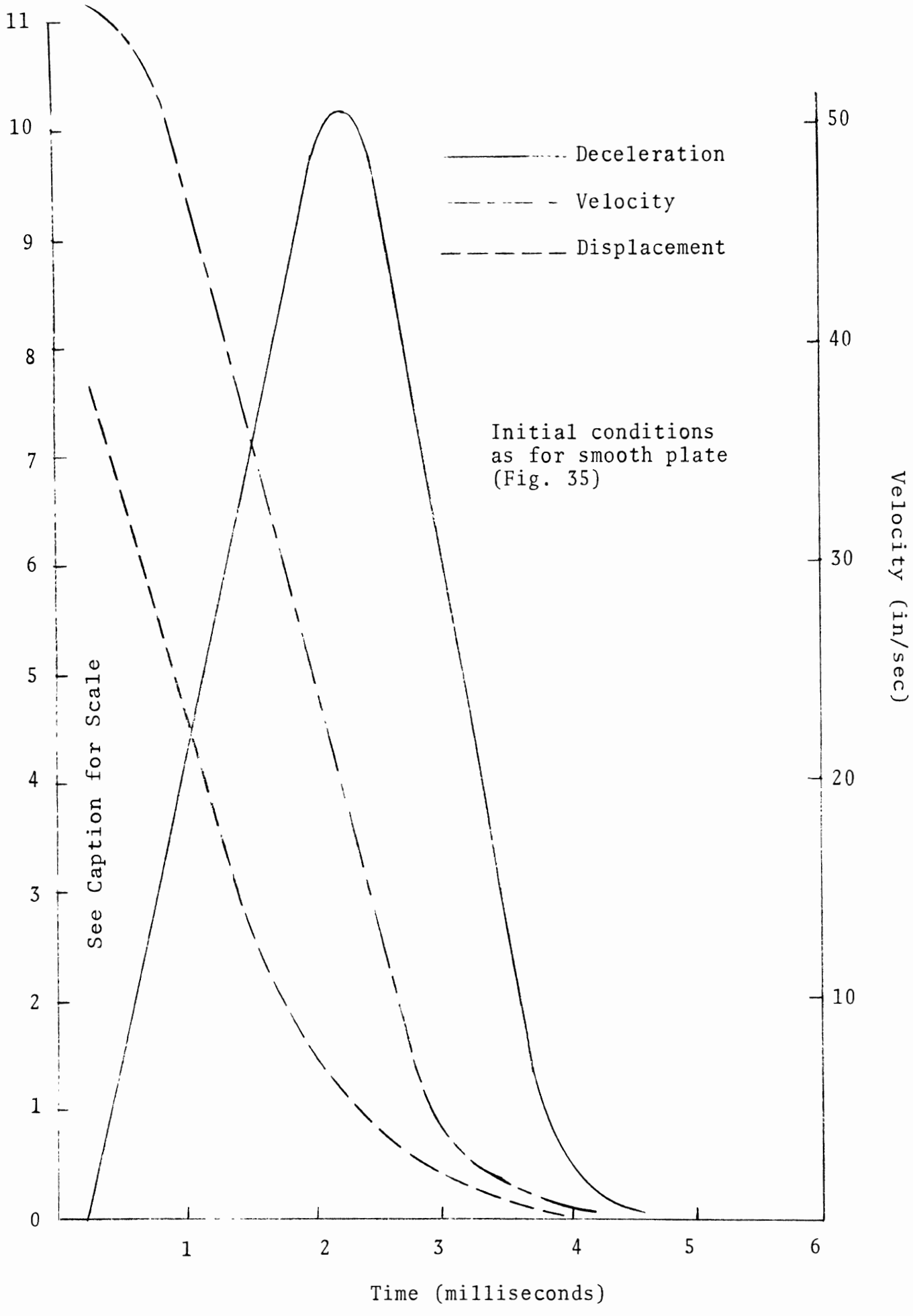

Figure 37. Grooved plate sinkage data. Left scale: angular deceleration (x 10^3 rad/sec^2) and displacement (x 10^{-2} in.).

is 52 in/sec, in comparison with 33 in/sec for the smooth tread; while hydrodynamic pressure is approximately the same* for both tread plates. For the grooved plate, however, the hydrodynamic force does not reach its peak until the water film is only a few thousandths of an inch thick. It seems that, for the grooved plate, the flow resistance is low until the water film thickness is reduced to the point where a viscous squeeze film is formed; while, for the smooth plate, hydrodynamic force is appreciable in thick squeeze films for which fluid inertia forces dominate.

A check on repeatability of the experimental results was made by dismantling the apparatus after the above tests on the 2-groove plate, reassembling, and repeating the test with the same initial conditions. Variations in the results of the second runs, compared with the first runs, could not be resolved on the photographs of the storage oscilloscope display.

At this point it has been established that the laboratory apparatus is capable of evaluating the water expulsion effectiveness of a grooved tread pattern vis à vis a smooth tread.

A series of tests were performed on tread plates having straight, longitudinally cut, groove patterns with the geometry given in Figure 38. Plates B through H constitute a series of increasing number of grooves (1 to 8) with groove volume held constant at .5 in^3. Since this pattern series has a groove volume per unit of gross contact area (groove capacity) fixed at .042 in., water will be forced to flow through the grooves when these patterns are operated in water depths greater than .042 in. The effect of groove capacity is studied with patterns I-K, each having three grooves of constant width (.25 in) but different depths.

*The removal of material in cutting the grooves only slightly alters the moment of inertia.

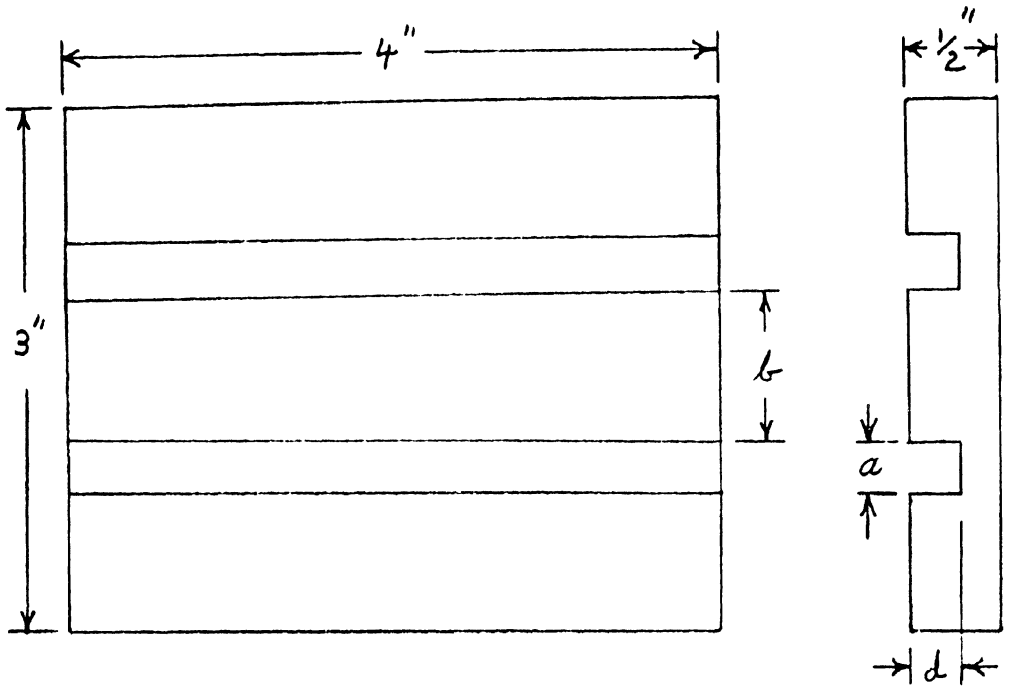

Plate	Number of Grooves	Groove Depth *d*	Groove Width *a*	Rib Width *b*	Groove Volume in.^{3}
A	Smooth	--	--	--	--
B	1	.250	.500	1.25	.50
C	2	.250	.250	.833	.50
D	3	.250	.167	.625	.50
E	4	.125	.250	.500	.50
F	5	.125	.200	.333	.50
G	6	.125	.167	.286	.50
H	8	.094	.167	.186	.50
I	3	.167	.250	.563	.50
J	3	.250	.250	.563	.75
K	3	.333	.250	.563	1.00

Figure 38. Geometry of tread pattern plates tested for water expulsion effectiveness.

Deep Water Test Results. For these tests, water depth was maintained at .3 in. to insure groove flow throughout the approach of the tread plate to the road surface plate. The test conditions correspond to a tire operating in water depths greater than the groove capacity.

Figure 39 shows tread displacement versus time curves (sinkage curves) for patterns A-H (Fig. 38). A motivating torque of 25 ft-lbs was used to produce an average hydrodynamic pressure of approximately 40 psi; a realistic value for a tire in total hydroplaning.

Relative to the sinkage rate of the smooth plate (A), improvement in tread pattern effectiveness was found for one groove and additional improvement was found for two grooves. No further improvement in water expulsion effectiveness was detected with the 3, 4, 5, 6, and 8-groove patterns. These data (Fig. 39) suggest the existence of a critical rib width, below which no improvement in tread pattern effectiveness is obtained. For the groove volume of .05 in^3, used in these tests, the critical rib width is approximately .8 in. An explanation for this finding will be offered later when the experimental results are discussed in greater depth.

To study the effect of groove capacity on tread pattern effectiveness, patterns I-K were tested with the same initial conditions (water depth: .3 in., torque: 25 ft-lbs) as patterns A-H. The results of the groove capacity study are shown in Figure 40. It was found that the sinkage curve for Plate I is identical to the sinkage curve for plate D, a 3-groove pattern having the same groove volume as plate I but with different groove width and depth. Plates J and K, which have greater groove volume, show higher sinkage rates and thus are more effective in deep water than any of the patterns shown in Figure 39.

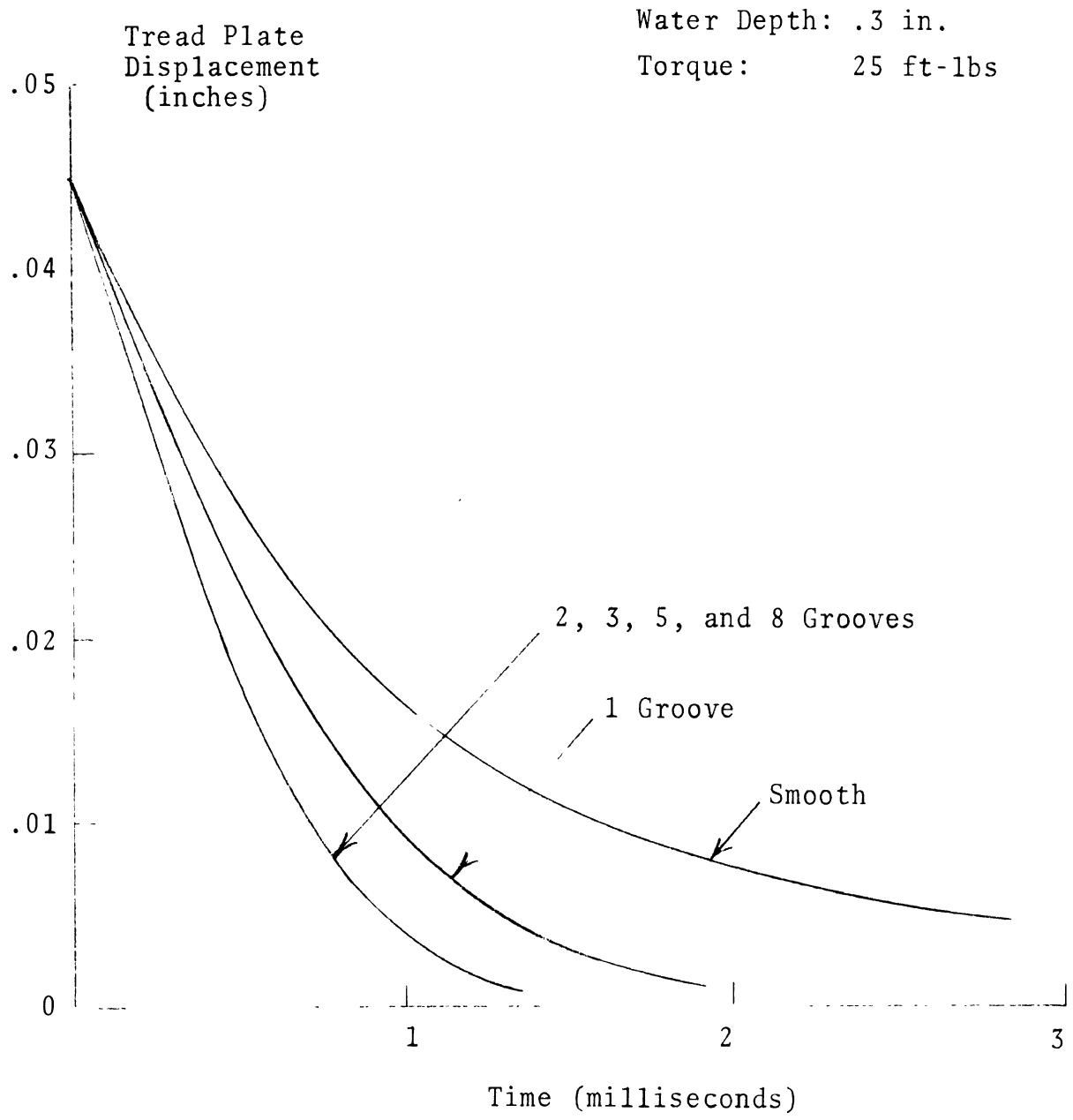

Figure 39. The effect of groove number on the sinkage of tread plates with the same groove volume (.5 in^3).

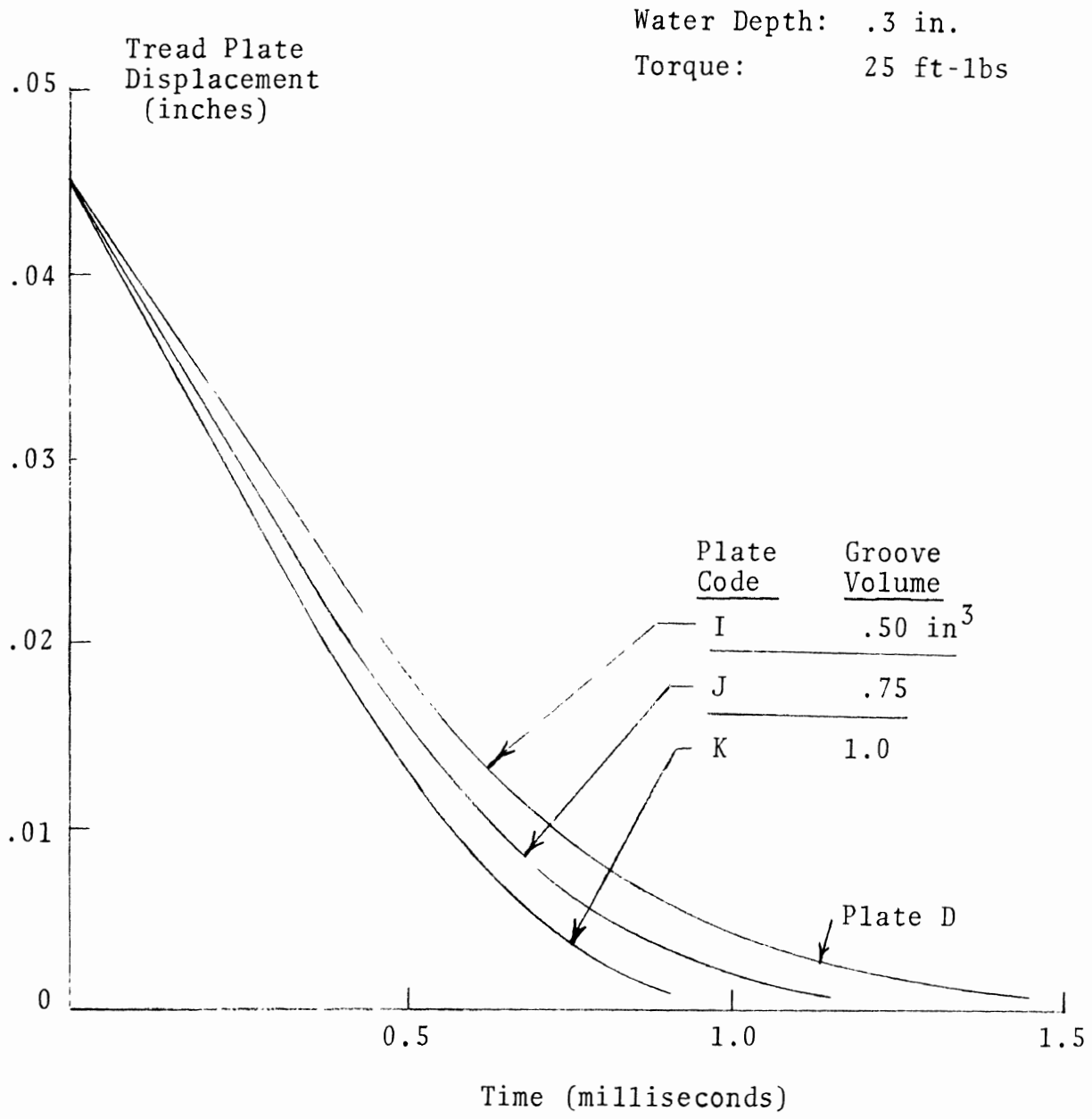

Figure 40. The effect of groove volume on the sinkage of tread plates with 3 grooves.

Test Results for Various Water Depths. If the grooves are not flooded during the entire approach of the tread plate to the road surface plate, water depth will have an influence on the test results. The following test procedure was used to study the influence of water depth on tread pattern effectiveness.

For each pattern to be tested in various water depths, a reference run was first made with the water depth at .3 in. (to assure groove flooding) and a motivating torque of 25 ft-lbs. Tests are then conducted at lower water depths with the motivating torque adjusted such that the displacement and approach speed versus time curves closely approximate those obtained with 25 ft-lbs of torque and .3 in. of water. Motivating torque thus becomes a measure of the ease with which water is expelled from beneath the tread plate; the lower the torque, the lower is the hydrodynamic pressure distribution associated with a given rate of sinkage. Tread plates A-H and K were tested in this manner.

Figure 41 shows the variation of motivating torque with water depth for tread patterns A-H (solid lines) and K (dashed line). It is interesting to note that at the water depth of .06 in., an improvement in water expulsion effectiveness (relative to the smoooth tread plate) was obtained with the 1, 2, 3, 4, and 5-groove patterns; in deep water, improvement was obtained only for the pattern with higher groove volume (K).

Another interesting feature of these results is that all of the curves in Figure 41 for tread plates B-H (all of equal groove volume) begin to deviate from the smooth tread plate at approximately the same water depth (.10 in.). However, plate K, which has twice the groove volume, begins to deviate at a higher water depth (approximately .15 in.).

Finally, it is important to observe that the smooth plate is insensitive to water depth, while the patterned plates are all water depth sensitive. The smooth plate would, of course, show depth sensitivity at very small water depths—smaller than those used in these experiments.

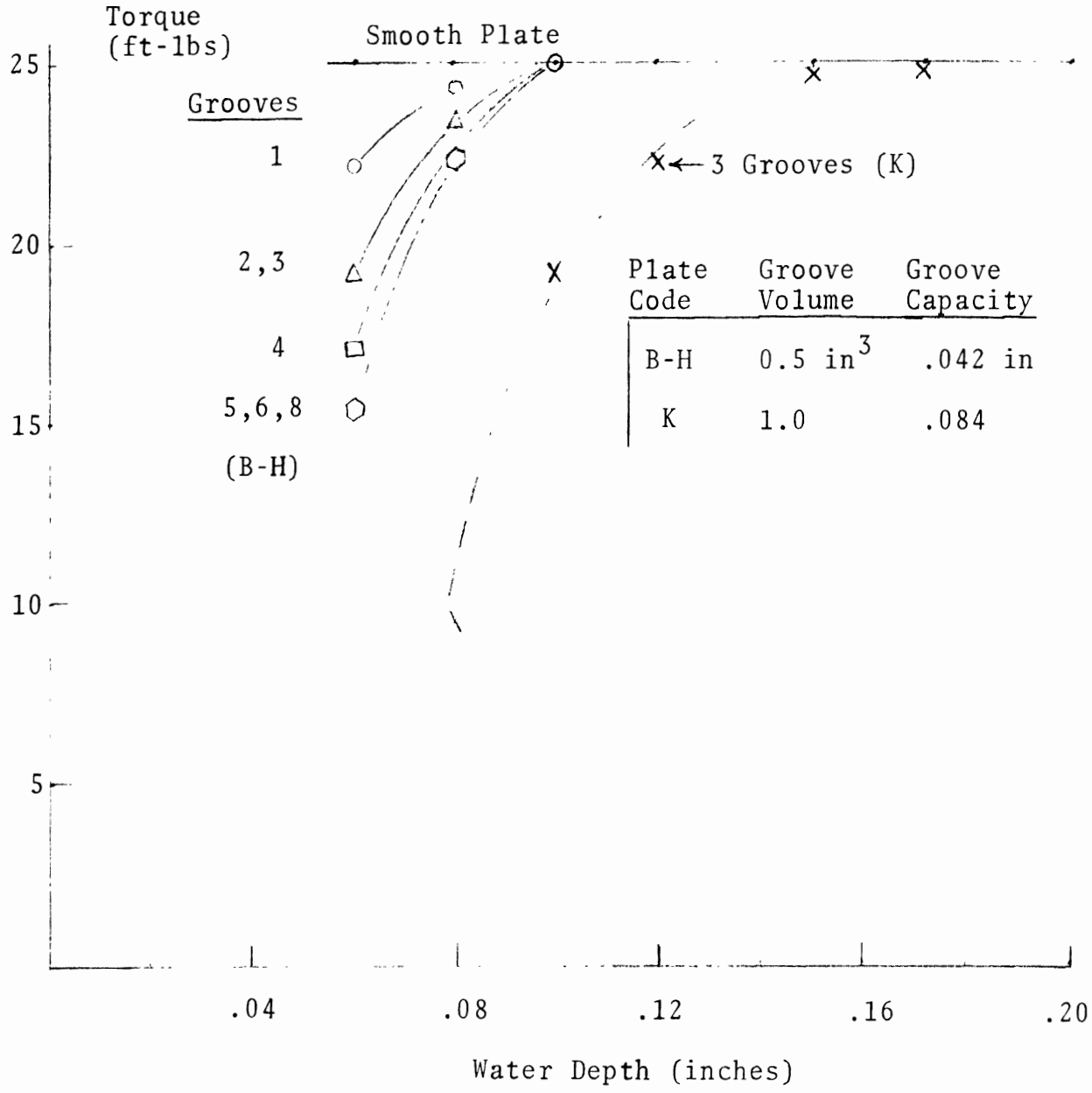

Figure 41. Ease of water expulsion versus water depth. Motivating torque (ordinate) is that required to duplicate the deep water (h = .3 in) sinkage curve obtained with 25 ft-lbs torque.

An inconsistency apparent in these data is that the 2 and 3-groove patterns fall on the same point in Figure 41. The reason for this is not known conclusively but it is believed to be due to either a misalignment between the tread plate and the road surface plate or by an error in calibration of the instrumentation.

5.4 DISCUSSION OF THE RESULTS

The existence of a critical rib width, such as observed in the deep water experiments (Fig. 39), may be explained by consideration of the hydrodynamic pressure distribution developed beneath the tread plate. It will be hypothesized that the pressure gradient required to motivate the flow of a particle of water from beneath a tread rib to a groove or the periphery of the contact region is made up of two components.

1. A pressure gradient associated with squeeze film flow (in the rib region).
2. A pressure gradient which motivates groove flow.

The squeeze film component (1) is a function of rib width while the groove flow component (2) depends on groove volume and water depth. Thus, for a given water depth and groove volume, it is clear that an improvement in tread pattern performance can be obtained by decreasing the rib width. However, when rib width is sufficiently small that the pressure gradient associated with groove flow becomes dominant, no further improvement with decreasing rib width will be obtained. In deep water (e.g., .3 in.) and with a groove volume of .5 in^3, the critical rib width found by the laboratory apparatus appears to be about .8 in.

If the above theory is correct, a decrease of the critical rib width could be obtained by either (a) increasing the groove volume, or (b) decreasing the water depth. The tests performed at decreased water depths (see Fig. 41) tend to confirm the theory since at a lower water depth (.06 in) a reduced critical rib width (.33 in) was found.

The data from tests performed on the 3-groove patterns J-K, which have greater groove volumes (.75 in and 1.00 in), are also consistent with this theory, since the increased groove volume patterns showed an increased sinkage rate that can only be explained by a decrease in groove flow resistance (see Fig. 40). However, the effect of an increase of groove volume on critical rib width has not clearly been established because tests have not been performed on tread plates having various rib widths as well as increased groove volume (patterns I-K were of constant rib width).

The preceding discussion is concerned with the role of tread grooves in deep water operation or in water depths which produce groove "flooding" at highway speeds. It is well known, from investigations of the hydroplaning phenomenon, that when hydrodynamic pressures associated with groove flow become equal to the tire-road contact pressure, the grooves become "choked" and there is no longer a pressure gradient existing between the tread ribs and the grooves to motivate expulsion of the squeeze film from beneath the ribs. A similar situation may prevail in the laboratory experiment when rib width is below the critical value.

It is recalled that Maycock [5] found a critical rib width of approximately .65 in. from tests performed on a smooth road surface with a water depth of .02-.04 in. At such low water depths the grooves could not have been flooded and the theory proposed above cannot be used to explain Maycock's finding. It seems more reasonable to hypothesize that, for low water depths

(no groove flooding), a rib width of .65 in. provides for a squeeze film expulsion rate in zone 2 of the contact region (Fig. 26) which is sufficiently rapid that partial dynamic hydroplaning cannot occur to any significant extent at normal highway speeds. In this case, a smaller rib width would not yield a measurable improvement in traction performance.

The hypothesis proposed in the preceding paragraph is consistent with the squeeze-film theory discussed in Chapter 3. A rib of .65 in. width has an average flow distance, AFD, of .16 in. A circular plate of .25 in. radius has approximately the same AFD. Referring to Figure 30, it is seen that the circular plate of .25 in. radius requires .45 milliseconds to sink from an initial height of .05 in. to .005 in. Under more realistic conditions of inclined sinkage to a surface having some roughness, the sinkage rate would be even greater. Since, at 60 mph, the time required for a tread element to pass through the contact patch is typically 5 or 6 milliseconds, zone 2 can be expected to comprise only a small fraction of the contact region. Although a smaller rib width would still further reduce the size of zone 2, it is not expected that a significant improvement in traction would result if the zone were already very small.

The experiments performed on the 3-groove pattern, D, tend to support the above hypothesis. Approximately .5 milliseconds was required for this pattern to sink from .05 in. to .005 in.—roughly the time predicted by inertial squeeze-film theory.

In the presentation of the data obtained in varying water depths (Fig. 41), it was noted that there are critical water depths above which water depth has no effect on tread plate sinkage. Although this laboratory finding appears to be analogous to the critical water depth observed in experiments on hydroplaning tires (see Section 2.2.3), the critical water depths seen in Figure 41 occur for a different reason and are not directly related to the hydroplaning tire.

The critical water depths seen in Figure 41 can be explained by hypothesizing that, at depths above the critical levels, the grooves are flooded during the entire approach, while at depths below the critical levels, the grooves are merely filling up without appreciable longitudinal flow to the tread plate periphery. Obviously, treads having lower groove volumes will flood at lower water depths. Thus it is not surprising to find that tread plates B-H, all of which have the same groove volume (.5 in^3), exhibit a bifurcation point at a lower water depth than plate K, which has a higher groove volume (1.0 in^3).

The preceding observations lead to the suspicion that the striking bifurcation points seen in Figure 41 can be correlated with the proposed tread pattern performance parameter γ_1

$$\gamma_1 = \frac{\text{groove capacity}}{\text{water depth}}$$

Unfortunately, due to surface tension effects, the measured value of water depth is not a true indicator of the amount of water being displaced by the tread pattern. This problem will be considered in the next section, which discusses the limitations of the laboratory apparatus.

5.5 LIMITATIONS OF THE EXPERIMENT

Although the experimental apparatus provides a realistic simulation of many aspects of the water expulsion process which takes place when a tire rolls over a wet surface, there are some significant limitations of the experiment which limit the extent to which the experimental data can be related to real tire behavior.

Boundary Conditions. The mechanical boundary conditions governing the water flow in the laboratory apparatus may be considered unrealistic in three major aspects.

1. A real tire experiences hydrodynamic pressure deformation of the tread in the contact region, while the experiment employs a flat and rigid tread plate. It is known from measurements [2,25] and glass plate observations [1,3,11] of hydroplaning tires that, for an automobile tire, the water film is thickest along the longitudinal center line of the contact patch and thinnest at the edges. In this experiment, the water film thickness is constant across the contact width.

Daughaday and Tung [24] have analytically investigated the effect of tread deformation on the pressure distribution beneath a fully hydroplaning tire. Figure 42 shows a hydrodynamic pressure distribution computed on the assumption of a flat tread surface

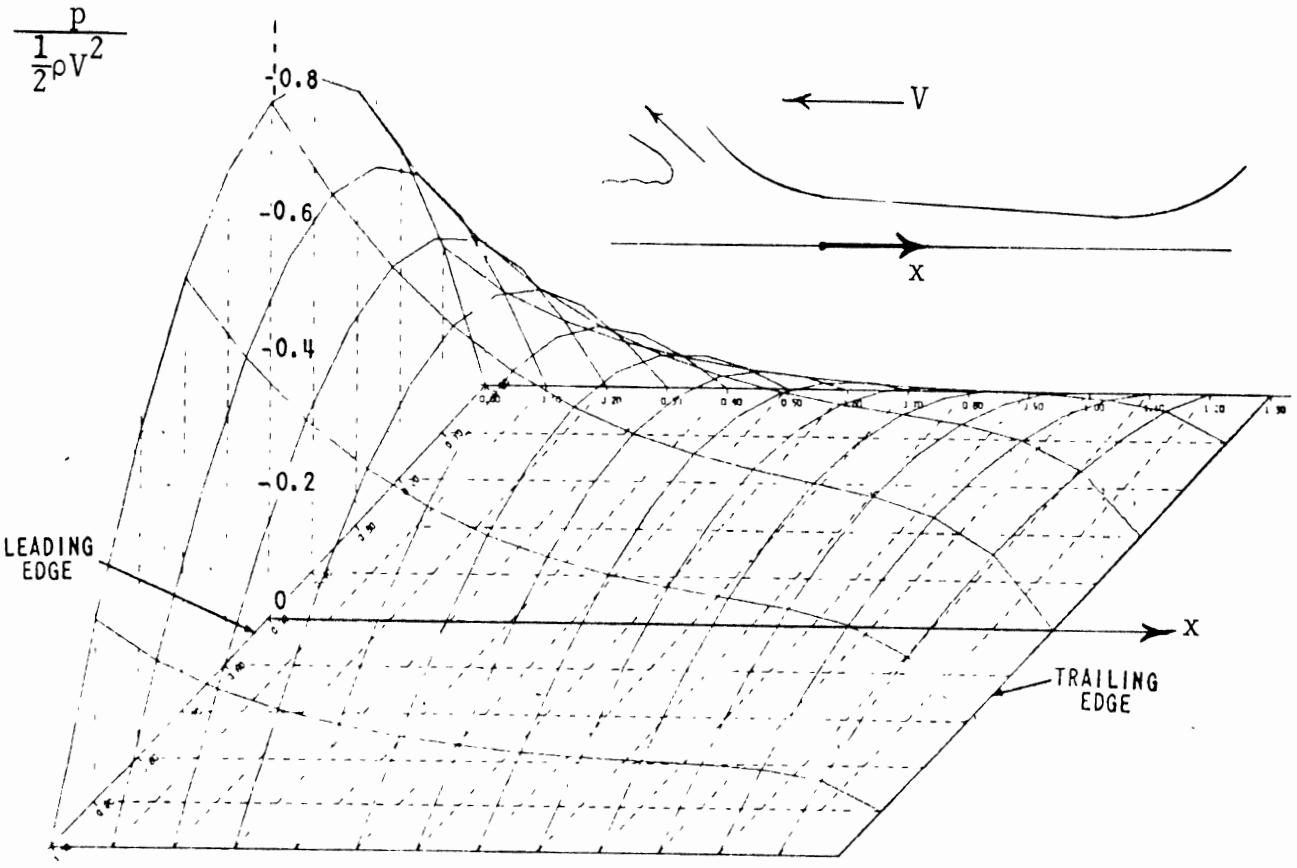

Figure 42. Hydodynamic pressure distribution computed for a totally hydroplaning tire with flat tread surface in the contact region. From [24]

in the contact region. The pressure distribution is found to be parabolic in the lateral direction. In the longitudinal direction, the high pressure (due to water-wedge impact) at the leading edge drops off rapidly to become nearly uniform in the central region and then drops off to zero at the trailing edge. The resultant lift developed by this pressure distribution is too small to produce total hydroplaning at the speeds at which it is commonly observed; thus, the authors have shown that the tread surface supported by hydrodynamic pressure must be curved in some manner.

Figure 43(a) shows a hydrodynamic pressure distribution computed by Daughaday and Tung [24] on the assumption of a curved tread surface (shown in Fig. 43(b)). The pressure distribution is now found to be nearly uniform in the central contact region and the resultant lift developed is sufficiently large to produce total hydroplaning at speeds comparable to those observed experimentally.

The recent and more comprehensive theoretical analysis of Browne [21] shows that tire hydroplaning must be accompanied by inward buckling [sic] of the tread in the central portion of the contact region. Browne's analysis shows that viscous effects are not important in hydroplaning where the amount of water encountered by the tire exceeds the combined drainage capacity of the tread pattern and the pavement macrotexture.

It is now clear that the hydrodynamic pressure distribution is highly sensitive to the deformed slope of the tire tread in the contact region. The flat and rigid surfaces employed in the laboratory apparatus described in this report may, therefore, not generate realistic hydrodynamic pressure distributions.

2. The rotational motion of the tread pattern in the laboratory apparatus is not similar to the motion of a real tire tread in conditions of partial hydroplaning. Figure 44 illustrates the motion of tread surface points in the laboratory experiment which constrains the tread plate to rotate about a fixed axis (A). Points 1 and 2 on the laboratory tread, traveling along circular arcs, do not move equal distances during the rotational motion.

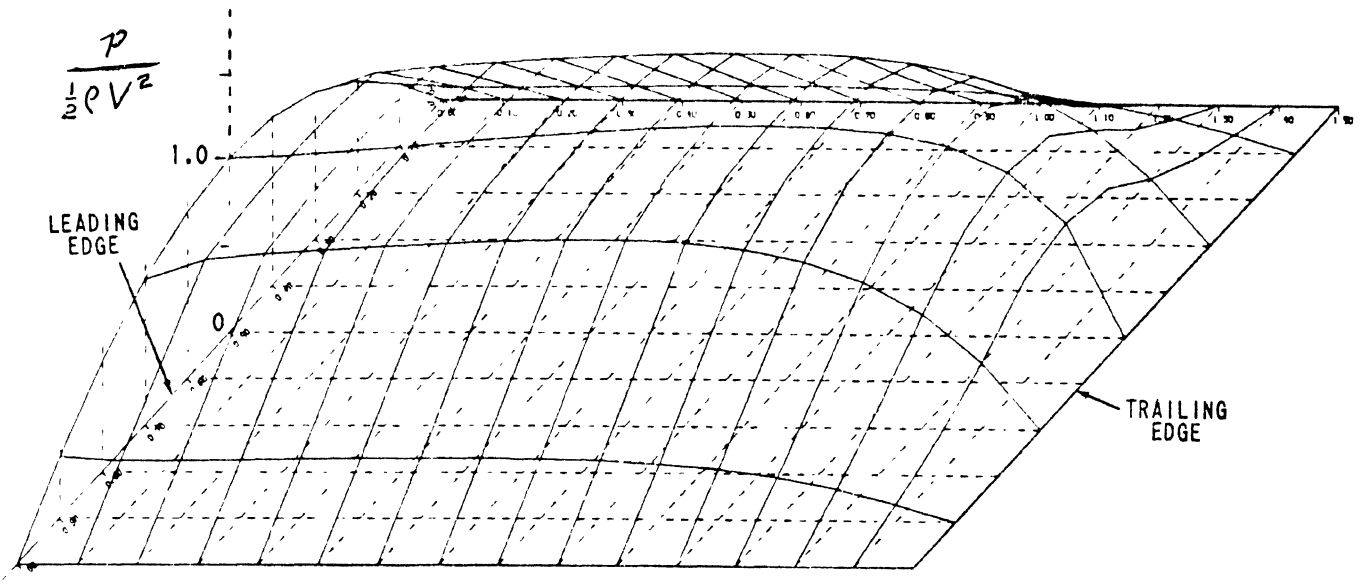

(a) pressure distribution

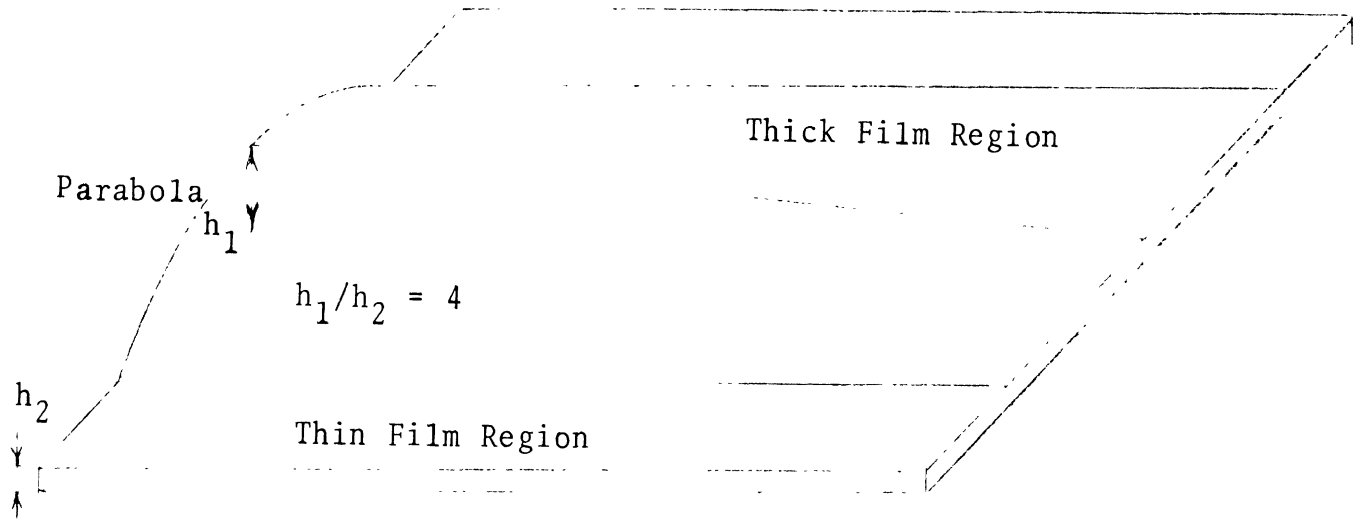

(b) tread curvature in the contact region

Figure 43. Hydrodynamic pressure distribution (a) computed for a totally hydroplaning tire with a curved tread surface (b) in the contact region. From [24]

In the highway situation, shown in Figure 45, the non-contacting tread surface exhibits a translational motion toward the road surface and all surface points move equal distances before contact is made. The line of contact (C), which is represented by the axis of rotation in the laboratory apparatus, travels along the road surface with the speed of the vehicle. As the tread on a real tire conforms to the road surface by bending along the line of contact, motion of noncontacting tread surface points may deviate slightly from pure translation due to bending deformation which propagates out to the noncontacting tread.

The extent to which the hydrodynamic pressure distribution is influenced by pure rotational motion , vis-à-vis pure translational motion of the type illustrated in Figure 45 , is difficult to analyze. The evaluation of the relative influence of these two tread motions would require an analytical solution for each (with the assumption of smooth tread and road plates). The flow produced in the highway situation (Fig. 45) has been tested analytically by Browne [21] and by Daughaday and Tung [24]. These researchers were able to achieve analytical solutions by choosing a flow coordinate system which moves with the tire and thus transforms the non-steady flow problem to one of steady flow. No similar choice of coordinates is possible for the pure rotational motion of the laboratory apparatus and the extremely complicated non-steady flow associated with this device has yet to be treated analytically.

3. The water wedge, which always exists when a real tire is operating on a wet pavement, is absent in the laboratory simulation. The hydrodynamic pressure distribution in zone 2, which is simulated by the laboratory apparatus, is believed to be strongly influenced by the boundary condition associated with the water wedge in zone 1. Here, again, the absence of a rigorous analytical solution for the water-wedge pressure distribution makes the assessment of the influence of this boundary condition one of pure speculation.

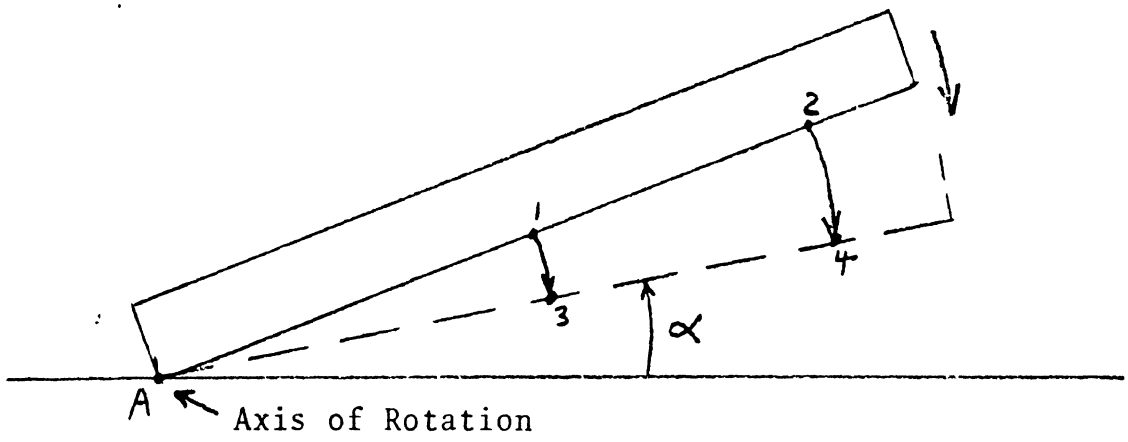

Figure 44. Laboratory situation: tread plate in pure rotation (fixed axis of rotation).

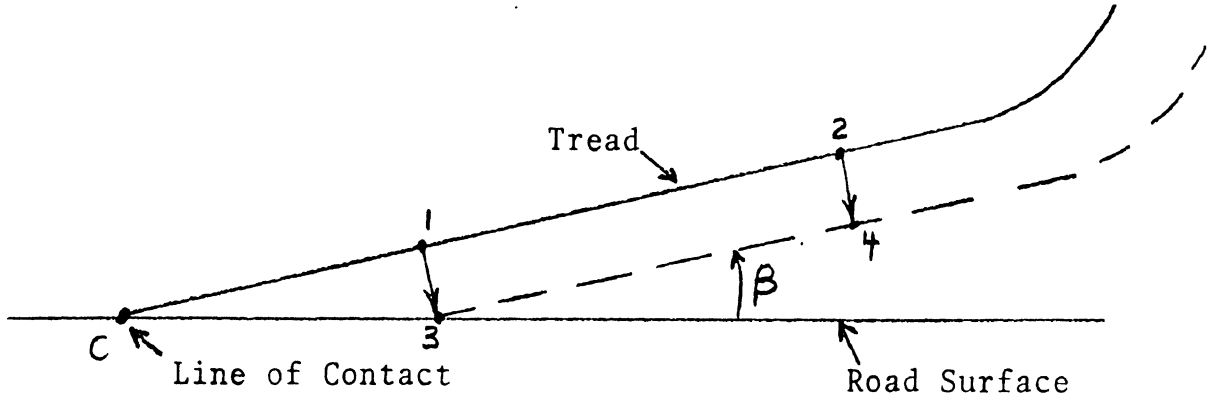

Figure 45. Highway situation: tread pattern in pure translation (moving line of contact).

Surface Tension Effects. It was previously mentioned, in the discussion of data, that the results of experiments performed at low water depths are difficult to interpret because of surface tension effects. The difficulty is illustrated in Figure 46 where it is seen that when the tread plate is raised to its initial position prior to release, additional water collects beneath the plate, behind a meniscus due to surface tension of the water. The measured value of the standing water depth is therefore not a true indication of the amount of water actually displaced by the tread. A modification of the apparatus to overcome this difficulty is suggested in Section 5.6.

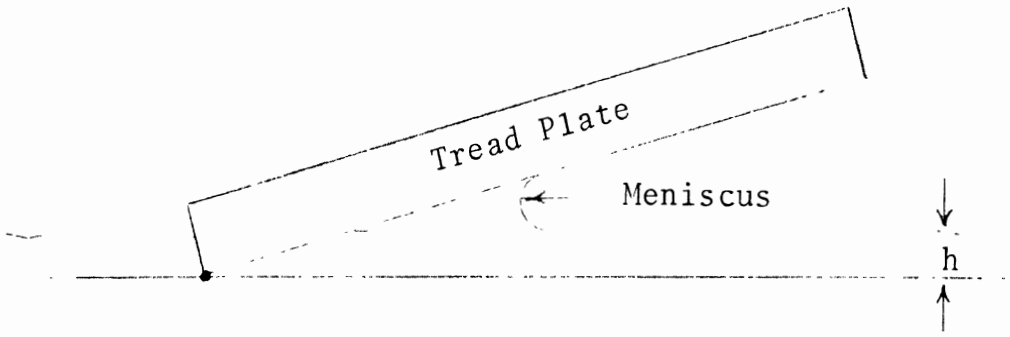

Figure 46. The effect of surface tension on the amount of water displaced by the tread plate.

5.6 SUGGESTIONS FOR FURTHER WORK

Mechanical Improvements. The bifurcation points in Figure 41 could be correlated with the dimensionless tread operation γ_1

$$\gamma_1 = \frac{\text{groove capacity}}{\text{water depth}}$$

if the experiment were modified to overcome the problems caused by the surface tension effect. This modification could be accomplished in two ways.

1. The apparatus could be rebuilt in such a way that the tread plate approaches the road surface plate in the parallel manner shown in Figure 47. This approach would necessitate a complete redesign of the apparatus and considerable difficulty may be encountered in maintaining a perfectly parallel approach under the loads and accelerations to which the tread plate is subjected. Obviously, a pure rotational approach is much easier to maintain than a pure translational approach.

2. A relatively simple modification could be made to the existing apparatus, as shown in Figure 48. Here, the tread plate is re-positioned so that its trailing edge no longer coincides with the axis of rotation. This will provide some clearance for a shallow water film when the tread plate is raised to its pre-release position. The formation of a meniscus with deep water films is not a serious problem as the water displaced from the meniscus is then insignificant compared to the deep water film displacement.

A meniscus will still form at the time the tread surface makes contact with a shallow water film. However, in this case it can be shown that the surface tension force, which produces the meniscus, is negligible compared to the fluid inertia forces involved in the water expulsion process. An analysis supporting this statement is given in Appendix A of this report.

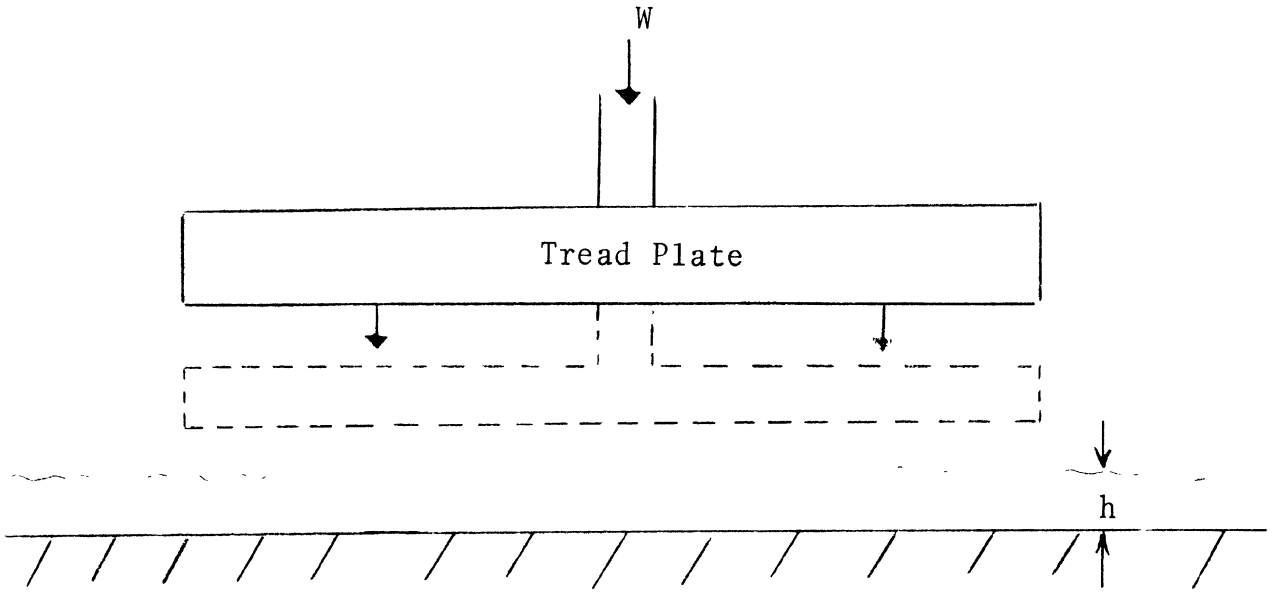

Figure 47. Tread plate in parallel approach.

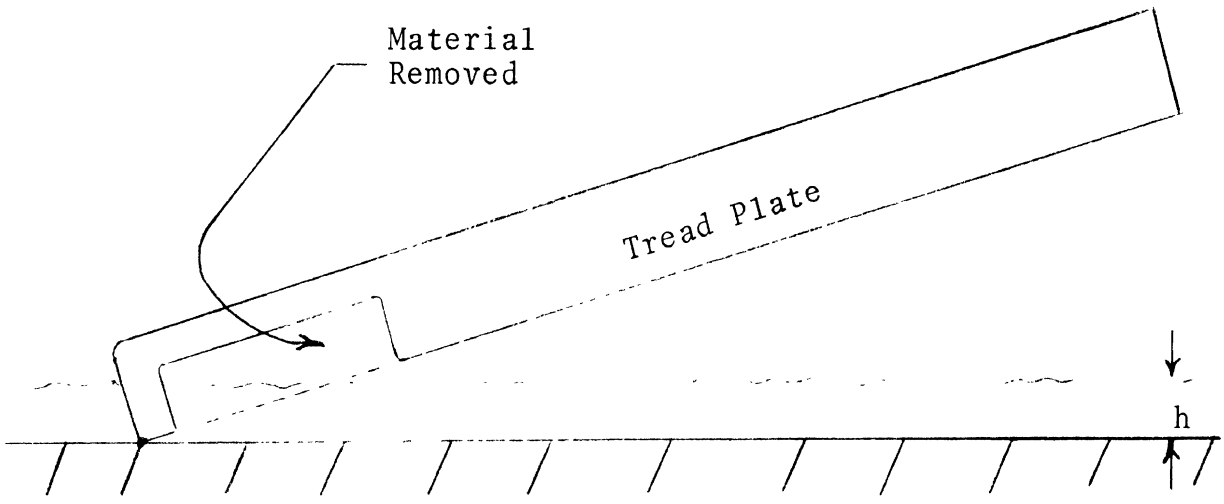

Figure 48. A modification of the existing apparatus to overcome the adverse effect of surface tension.

Additional Applications. At this time, the laboratory apparatus has been applied only to the study of longitudinally grooved tread patterns. In order to evaluate the relevance of the flow distance parameter γ_2,

$$\gamma_2 = \frac{A/C}{L}$$

it will be necessary to test a much broader variation of patterns incorporating zig-zag grooves, transverse grooves, and some block-type patterns. It may prove feasible to test actual rubber treads cut from production tires, provided a method of assuring a sufficiently flat tread surface can be found.

Another potential application of this laboratory apparatus lies in the study of surface texture effects. By covering the smooth road surface plate with surfaces of various textures, the effect of surface drainage on tread plate sinkage could be studied.

Finally, in Section 4.0 of this report, it was suggested that there is need for a parameter which can be correlated with the resistance to groove flow. A design of a laboratory apparatus for the study of groove flow resistance is described in Appendix B.

REFERENCES

1. Horne, W.B. and Dreher, R.C., "Phenomena of Pneumatic Tire Hydroplaning," NASA Technical Note D-2056, November 1963.

2. Horne, W.B. and Joyner, U.T., "Pneumatic Tire Hydroplaning and Some Effects on Vehicle Performance," SAE Paper No. 970C, January 1965.

3. Leland, T.J.W., "An Evaluation of Some Unbraked Tire Cornering Force Characteristics," NASA Technical Note D-6964, November 1972.

4. Staughton, G.C. and Williams, T., Tyre Performance in Wet Surface Conditions, Road Research Laboratory Report LR 355, 1970.

5. Maycock, G., Experiments on Tyre Tread Patterns, Road Research Laboratory Report LR 122, 1967.

6. Leland, T.J.W., et al., "Effects of Pavement Texture on Wet-Runway Braking Performance," NASA Technical Note D-4323, 1968.

7. Grime, G. and Giles, C.G., "The Skid-Resisting Properties of Roads and Tyres," Proceedings of the Automobile Division, Institution of Mechanical Engineers, No. 1, 1954-55.

8. Kummer, H.W., Pavement Wetting and Skid Resistance, Joint Road Friction Program, Pennsylvania State University, Report No. 8, December 1963.

9. Gengenbach, W., "Experimentelle Untersuchung von Reifen auf nasser Fahrbahn (Experimental Investigation of Tires on a Wet Roadway)," ATZ, Vol. 70, No. 9, 1968.

10. Staughton, G.C., The Effect of Tread Pattern Depth on Skidding Resistance, Road Research Laboratory Report LR-323, 1970.

11. Yeager, R.W. and Tuttle, J.L., "Testing and Analysis of Tire Hydroplaning," SAE Paper No. 720471, May 1972.

12. Sabey, B.E., Road Surface Texture and the Change in Skidding Resistance with Speed, Road Research Laboratory Report No. 20, 1966.

13. Moore, D.F., "A Theory of Viscous Hydroplaning," Int. J. Mech. Sci., Vol. 9, pp. 797-810, 1967.

14. Moore D.F., A Study of Tire-Surface Interaction for the Case of Rolling on a Wet Surface, C.A.L. Report No. YD-1969-V-2, July, 1965.

15. Reynolds, O., "On the Theory of Lubrication," Trans. Roy. Soc. (London), 177, p. 190, 1886.

16. Hays, D.F., "Squeeze Films for Rectangular Plates," ASME Lubrication Symposium Paper No. 62-LubS-9, 1962.

17. Moore, D.F., "On the Inclined Non-Inertial Sinkage of a Flat Plate," Journal of Fluid Mechanics, Vol. 20, Part 2, pp. 321-330, 1964.

18. Moore, D.F., "The Sinkage of Flat Plates on Smooth and Rough Surfaces," Doctoral Dissertation, Mechanical Engineering Department, Pennsylvania State University, December 1963.

19. Saal, R.N.J., "Laboratory Investigations into the Slipperiness of Roads," Chemistry and Industry, Vol. 55, pp. 3-7, January 1936.

20. Allbert, B.J. and Walker, J.C., "Tyre to Wet Road Friction at High Speeds," Proceedings of the Institution of Mechanical Engineers, Vol. 180, Part 2A, No. 4, 1965-66.

21. Browne, A.L., "Dynamic Hydroplaning of Pneumatic Tires," Doctoral Dissertation, Mechanical Engineering Department Northwestern University, June 1971.

22. Kuzma, D.C., "Fluid Inertia Effects in Squeeze Films," Applied Science Research, 18, August 1967.

23. Li, W.H. and Lam, S.H., Principles of Fluid Mechanics, Addison-Wesley, Reading, Mass., 1964, p. 4.

24. Daughaday, H. and Tung, C., A Mathematical Analysis of Hydroplaning Phenomena, C.A.L. Report No. AG-2495-S-1, January 1969.

25. Browne, A.L., Tire Deformation During Dynamic Hydroplaning, General Motors Research Report No. GMR-1701, September, 1974.

SYMBOLS AND TERMINOLOGY

A	contact area (actual)
a	groove width
b	rib width
C	contact perimeter
d	groove depth
F_A	local inertia force
F_C	convective inertia force
F_V	viscous force
F_x	longitudinal component of hydrodynamic force
F_z	vertical component of hydrodynamic force
g	groove capacity (groove volume/gross contact area)
h	water depth, film thickness
h_o	initial film thickness
h_c	critical water depth
L	contact length
ℓ	water wedge length, characteristic length
m	mass
P	water wedge pressure
P_{avg}	average hydrodynamic pressure
P_i	tire inflation pressure
$p(x,y)$	hydrodynamic pressure distribution
p_m	maximum hydrodynamic pressure
$\dot{Q}$	water volume interception rate
$\dot{Q}_g$	groove flow rate
R	groove flow resistance pressure

r	rib width
t	time
V	traveling velocity
V_C	average flow velocity (across a perimeter)
V_h	total dynamic hydroplaning speed (Horne , eq. (10))
V_p	partial hydroplaning initiation speed (eq (16))
v	groove volume
W	tread plate load
w	contact width
x	longitudinal contact coordinate
y	lateral contact coordinate
γ	fraction of water volume recycled by forward spray
$\gamma_1 = \frac{g}{h}$	groove capacity parameter
$\gamma_2 = \frac{A/C}{L}$	flow distance parameter
η	fluid dynamic viscosity
ρ	fluid mass density
AFD	average flow distance
BFC	brake force coefficient
$(\dot{})$	derivative with respect to time

UNIT CONVERSION GRAPHS

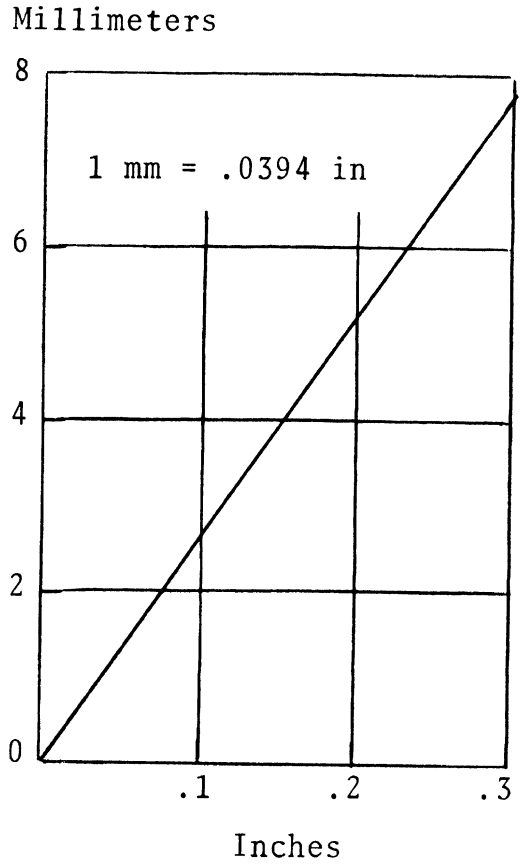

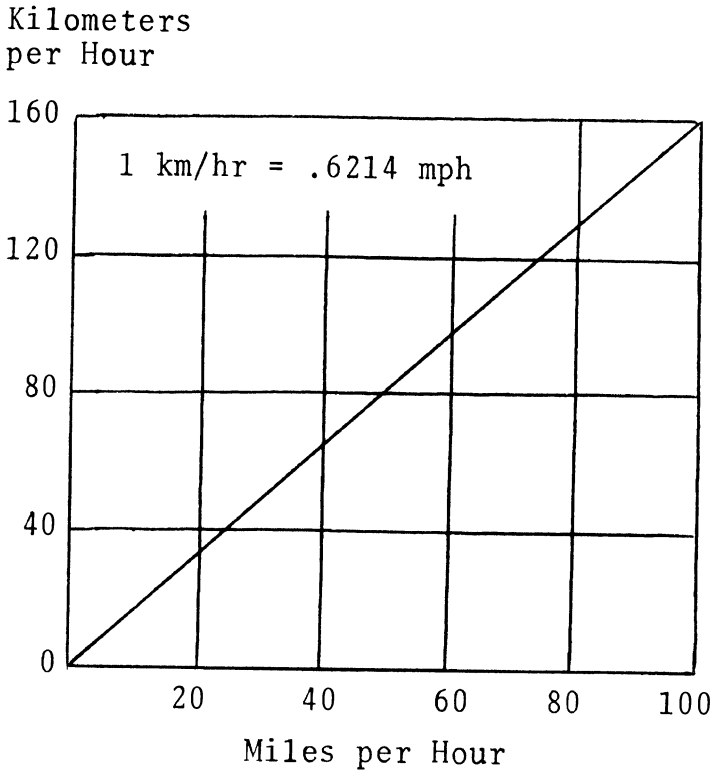

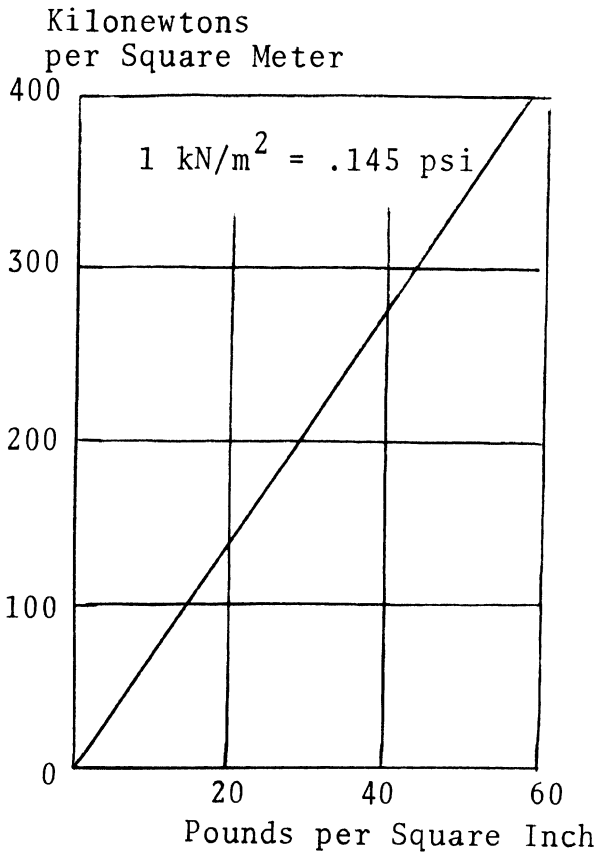

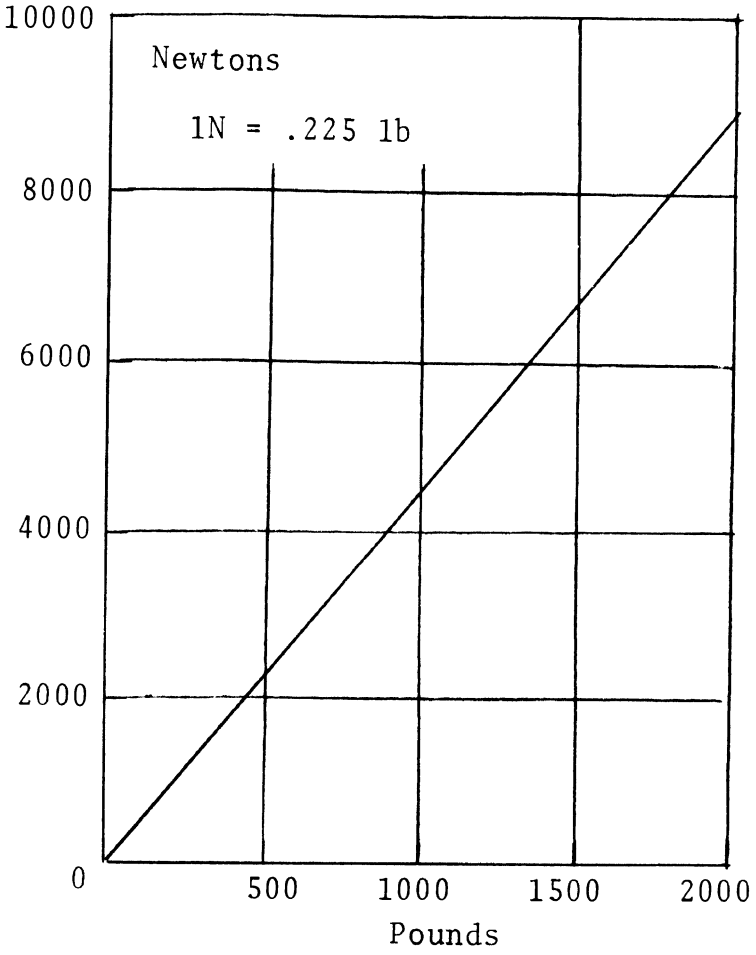

APPENDIX A

THE EFFECT OF SURFACE TENSION

It can be shown [23] that the pressure differential, ΔP, across an interface (meniscus) between two different fluids is given by

$$\Delta P = \sigma\left(\frac{1}{R_1} + \frac{1}{R_2}\right) \qquad \text{(A-1)}$$

where R_1 and R_2 are the principal radii of curvature of the meniscus and σ is the surface tension. If the meniscus, which appears when the tread plate is partially submerged, is approximated by a cylinder tangent to both the tread plate and the water surface, as shown in Figure A-1, the radii are

$$R_1 = \infty$$

$$R_2 = x \tan\left(\frac{\alpha}{2}\right)$$

For a tread plate angle of α = 3 deg. and the air-water surface tension value of σ = .000417 lb/in, the pressure differential across a typical meniscus formed during operation of the tread pattern effectiveness experiment is

$$\Delta P = \frac{.016}{x} \text{ psi} \qquad \text{(A-2)}$$

where x (inches) is the horizontal distance from the tread pivot point to the center of curvature of the meniscus (Fig. A-1). It is this pressure differential which motivates water to flow behind the meniscus and build up beneath the tread plate. It is seen,

eq (A-2), that ΔP is inversely proportional to x so that the meniscus will propogate rapidly at first, before stabilizing to an equilibrium configuration.

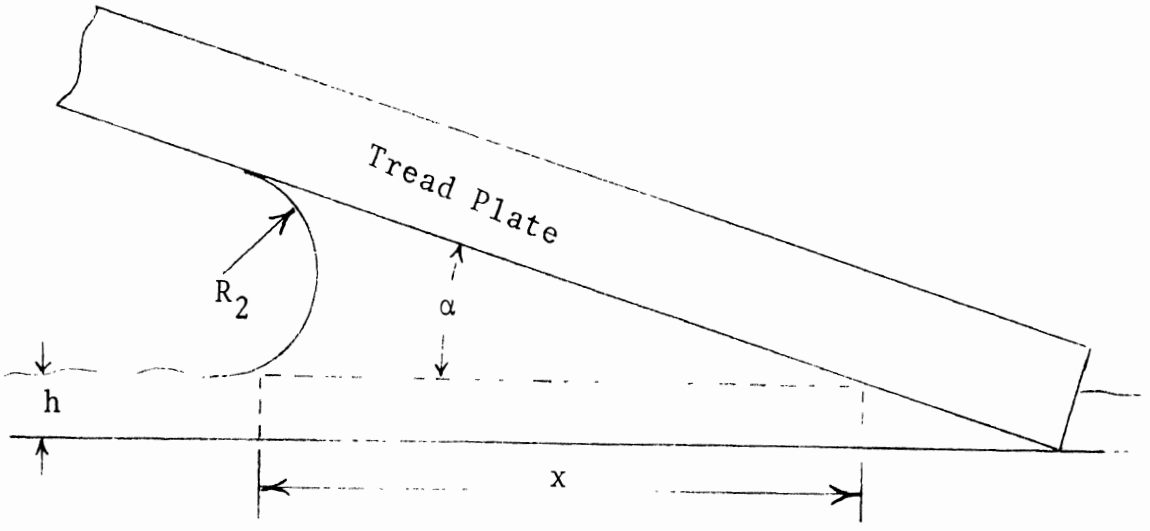

Figure A-1. Surface tension meniscus geometry

Assuming a well-formed meniscus to occur at x = .25 in, Equation (A-2) predicts a pressure gradient of ΔP = .064 psi. In the main text of the report, it was calculated that hydrodynamic pressure due to fluid inertia forces is, on the average, 30-40 psi, which is more than two orders of magnitude higher than the surface tension pressure. As the entire water expulsion experiment takes place in a few milliseconds, it is clear that the surface tension effect of a meniscus which forms during the plate approach is negligible. As explained in Section 5.5, however, it is very important that the formation of a surface tension meniscus be prevented when shallow water experiments are run. The suggested modification to the laboratory apparatus shown in Figure 48 would fulfill this requirement.

APPENDIX B

THE MEASUREMENT OF GROOVE FLOW RESISTANCE

In Chapter 4 of the report, which describes the formulation of tread pattern performance parameters, the necessity for the development of certain parameters which can be correlated with groove flow resistance was pointed out. This appendix will describe a laboratory apparatus (as yet unbuilt) designed to measure the flow resistance property of simple groove patterns.

This device would utilize a contact-patch-size section of tire tread bonded to a smooth, flat plate. Water is supplied under pressure at the leading edge of the tread and flow rate and pressure are measured at the leading edge, as shown in Figure B-1. The flow resistance, R, can then be calculated as

$$R = \frac{P}{\dot{Q}_g}$$

where P = pressure at the leading edge

$\dot{Q}_g$ = volume flow rate (through the tread grooves)

Techniques for the analysis of steady flow of incompressible fluids in pipe networks are already well developed. Possibly, with the aid of a digital computer, these techniques can be applied to the analysis of groove flow resistance. Such an analysis, verified by the experiment sketched in Figure B-1, would lead to one or more dimensionless parameters involving certain tread features (groove geometry, transverse grooves, etc.) which can be correlated with the resistance to flow.

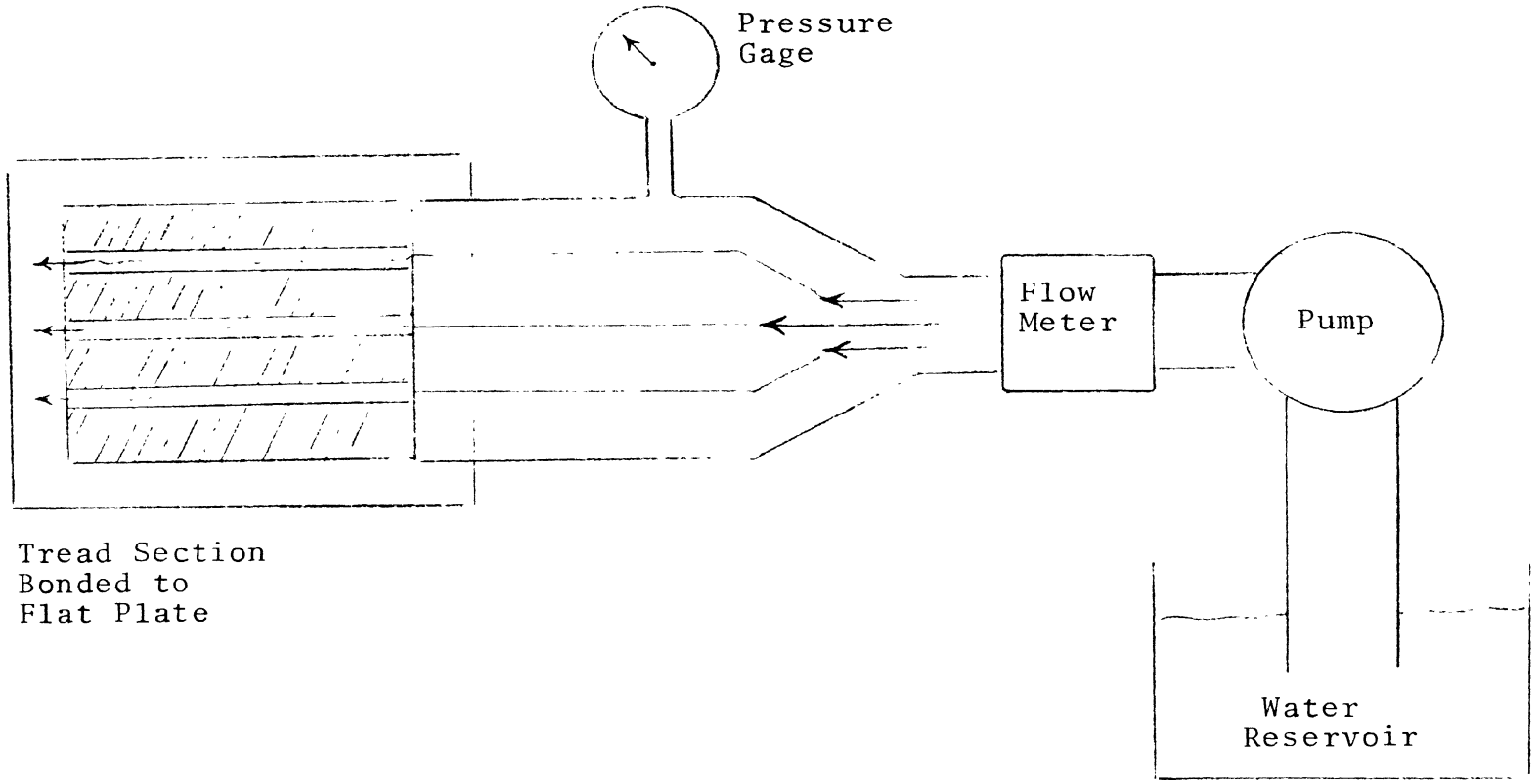

Figure B-1. Schematic diagram of an apparatus to measure the flow resistance of a tread pattern.